UNIVERSITY OF CALIFORNIA

Santa Barbara

Contributions of Glacial Melt, Snowmelt, and Groundwater to Streamflow During Low-Flow Periods: A Paired Catchment Approach in the Arun Watershed, Eastern Nepal

A dissertation submitted in partial satisfaction of the

requirements for the degree Doctor of Philosophy

in Geography

by

Katalyn A. Voss

Committee in charge:

Professor Oliver Chadwick, Co-Chair

Professor Bodo Bookhagen, Co-Chair

Professor Christina (Naomi) Tague

June 2019

The dissertation of Katalyn A. Voss is approved.

_____

Christina (Naomi) Tague

_____

Bodo Bookhagen, Co-Chair

_____

Oliver Chadwick, Co-Chair

June 2019

Contributions of Glacial Melt, Snowmelt, and Groundwater to Streamflow During Low-Flow Periods: A Paired Catchment Approach in the Arun Watershed, Eastern Nepal

ACKNOWLEDGEMENTS

There is a Nepali proverb: *saas cha unjel aas* (as long as there's breath there's hope). This dissertation would not have been possible without an incredible cadre of people who helped to shape my ideas, push my intellectual boundaries, and provide constant guidance, field support, and joy over the course of my graduate school experience. Nor would it have been possible to conduct this research project as I envisioned it without generous funding from the National Science Foundation Graduate Research Fellowship Program (grant number DGE 1144085), the Robert and Patricia Switzer Foundation, the American Geophysical Union Horton Hydrology Research Grant, P.E.O. International, the UCSB Department of Geography, and UCSB Broom Center for Demography.

First and foremost, I would like to thank my dissertation committee – Oliver Chadwick (chair), Bodo Bookhagen, Naomi Tague – for their phenomenal insights to my research. You each helped cultivate my creativity and technical skills via your own unique scientific backgrounds and perspectives. Thank you for your patience as you mentored and advised me as I dug into hydrology, geochemistry, and remote-sensing. I've become a more well-rounded scientist because of the questions that you've posed and the conversations we've shared. Thank you for encouraging me to explore and push my personal boundaries.

Equally important, this project would not have been possible without the people of Nepal who supported the field components of this research. They truly helped give me breath as we trekked through the Himalaya and provided nuanced insights to their water resources, endless laughs, and genuine friendship. In particular, I would like to thank Dr. Dhananjay Regmi and the Himalayan Research Expedition team for their support during fieldwork. Special thanks to Shanker Rai, Labina Rai, Kedar Prasad Rai, Bhuvan Halide Rai, Guman Rai, Jabbar Rai, Chandra Rai, and Bikum Rai for their work as field assistants.

The data analysis for this dissertation required the support of a wide range of facilities and individuals, in particular: Dirk Sachse and Oliver Rach (GFZ), Amanda Strom (UCSB TEMPO Lab at the Materials Research Laboratory; NSF DMR-1121053), and Guangchao Li (Earth Measurements Lab at Stanford). Many thanks to William Turner for his support pulling CHIRPS rainfall data for my region and Taylor Smith for his assistance and insights to snowpack across the region. In addition, I am incredibly grateful for the technical training I received from Michel Baraer, Jeff McKenzie, and Bryan Mark at the HBCM Training Course at McGill University as well as the phenomenal lessons from IsoCamp at the University of Utah. A special thank you to Banu and Shambu Oja, who gifted me with many Nepali proverbs during Cornell University's Intensive Nepali Language Course that facilitated endless laughs on the trails of Nepal.

I've been lucky to be supported by phenomenal communities of individuals from the peaks of the Himalaya and the Andes to the beachside bliss that is Santa Barbara. I am incredibly appreciative of the endless support from and fun conversations with our UCSB Geography Department Staff. The Terrestrial Earth Surface Processes (TESP) Lab offered countless insights, technical critiques, and side-splitting laughs over the past 6 years. In particular, I would like to thank Jennifer King for her mentorship as a woman in science as well as access to her fridge for sample storage. In a similar vein, many thanks to the Tague Team Lab for their insights to ecohydrology and fun conversations.

To all my friends and family who offered joy, conversations, and a listening ear over the past six years: this acknowledgement is just a cumin seed in the elephant's mouth. My

whole heart and soul is grateful that I have you in my life. Whether preparing over 500 sample bottles, exploring the octopus' garden off of Mesa Lane, enjoying ocean swims followed by Americanos at Handlebar Coffee, pizza Fridays and doodle love, exploring the world from Rapa Nui to Burma to the Goyko Valley, sharing you ideas, creativity, and excitement, or simply offering a smile and a hug: thank you.

VITA OF KATALYN A. VOSS
May 2019

Dept. of Geography, University of California, Santa Barbara
Room 4809, Ellison Hall, Santa Barbara, CA 93106
katalynvoss@geog.ucsb.edu

EDUCATION

Exp. 2019 Ph.D., Department of Geography, University of California, Santa Barbara

2011 B.S. in Science, Technology, and International Affairs, School of Foreign Service, Georgetown University. *Honors Thesis*: Water Storage Trends in the Tigris-Euphrates Basin and Middle East from GRACE

PUBLICATIONS

Refereed Articles

Giordano, M., **K.A. Voss**, S. Stroming (2019), Supply, Use, and Implications of Groundwater in the Mideast/North Africa: A Review, *in review with Oxford University Press*

Kargel, J.S., G. J. Leonard, D. H. Shugar, U. K. Haritashya, A. Bevington, E. J. Fielding, K. Fujita, M. Geertsema, E. S. Miles, J. Steiner, E. Anderson, S. Bajracharya, G. W. Bawden, D. F. Breashears, A. Byers, B. Collins, M. R. Dhital, A. Donnellan, T. L. Evans, M. L. Geai, M. T. Glasscoe, D. Green, D. R. Gurung, R. Heijenk, A. Hilborn, K. Hudnut, C. Huyck, W. W. Immerzeel, Jiang Liming, R. Jibson, A. Kääb, N. R. Khanal, D. Kirschbaum, P. D. A. Kraaijenbrink, D. Lamsal, Liu Shiyin, Lv Mingyang, D. McKinney, N. K. Nahirnick, Nan Zhuotong, S. Ojha, J. Olsenholler, T. H. Painter, M. Pleasants, Pratima KC, QI Yuan, B. H. Raup, D. Regmi, D. R. Rounce, A. Sakai, Shangguan Donghui, J. M. Shea, A. B. Shrestha, A. Shukla, D. Stumm, M. van der Kooij, **K.A. Voss**, Wang Xin, B. Weihs, D. Wolfe, Wu Lizong, Yao Xiaojun, M. R. Yoder, and N. Young (2016), Geomorphic and geologic controls of geohazards induced by Nepal's 2015 Gorkha earthquake, *Science*, 351, aac8353, *doi*: 10.1126/science.aac8353. Emergency response team member: analyzed satellite imagery and identified landslide, avalanche, and other natural hazards across Nepal.

Richey, A. S., B. F. Thomas, M.-H. Lo, J. T. Reager, J. S. Famiglietti, **K.A. Voss,** S. Swenson, and M. Rodell (2015), Quantifying renewable groundwater stress with GRACE, *Water Resources Research,* 51, *doi:*10.1002/2015WR017349. Supported project design and conceptualization, including methodological approaches to quantify groundwater stress.

Voss, K.A., J. S. Famiglietti, M. Lo, C. de Linage, M. Rodell, and S. C. Swenson (2013), "Groundwater depletion in the Middle East from GRACE with implications for transboundary water management in the Tigris-Euphrates-Western Iran region", *Water Resources Research,* 49, *doi:*10.1002/wrcr.20078

Other Publications

Voss, K.A. (2013, February 27), Parallel Worlds: Water Management in Israel and California [Blog post]. Available online at: https://blog.nationalgeographic.org/

Voss, K.A. (2013, May 13), Political Currents of Water Management: Challenges in Israel, Palestine, and Jordan [Blog post]. Available online at: https://blog.nationalgeographic.org/

Gassert, F., T. Shiao, and M. Luck (2013) "Colorado River Basin Study." Working Paper. Washington, DC: World Resources Institute. Available online at: http://www.wri.org/

Reig, P., T. Shiao and F. Gassert (2013) "Aqueduct Water Risk Framework." Working Paper. Washington, DC: World Resources Institute. Available online at: http://www.wri.org/

Voss, K.A. (2012, Winter), High Mountain Glacial Watershed Program Quarterly Newsletter. Available online at: http://www.highmountains.org/

Voss, K.A. (2012, Fall), High Mountain Glacial Watershed Program Quarterly Newsletter. Available online at: http://www.highmountains.org/

Voss, K.A. (2012, Summer), High Mountain Glacial Watershed Program Quarterly Newsletter. Available online at: http://www.highmountains.org/

Voss, K.A. (2012, Spring), High Mountain Glacial Watershed Program Quarterly Newsletter. Available online at: http://www.highmountains.org/

Statement of Dr. J.S. Famiglietti for United States Congressional House Committee on Natural Resources, Subcommittee on Water and Power, *Oversight Field Hearing on Perspectives on California Water Supply: Challenges and Opportunities*, 25 January 2010, 111th Congress, 2nd session, Los Angeles, CA. Available online at: https://naturalresources.house.gov/

PRESENTATIONS

Voss, K., O.A. Chadwick, B. Bookhagen (2018), "Tracking the spatiotemporal patterns of the high mountain water cycle with isotopic and geochemical data in the Arun watershed, eastern Nepal", poster presentation C21F-1421, American Geophysical Union Fall Meeting, Washington, D.C.

Voss, K., O.A. Chadwick, B. Bookhagen, D. Sachse (2017), "Spatiotemporal Characteristics of Water Sources in the Eastern Himalayas: A case study of the Arun watershed, Nepal", oral presentation C41F-05, American Geophysical Union Fall Meeting, New Orleans, LA

Voss, K. (2016), "Citizen Science in Developing Countries: Why We Need to Move Away from Data Colonialism and Towards Local Engagement", oral presentation in the *Social Dimensions of Geosciences Pop-up Talks*, American Geophysical Union Fall Meeting, San Francisco, CA

Voss, K. (2015), "But What Do the Data Say? Lessons in Integrating Science and Policy to Inform International and Domestic Water Management Decisions", oral presentation ED13H-07, American Geophysical Union Fall Meeting, San Francisco, CA

Voss, K., D. Lopez-Carr, B. Bookhagen, C. Tague (2014), "Evaluating Coupled Human-Hydrologic Systems in High Altitude Regions: A Case Study of the Arun Watershed,

Eastern Nepal", poster presentation GC13E-0691, American Geophysical Union Fall Meeting, San Francisco, CA

Voss, K., J. Famiglietti, J.T. Reager, M. Lo, S. Ho, C. De Linage, M. Rodell (2012), "Asia's Changing Water Resources: Trends from GRACE and Implications for Water Management", poster presentation G33A-0939, American Geophysical Union Fall Meeting, San Francisco, CA

Voss, K., J. Famiglietti, M.Lo, and C. de Linage (2011), "Water Storage Changes in the Tigris-Euphrates River Basin and the Middle East from GRACE with Implications for Transboundary Water Management", poster presentation PA33A-1816, American Geophysical Union Fall Meeting, San Francisco, CA

FELLOWSHIPS AND AWARDS

Externally Funded

2017 Philanthropic Educational Organization (P.E.O.) Scholar Award	*$15,000*
2016 American Geophysical Union Horton Hydrology Research Grant	*$10,000*
2016 Robert and Patricia Switzer Foundation Fellowship	*$15,000*
2015 U.S. Dept. of Education Foreign Language and Area Studies Fellowship	*$5,000*
2014 National Science Foundation Graduate Research Fellowship (2014-2017)	*$100,000*
2014 National Aeronautics and Space Administration Earth System Science Fellowship (declined for NSF GRFP)	*$90,000*
2011 Princeton in Asia Fellow (The Mountain Institute, Nepal)	
2010 Honorable Mention, Morris K. Udall Undergraduate Scholarship	
2009 National Science Foundation Research Experiences for Undergraduates Summer Fellowship in Biogeochemistry and Climate at University of California, Irvine	*$3,600*

Internally Funded

2017 UCSB Faculty Outreach Grant, CASTLES: Creating an Augmented-reality Sandbox for Teaching and Learning about Earth Surfaces	*$15,000*
2016 UCSB Department of Geography Leal Ann Mertes Scholarship	*$1,000*
2015 UCSB Broom Center for Demography Research and Training Grant	*$1,800*
2014 UCSB Broom Center for Demography Research and Training Grant	*$2,000*
2013 UCSB Graduate Opportunity Fellowship	*$22,000*

Trainings

2018 NSF/Mitchell Hamline Law School Expert Witness Training Academy participant

2014 American Meteorological Society Summer Policy Colloquium participant

2014 NSF/William Mitchell Law School Expert Witness Training Academy participant

PROFESSIONAL EXPERIENCE

2011 – 2013 Program Officer | The Mountain Institute, Nepal and Peru

- Developed local adaptation plans of action to reduce risk in the floodplain of glacial lakes
- Assessed the stability of glacial lakes in Nepal and Peru using ground-penetrating radar and bathymetric surveys of glacial lakes
- Determined engineering mitigation and community adaptation options for water management related to glacial lake outburst floods
- Led policy briefs, formal meetings, and training workshops with U.S. Agency for International Development (USAID), U.N. Development Program, and national policy-makers in Nepal, Peru and Washington, D.C.
- Developed and maintained a website, quarterly newsletter, and webinars for practitioners, researchers, and communities in alpine regions

2009 – 2013 Water Policy Fellow | UC Center for Hydrologic Modeling, UC Irvine

- Evaluated water security of groundwater depletion in Beijing, northwestern India, and the Tigris-Euphrates River Basin by integrating water storage data from the GRACE satellite mission and social, political, economic data
- Organized and led "water for peace" diplomatic trips to Israel, Jordan, Palestine, and China with the U.S. Department of State and USAID
- Wrote science pieces for National Geographic's *Water Currents* blog (see Publications)
- Drafted Dr. James Famiglietti's Congressional testimony on California's water supply for the House of Representatives Subcommittee on Water and Power (see Publications)
- Represented UCCHM at Stockholm World Water Week (Stockholm, Sweden – 2013), the Global Water Forum (Marseilles, France – 2013), and the Global Water Summit (Berlin, Germany – 2010)

2010 – 2011 Aqueduct and New Ventures Intern | World Resources Institute, D.C.

- Developed Aqueduct water index for the Colorado River basin (See Publications)
- Improved the metrics for the Aqueduct tool to integrate hydrologic, social, economic, legal, and political water risk indicators (See Publications)
- Validated prior Aqueduct case studies of the Yellow River Basin in China, Mekong River Basin in southeast Asia, and the Orange-Sengue River Basin in southern Africa
- Communicated implications of water scarcity for business and industry via Bloomberg, Circle of Blue, and direct meetings with the Aqueduct Water Alliance
- Planned the Global Investor Forum for March 2011 to connect entrepreneurs with investors
- Developed environmental and social metrics to assess the impact of WRI-funded New Ventures social entrepreneurs

2009 Project Lead, Na Nong Bong Community Organizer | ENGAGE, Thailand

- Developed a multimedia presentation about the impacts of mining on soil and water

2008 Intern | Surfrider Foundation, San Clemente, California

- Researched and developed programs to for the National Membership Drive

TEACHING EXPERIENCE

2019	Teaching Assistant, GEOG 136: Field Studies in Water, Energy, and Ecosystems (UCSB)
2018	Teaching Assistant, GEOG 137/237: Quantitative Geomorphology (UCSB)
2018	Teaching Assistant, GEOG 115B: Remote Sensing (UCSB)
2017-2018	Teaching Assistant, GEOG/ENVS 114A: Soil Science (UCSB)

MEDIA COVERAGE

BBC: Nepal Quakes Could Have Been Far Worse

KCRW/NPR: Desalination to Fight Drought?

National Geographic: Parallel Worlds- Water Management in Israel and California

Nature Middle East: Massive losses of freshwater in Middle East revealed

The Economist: The Tigris and Euphrates, Less fertile crescent

ACADEMIC SERVICE AND OUTREACH

Ongoing	Reviewer, *Water Policy, Water Resources Research, Hydrologic Sciences Journal, Elementa*
2017	Organizer, *UCSB Let's Talk About Water*, a regional public event that connected UCSB researchers, the general public, and local community organizations to discuss water in the west
2016-2017	Student Representative, UCSB Dept. of Geography Geomorphology Faculty Hire
2015-2016	Internal Review Board*, Journal of Environment and Development*
2014	Speaker, Geography Awareness Week at The Anacapa School, Santa Barbara, CA
2010-2011	Peer Advisor*,* International Development Minor (Georgetown University)

PROFESSIONAL SKILLS

Spanish (advanced speaking, reading, and writing)

Nepali (intermediate speaking; beginning reading and writing)

ABSTRACT

Contributions of Glacial Melt, Snowmelt, and Groundwater to Streamflow During Low-Flow Periods: A Paired Catchment Approach in the Arun Watershed, Eastern Nepal

by

Katalyn A. Voss

My dissertation research investigates the spatial and temporal variability of water sources in the Arun watershed, a river basin in the eastern Himalaya, using a combination of geochemical and isotopic tools to assess the hydrologic and climatic processes that control water resources in the region. Broadly, I aim to answer the questions: (1) what are the spatiotemporal patterns of the Indian Summer Monson versus Winter Westerly Disturbance storm systems as they contribute to water supply, and (2) how do contributions of snowmelt, glacial melt, groundwater, and rain vary from local-to-regional scales in the eastern Himalaya? I address these questions by exploiting the natural variability in the geochemical and isotopic composition of meteoric water, which is controlled by distinct hydrologic and climatic processes. I explore these data across spatial scales that include the Tibetan Plateau headwaters of the Arun River, a high-elevation glacierized tributary, a low-elevation tributary, and the downstream outlet of the Arun River.

In Chapter Two, I find that deuterium excess emerges as valuable tracer to partition regional precipitation systems while high sulfate levels are correlated to glacial melt source waters. I use these two tracers to qualitatively describe broad patterns in regional water

supply for the Arun watershed and its tributaries, and highlight differences that arise from the varying hydroclimatic characteristics throughout the basin. In Chapter Three, I explore the variability in $\delta^{18}O$ and δD stable isotope values along a 6000-m elevation gradient and identify non-linear $\delta^{18}O$ and δD lapse rates in river water controlled by regional precipitation patterns and local mixing with glacial melt. In Chapter Four, I use a combination of dissolved ion concentrations and $\delta^{18}O$ and δD stable isotope values in a mixing model approach to partition streamflow during low-flow periods before and after the monsoon, and I identify the tracers that offer the highest utility to identify water sources in these Himalayan catchments.

The dissertation provides evidence that seasonality and elevation act as strong controls on Himalayan water supply with low-elevation catchments dependent on monsoon rainfall and high-elevation catchments relying more heavily on glacial melt. Contributions of snowmelt to river discharge are seasonally discrete in the pre-monsoon season and spatially constrained to high-altitude regions or headwaters. I elucidate the potential applications of isotopic and geochemical tracers to differentiate snowmelt from glacial melt and to identify seasonal precipitation cycles. This work advances an emerging body of literature focused on Himalayan water resources and provides a practical framework to assess water budgets across local and regional scales. Critically, the dissertation provides insights and direction for future research to accurately quantify water resources in the Himalaya and, ideally, inform water management decisions.

TABLE OF CONTENTS

Chapter 1. Introduction

Water resources are the crux of our global well-being: from sustaining human populations as drinking water to nourishing agriculture and flowing through turbines to generate electricity. Demand for water is increasing as populations grow, industry thrives, and societies transition to a modernized, albeit water-intensive, society. This escalated demand is juxtaposed by increased variability in water supply. With climate change, the global water cycle is accelerating, and the result is a redistribution of water resources both spatially and temporally: wet regions are becoming wetter while dry regions are becoming drier, droughts and floods are increasing, and formerly predictable precipitation cycles are now erratic (Jimenez Cisneros et al., 2014). With diverging patterns in water supply and demand, many regions are experiencing increased vulnerability to water stress or water-related hazards (Vörösmarty et al., 2000).

In high mountain regions, these trends are magnified because the dramatic elevation gradients of mountain regions amplify small perturbations in climate and anthropogenic activities. Across the globe, high mountain regions are experiencing rapid increases in temperature that alter several components of the mountain hydrologic system: glacier retreat is accelerating and some glaciers are disappearing entirely; snowpack is diminishing and the timing of melt events is increasingly variable; and, high-intensity rainfall events are becoming more frequent, resulting in increased hazards from floods and landslides (Beniston, 2003). At the same time, the populations living in high mountain regions or dependent on mountain resources are attempting to minimize risk from natural hazards, maintain food security, and achieve energy independence. High mountain regions and the populations that live in them are on the frontlines of climate change. Indeed, climate-driven shifts in water

resources are happening *now,* and the nations, cities, and communities in these regions are rapidly attempting to adapt, manage, and thrive in these dynamic environments.

The Himalaya, the water towers of Asia, are an archetypal mountain landscape in flux. Critically, rivers originating in the Himalaya and Tibetan Plateau eventually drain through the Indian subcontinent and supply water for agriculture, domestic use, and energy generation (Immerzeel et al., 2010; National Research Council, 2012; Viviroli et al., 2007). Yet, the Himalayan ecosystem – both its physical land and water resources as well as its political and socioeconomic structures – remain enigmatic despite their geopolitical significance (Wirsing, 2013; Wirsing et al., 2012). Our weak understanding of the Himalaya is partially due to the rapid hydrologic changes occurring the region, but also because the rugged region is remote and inaccessible. Consequently, the vast majority of rivers in the Himalaya are ungauged and lack traditional meteorological or hydrologic monitoring infrastructure to accurately quantify water resources. Instead, a combination of local field-based studies and regional remote-sensing studies shape our foundational understanding of the hydroclimatic dynamics of watersheds throughout the region.

Broadly, water supply in the Himalaya is derived from rainfall, snowmelt, glacial melt, and groundwater, and the relative importance of these water sources varies across spatial scales from small, localized watersheds to the expansive river basins that span the continent. Geographically, the Himalaya act as a significant physical barrier that drives hydroclimatic patterns across the region. The Himalaya are influenced by two moisture regimes: the Indian Summer Monsoon (ISM) and the Winter Westerly Disturbances (WWD). The ISM brings rainfall to the region from May to October while the WWD deposit snowpack from November to April; however, the spatial distribution of these precipitation

sources is divergent with the influence of the ISM decreasing from east-to-west and the WWD increasing (Bookhagen & Burbank, 2010). Additionally, the Himalaya block the two storm systems from moving north and result in a rainshadow across the Tibetan Plateau. Glaciers are a component of river discharge; however, their relative contributions vary spatially and temporally. High-elevation catchments and the headwaters of glacierized rivers have the greatest contributions of glacial melt to streamflow, and that contribution decreases as rivers flow downstream and into low-elevation regions with greater inputs from rain, snow, and groundwater (Armstrong et al., 2018; Bolch et al., 2012; Lutz et al., 2014). That said, the melt dynamics of glaciers and snow are still poorly understood and dependent upon a variety of factors including debris-cover, redistribution of snow from avalanches or landslides, regional climate patterns, and variability in the local energy balance (Bolch et al., 2012; Rounce et al., 2017; Smith & Bookhagen, 2018). Our knowledge of groundwater in Himalayan catchments is also limited, but groundwater is suggested to be a significant source of water depending on catchment elevation, season, and local soil or bedrock characteristics (Andermann et al., 2012).

Climate change adds another layer of complexity to the already dynamic baseline of Himalayan water resources. Rainfall from the ISM is increasingly variable: the frequency and magnitude of high intensity storms is increasing but the gaps between these storms are lengthening (Malik et al., 2016). Snowpack is decreasing throughout the central and eastern Himalaya with shorter and earlier melt periods (Smith & Bookhagen, 2018). Glacier retreat is accelerating (with the exception of the Karakoram region), and proglacial lakes now dot the Himalayan landscape (Bolch et al., 2012). Groundwater recharge and flow patterns evolve with land use and land cover change, and predicted to be highly variable given

patterns of deforestation, cropland conversion, and terracing. Combined with our baseline framework of water resources in the Himalaya, we can anticipate potential tension points that will arise in water supply. First, the fluctuations between high and low flow periods may increase in magnitude and diverge temporally. This could result in increased water scarcity, and simultaneously, increased frequency of floods. Second, the already convoluted mix of sources contributing to Himalayan rivers will only become more variable and, consequently, river discharge will likely become more unpredictable.

The intricate Himalayan hydroscape presents a challenge for water management and the potential implications for regional security situate Himalayan rivers as a geopolitical hotspot (National Research Council, 2012). Innovative research that utilizes alternative methodologies to quantify Himalayan water resources is indispensable and provides critical assessments of water budgets for the region despite the isolated terrain and the lack of traditional water monitoring infrastructure. This dissertation seeks to contribute to an emerging body of research to provide new insights to the spatiotemporal variability of water supply in Himalayan watersheds. The dissertation seeks to answer the broad questions: What are the main sources of water contributing to river discharge? How do the contributions of source waters vary across space and time? The methodology used in the dissertation bypasses the lack of traditional gauge and observational data to explore the potential applications of geochemical and isotopic tracers to track distinct source waters in the eastern Himalaya across spatial and temporal scales. Specifically, the dissertation aims to elucidate several gaps in our current understanding of Himalayan rivers, including: (1) the relative influence and timing of ISM versus WWD precipitation; (2) differentiation between snow

and glacial meltwaters as they contribute to discharge; and, (3) variation in source waters across spatial scales from tributary headwaters to a larger transboundary river basin.

To investigate these questions, we target a single river basin, the Arun watershed in eastern Nepal, as a case study. The Arun watershed is an ideal study site for several reasons. First, it's lower reaches receive precipitation from both WWD and the ISM moisture sources while its headwaters are located in the Tibetan Plateau, which will allow us to disentangle spatiotemporal variation in precipitation contributions from the two storm systems. Second, it contains tributaries with a variety of physical features that can be compared to explore and extrapolate the unique geochemical and isotopic signatures of glacial melt, snowmelt, groundwater and rainfall. Third, it is physically accessible with extensive trail systems and villages, which allowed for data collection across large portions of the watershed and collaboration with local community members as citizen scientists to collect a spatially and temporally dense dataset.

The first chapter of this dissertation explores broad patterns in the geochemical and isotopic characteristics of water sources in the Himalaya. Specific dissolved ions and isotope values are correlated to distinct source waters, such as glacial melt and snowmelt, and used to qualitatively describe seasonal transitions of source waters in the Arun River and two of its tributaries. Sulfate emerges as a useful tracer for glacial melt while variation in deuterium excess values are linked to ISM versus WWD sourced precipitation (rainfall versus snowmelt, respectively). Across the Arun River and its tributaries, we identify snowmelt as a key contributor to streamflow in the pre- and early-monsoon season followed by a flushing of the river systems with ISM-sourced rainfall through the summer. Glacial melt is a key

source for the Tibetan Plateau headwaters and glacierized tributaries of the Arun, particularly in the mid- to post-monsoon season as temperatures increase.

Probing into Chapter One's results, Chapter Two leverages a 6000-m elevation gradient in the Arun watershed to examine the separate controls of elevation and moisture source on hydrogen and oxygen isotope values. We find non-linear trends in $\delta^{18}O$ and δD elevation lapse rates with strengthening lapse rates in meteoric water samples collected above 4000-m compared to low-elevation samples (<3000-m). We explore the seasonal variation in the isotopic composition of surface and groundwater that is driven by distinct transitions in moisture regimes from the continental-sourced WWD versus oceanic-sourced ISM precipitation. Our findings highlight the opportunity to utilize isotopic tracers to describe regional climate patterns and identify potential complications for $\delta^{18}O$ and δD values in paleoclimate and paleoelevation interpretations.

Chapter Three integrates aspects of the first and second chapters in a spatially and temporally explicit analysis of glacial melt, snowmelt, and groundwater contributions to river discharge in two tributaries of the Arun watershed during low-flow periods before and after the monsoon season. We find greater glacial melt contributions to streamflow than previously described in small- or mid-sized catchments in the eastern Himalaya as well as a seasonal reliance on snowmelt in the headwaters of low-elevation catchments. These results are compared to other studies with varying influence from the ISM, WWD, and glaciers as well as regional remote-sensing analysis to discuss role of spatial scale in our interpretation of Himalayan river water budgets.

Collectively, the results described in this dissertation advance our understanding of the hydrologic and climatic processes controlling water resources in the eastern Himalaya.

Notably, the analysis spans spatial and temporal scales to capture patterns in water resources that are controlled by local physical landscape conditions as well as regional climate dynamics. The results highlight potential tools to be used to further elucidate source water contributions in Himalayan rivers and, combined with other studies from the region, enhance our understanding of Himalayan water budgets.[1]

[1] The dissertation chapters are prepared as stand-alone manuscripts with the intention of future publication; therefore, there are sections of background, methods, and data in each chapter that may be repeated.

Chapter II. Exploring the geochemical and isotopic patterns of meteoric waters in the Arun watershed, eastern Nepal

1 Introduction

Spatiotemporal patterns in the geochemical and isotopic composition of meteoric waters are a useful tool to explore local-to-regional scale hydroclimatic processes. An extensive body of research describes the physical controls on $\delta^{18}O$ and δD stable isotope values, many of which are linked to temperature and, consequently, correspond to distinct climatic processes including orographic rainout, storm path or distance, and local evaporation or sublimation (Dansgaard, 1964; Kendall et al., 2014). The geochemical composition of meteoric waters reflects the physical characteristics of a landscape and the processes that control variability in the dissolved solute concentrations of surface water, which include chemical or physical weathering, soil-water interactions, and atmospheric pollution (Burt & Pinay, 2005; Faure, 1998). Combined, the isotopic and geochemical composition of meteoric waters represent the initial climatic conditions controlling water supply as well as the subsequent flowpaths of water through a watershed. With this in mind, river water captures the integrated geochemical and isotopic signal of a drainage area and can be used to infer the physical landscape and climate controls acting on a watershed.

High mountain regions offer a complex setting to explore variability in the geochemical and isotopic composition of river water that arises as a result of extreme elevation gradients. Specifically, high mountain catchments are characterized by orographic rainout and rapid ecological transitions. In the Himalaya, these characteristics are magnified across high-altitude glacierized headwaters, mid-altitude forested zones with seasonal

snowpack, and low-elevation areas that are often marked with agriculture terracing (Price et al., 2013). In this study, we exploit the elevation and ecosystem gradients of the Arun watershed, a Himalayan catchment in eastern Nepal, to explore the hydroclimatic factors that influence the spatiotemporal variability of the geochemical and isotopic composition of river water throughout the basin. We examine a unique dataset that spans a hydrologic year from April to November 2016 to capture seasonal water cycles and include three drainages with distinct physical attributes to investigate the role of both local and regional processes in the basin.

2 Hydroclimatic Contexts of the Arun and Anticipated Isotopic and Geochemical Patterns

The Arun watershed is a 33,000-km^2 basin that contains ~15% glacierized area and is marked by an extreme elevation gradient that spans from 200 m to 8480 m in altitude. Notably, the majority of the basin (~85%) is located in the Tibetan Plateau before the Arun River drains into Nepal and, eventually, combines with the Koshi River as a tributary to the Ganges. Since the Arun River spans a south-north transect from the Himalayan foothills to the Tibetan Plateau, it is marked by a distinct climate transition that includes a strong influence from the Indian Summer Monsoon (ISM) from May through September along the Himalayan front and a rainshadow on the Tibetan side of the basin (Gonga-Saholiariliva et al., 2016). In addition to the ISM, the Arun watershed also receives precipitation inputs from Winter Westerly Disturbances from November through March (Cannon et al., 2015). Overall, the Arun is estimated to receive ~25% of annual streamflow from snowmelt sourced from WWD and ~70% from ISM-sourced rainfall (Bookhagen & Burbank, 2010). Glaciers

in the Arun are retreating and their meltwaters also contribute to river discharge, particularly in the high-altitude regions of the watershed (Bolch et al., 2012; Meese et al., 2018). Ecologically, the Arun encompasses lowland regions along the Himalayan foothills with extensive forest cover and agriculture terracing as well as high-elevation alpine scrubland and tundra in the Tibetan Plateau (Carpenter & Zomer, 1996). Geologically, the Arun watershed drains from the Tethyan Tibetan Zone (carbonates and siliclastic sedimentary rocks) in the Tibetan Plateau region and the Greater and Lesser Himalayan Sequences (quartzite, gneiss, schist and phyllite) in the lower portion of the watershed.

With this general framework, we identified three distinct hydroclimatic settings in the Arun watershed that we expect will have discrete geochemical and isotopic signatures: (1) Tibetan headwaters, (2) high-altitude glacierized tributaries, and (3) low-altitude forested and terraced tributaries. Each of these regions is marked by seasonally variable influences from the ISM and WWD precipitation, glacier melt, and snowmelt (Immerzeel et al., 2013; Meese et al., 2018; Mölg et al., 2014; Smith & Bookhagen, 2018; Voss et al., 2018). With this baseline, we can broadly describe the seasonal sources of water supply throughout the Arun watershed. The Tibetan headwaters region is likely sourced predominantly from glacier and snowmelt throughout the year since it is located in the rainshadow of the Himalaya and receives little ISM rainfall. High-elevation glacierized tributaries are known to have a strong seasonal flux in water supply with ISM-sourced rainfall contributing to discharge from May to September and snow or glacial melt contributing significantly in the shoulder periods before and after the monsoon (Meese et al., 2016; Taylor Smith & Bookhagen, 2018). The discharge from low-elevation tributaries of the Arun, which receive limited WWD-sourced snowpack and do not contain glaciers, can be assumed to be predominantly sourced from

ISM precipitation as well as shallow and deep groundwater recharged from rainfall or snowmelt.

Each hydroclimatic setting of the Arun River should reflect a distinct geochemical and isotopic composition in its respective meteoric waters. Previous studies confirm that water collected from high-elevation sites in the Himalaya have depleted $\delta^{18}O$ and δD values relative to low-elevation sites as a result of orographic rise and decreasing temperatures at high altitudes (Hren et al., 2009). Deuterium excess is known to correspond to Himalayan moisture sources and differences emerge as a consequence of storm path and distance. Average deuterium excess values for WWD-sourced water higher (>15 $^{0}/_{00}$) because these storms travel a longer continental path before rainout as compared to ISM-sourced water (d-excess ~8-12 $^{0}/_{00}$), which travel a short distance across the Indian subcontinent (Gat & Carmi, 1970; Hren et al., 2009; van der Veen et al., 2018). Geochemically, glacier melt is marked with elevated concentrations of dissolved ions, particularly those associated with glacial silt: Ca^{2+}, Mg^{2+}, K^{+}, SO_4^{2-} (Tartari et al., 1998; Wilson et al., 2015). Additionally, glaciated landscapes have high rates of sulfide oxidation and carbonate weathering, which should be reflected in elevated values of SO_4^{2-}:Na^{+} and Ca^{2+}:Na^{+} ion ratios, respectively (Anderson, 2007; Torres et al., 2017). Groundwater, depending on its residence time and interaction with soil or bedrock, will have higher dissolved ion concentrations relative to precipitation from rain or snow, which is known to have low solute concentrations in this region of the Himalaya (Balestrini et al., 2016). By capturing the variation in the isotopic and geochemical composition of meteoric water across the Arun River, we will attempt to track regional climate patterns (i.e. the relative influence and timing of the ISM versus WWD) as well as local water sources (i.e. glacial melt) in each distinct hydroclimatic setting.

3 Study Sites and Data

We collected river water samples from each hydroclimatic zone across a hydrologic year to investigate the predicted spatiotemporal patterns described above. The sampling locations include: (1) an upstream Arun River site that drains from the Tibetan Plateau, (2) a downstream Arun River site located in the Himalaya foothills, (3) the Barun Khola, a glacierized tributary to the Arun River, and (4) the Sabha Khola, a low-elevation catchment with no glaciers but some seasonal snowpack and extensive agriculture terracing (Figure 1). The upstream Arun River site is located above the confluence of the Barun Khola and the Arun River, drains the ~28,900-km^2 headwaters from the Tibetan Plateau, and has a mean catchment elevation of 4900 meters above sea level (masl). The downstream Arun River site is located in the Himalayan foothills above the confluence of the Sabha Khola and Arun River with a drainage area of ~31,200-km^2 and a mean catchment elevation of 4780 masl. The Barun Khola tributary is a 468-km^2 watershed with a mean catchment elevation of 4758 masl and ~30% glaciated area. The Sabha Khola tributary is a 549-km^2 nonglacierized watershed with a mean elevation of 1503 masl and extensive agriculture terracing.

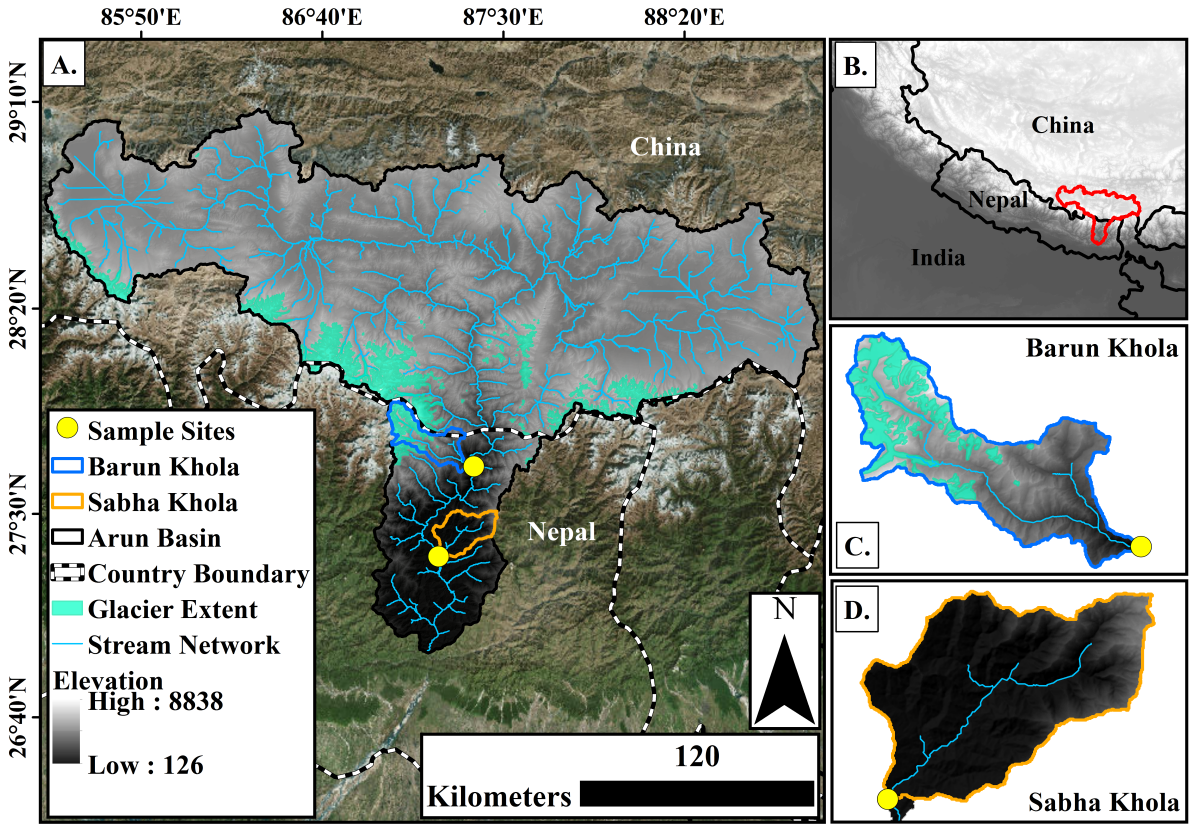

Figure 1. (A) Elevation and glacier extent of study areas in the Arun watershed. (B) Arun watershed (outlined in red) in the eastern Himalaya. (C) Barun Khola. (D) Sabha Khola. Glacier extent is from the Randolf Glacier Inventory derived from Global Land Ice Measurements from Space (GLIMS) (RGI Consortium, 2017).

Local Nepali schoolteachers were trained to collect samples at the confluence of the Barun and Sabha Kholas with the Arun River at Barun Bazaar and Tumlingtar, respectively. Samples were collected every 4 days from late April/early May through October 2016 (N = 41 for the Sabha Khola and Lower Arun sites; N = 45 for Barun Khola and Upper Arun sites). Two sets of water samples were collected and each sample was filtered through 0.45-µm glass filters into 30-mL polyethylene Nalgene bottles that were rinsed three times with filtered water. Bottles were filled completely to produce a positive meniscus, sealed tightly,

and wrapped with tape to prevent the formation of air bubbles and possible evaporation before laboratory analysis. Bottles were stored in a dark place until the completion of the field season and then stored in a refrigerator at 4°C at UC Santa Barbara.

Samples were analyzed for $\delta^{18}O$ and δD at the German Research Center for Geosciences (GFZ) Organic Surface Geochemistry Lab with a Picarro L-2140i Laser Spectrometer. Precision for $\delta^{18}O$ and δD measurements was $\pm 0.03\ ^{0}/_{00}$ and $\pm 0.3\ ^{0}/_{00}$, respectively. Analytical uncertainties for the oxygen and hydrogen stable isotope measurements are reported as standard deviation of triplicate measurements in the data repository. Deuterium excess was calculated for each sample as $d = \delta D - 8*\delta^{18}O$ (Dansgaard, 1964). Samples were also analyzed for Ca^{2+}, Mg^{2+}, Na^{+}, K^{+}, Si, Cl^{-}, and SO_4^{2-}. Major cations (Ca^{2+}, Mg^{2+}, Na^{+}, K^{+}, Si) were analyzed at the University of California Santa Barbara's TEMPO research facilities at the Materials Research Lab with a Thermo iCAP 6300 inductively coupled plasma spectrometer. The detection limit for each solute was <0.1 mg L^{-1} with precision for Ca^{2+}, K^{+}, Mg^{2+}, Na^{+}, and Si measurements of +/- 0.03 mg L^{-1}, 0.10 mg L^{-1}, 0.01 mg L^{-1}, 0.09 mg L^{-1}, and 0.03 mg L^{-1}, respectively. Major anions (Cl^{-}, SO_4^{2-}) were measured at Stanford University's Environmental Measurements Lab with a Dionex DX-500 Ion Chromatography (IC) System. The detection limit was <0.5 mg L^{-1} with precision for Cl^{-}, SO_4^{2-} measurements of +/- 0.11 mg L^{-1} and 0.33 mg L^{-1}, respectively. All ion data are reported in milligrams per liter (mg L^{-1}) and δD and $\delta^{18}O$ isotope data are reported in delta notation as parts per thousand as related to their deviation from Vienna Mean Standard Ocean Water (VSMOW). Data for individual samples are listed in Appendix A. Daily rainfall data were averaged over the Arun River basin with precipitation data from the U.S. Geological Survey and UC Santa Barbara Climate Hazards Group Infrared

Precipitation with Stations (CHIRPS) dataset (Funk et al., 2015) to supplement the interpretation of the isotope and geochemical data.

4 Results

4.1 Comparison of temporal patterns in δD and d-excess in the Arun watershed

The δD values of the sample sites in the Arun exhibit similar temporal trends that correspond to the onset and intensity of monsoon rainfall (Figure 2). In all of the sites, δD values at the onset of the monsoon (May to mid-June) are enriched relative to the remainder of the timeseries. Once ISM rainfall intensifies in mid-June, all sites undergo a rapid depletion in δD values that continues through mid-July. From mid-July to the end of the timeseries in October, δD values remain relatively stable in the Lower Arun, Barun Khola, and Sabha Khola while the δD values in the Upper Arun become enriched. The Sabha Khola consistently has the most enriched δD values relative to the other sites while the δD values from the Upper Arun sample site are the most depleted with the exception of two spikes in mid-August and early October. D-excess values follow a similar pattern as the δD data with increasing values from May through mid-June followed by a rapid decline through mid-July and relatively stable values through October (Figure 3). The Barun Khola has the highest d-excess values throughout the timeseries while the Upper Arun has the lowest.

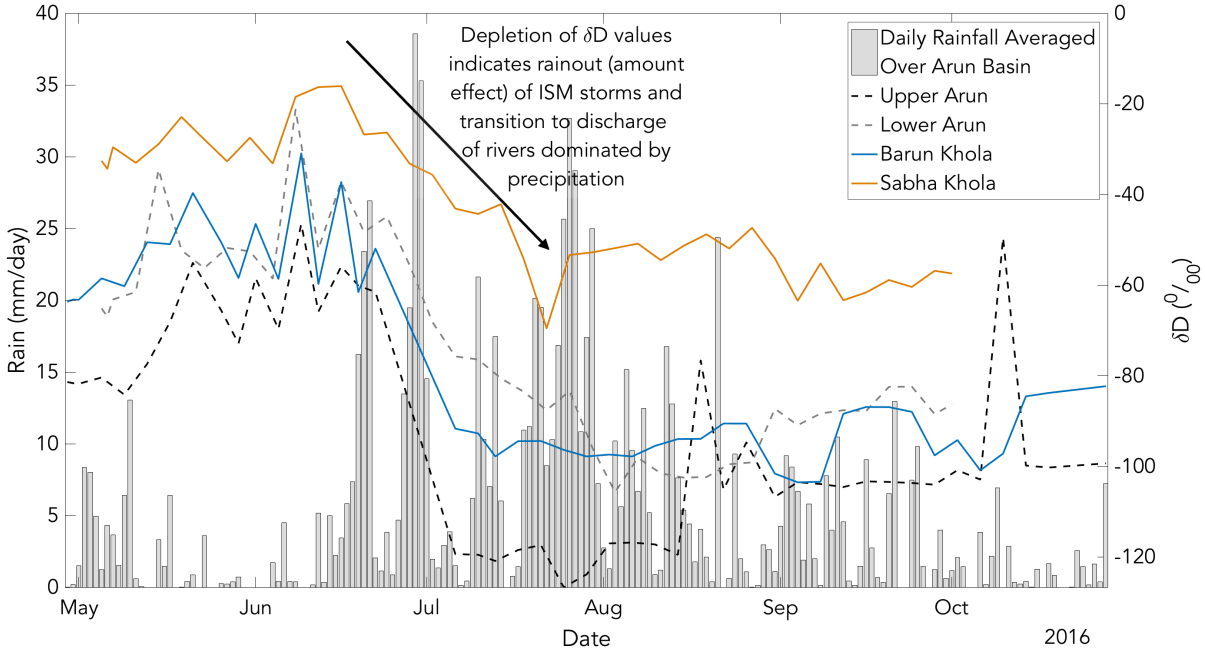

Figure 2. Comparison of δD values from the Upper Arun, Lower Arun, Barun Khola, and Sabha Khola sample sites from May through October 2016. Daily average rainfall from CHIRPS is included to elucidate the relationship between δD values and the ISM (Funk et al., 2015).

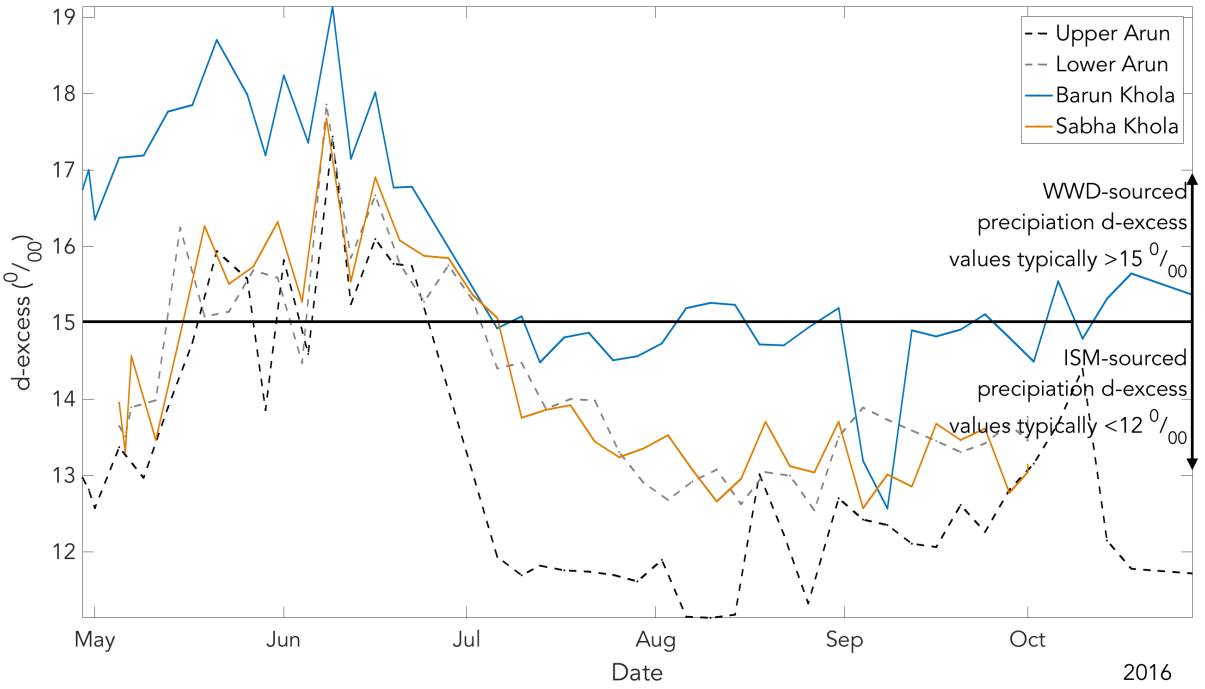

Figure 3. Comparison of d-excess values from the Upper Arun, Lower Arun, Barun Khola, and Sabha Khola sample sites from May through October 2016. A line at 15 $^{0}/_{00}$ indicates the known transition between WWD- and ISM-sourced precipitation (Gat & Carmi, 1970).

4.2 Comparison of temporal patterns of dissolved ion concentrations in the Arun watershed

At the onset of the monsoon (May to June) total dissolved cations are highest in the Sabha Khola and lowest in the Barun Khola with the Arun River sites' concentrations falling between the two tributary values (Figure 4). This pattern changes during the height of the monsoon with the highest dissolved cations found in the Arun River sites from July through the end of the timeseries in October. The Barun Khola dissolved ion concentrations appear to increase from June through September and have a notable spike in early September. The Sabha Khola values decline from May through mid-June and then remain relatively stable through October. The Lower Arun dissolved cation concentrations are consistently lower than the Upper Arun site and exhibit similar temporal patterns in its spikes and dips though these patterns are delayed and dampened relative to the Upper Arun.

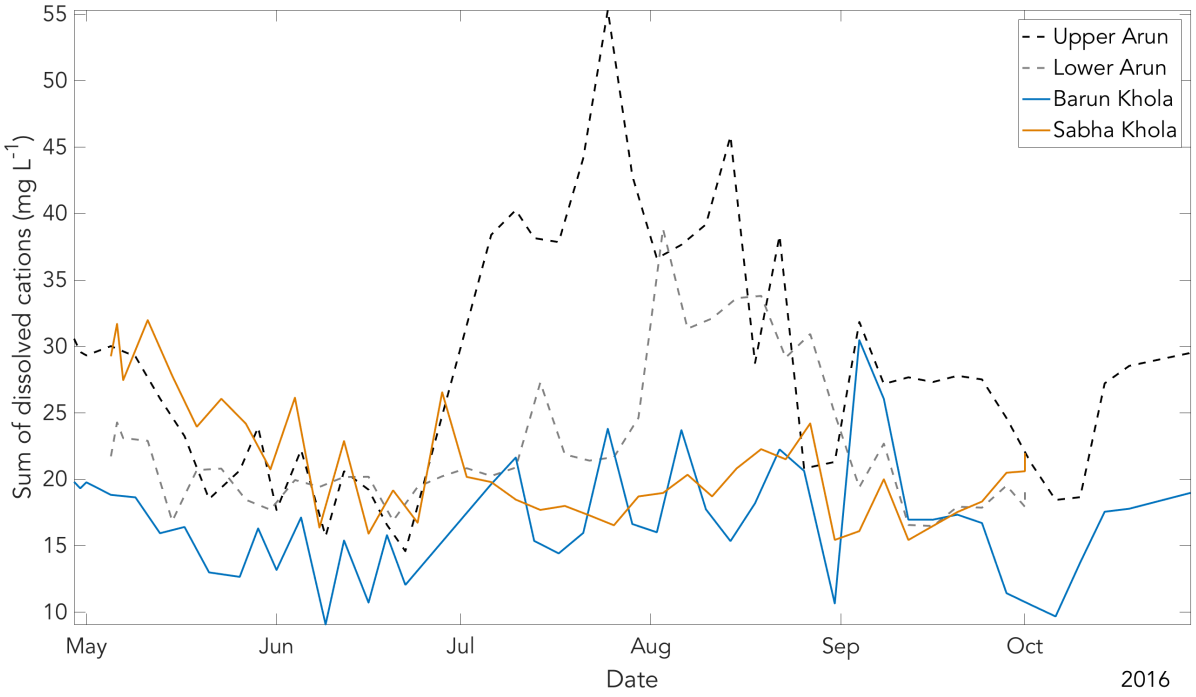

Figure 4. Comparison of total dissolved cation concentrations at each site for the duration of the timeseries sampling from May through November.

Timeseries of ion ratios between SO_4^{2-}:Na^+ and Ca^{2+}:Na^+ reveal distinct spatiotemporal patterns across the basins. SO_4^{2-}:Na^+ ratios are highest in the Barun Khola at the onset of the monsoon (May-June) at which point the Arun River sites have the highest ratios for the duration of the timeseries (Figure 5). Similar to the total dissolved cation results, the Upper Arun is consistently higher than the Lower Arun, which appears to have a dampened and lagged signal, with the exception of a spike in late August. The two Arun River sites appear to increase from May through late August and then decline and stabilize through October. SO_4^{2-}:Na^+ ratios are consistently higher in the Barun Khola relative to the Sabha Khola. The Sabha Khola SO_4^{2-}:Na^+ values slightly decline throughout the timeseries,

whereas the Barun Khola declines from May to mid-August and then increases through October.

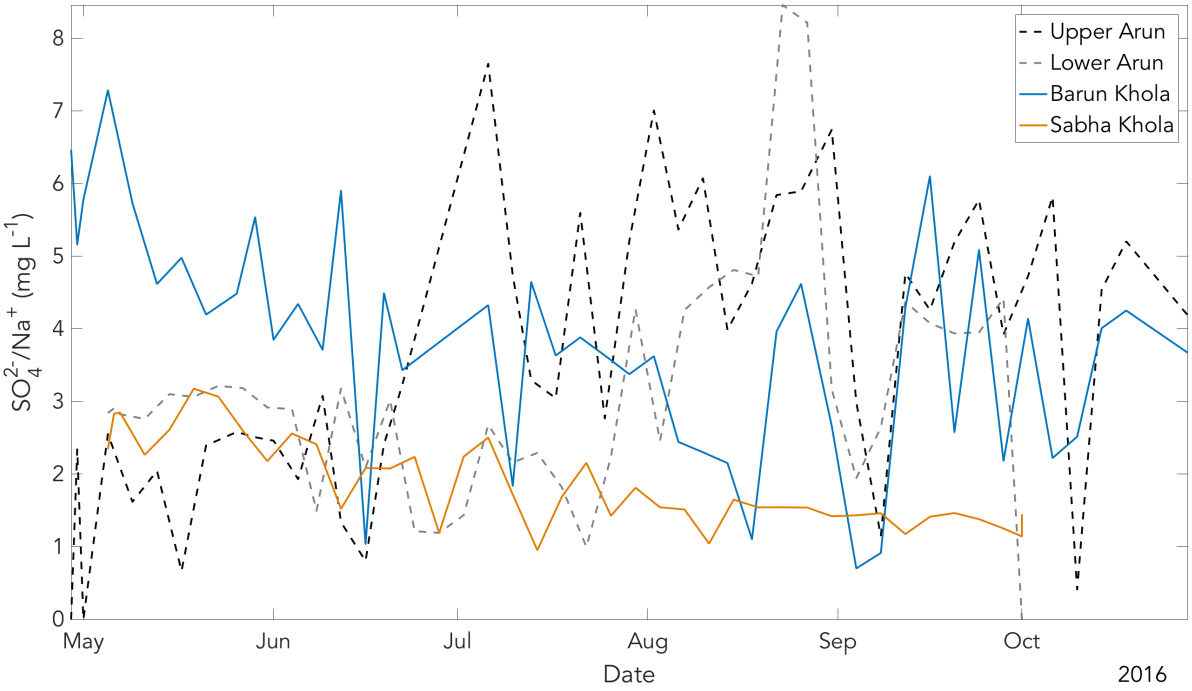

Figure 5. Comparison of SO_4^{2-}:Na^+ concentrations at each site for the duration of the timeseries sampling from May through November.

The temporal pattern of Ca^{2+}:Na^+ in the sites is more complex and has greater variability compared to the SO_4^{2-}:Na^+ timeseries. In the Sabha Khola, Ca^{2+}:Na^+ values in May are relatively high and decrease until August, albeit with large variability in magnitude, followed by a stabilization through October. The Barun Khola Ca^{2+}:Na^+ ratios decline from May to July then increase again in August through the duration of the timeseries. The Barun Khola Ca^{2+}:Na^+ ratios exhibit the greatest variability across the timeseries. Ca^{2+}:Na^+ ratios in the Upper and Lower Arun sites generally increase through the timeseries and remain relatively similar with the exception of May, when the Lower Arun values are higher than the

Upper Arun. The Barun Khola and two Arun River sites both have a dramatic peak in their Ca^{2+}:Na^{+} ratios in late August.

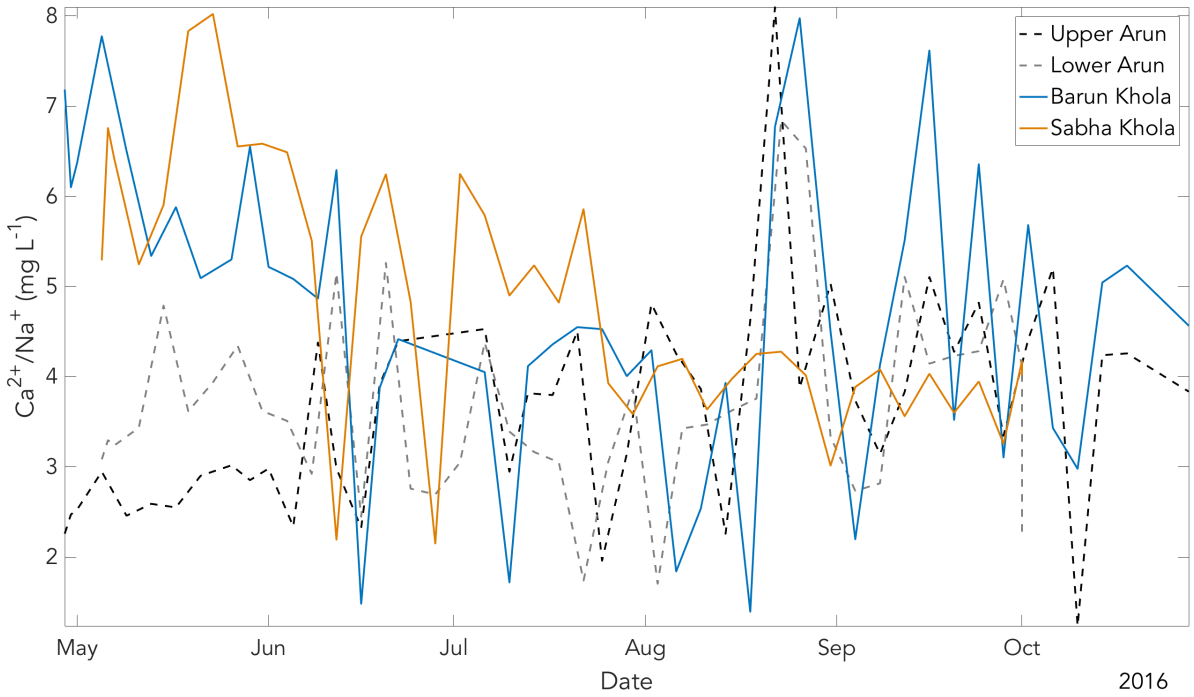

Figure 6. Comparison of Ca^{2+}:Na^{+} concentrations at each site for the duration of the timeseries sampling from May through November.

5 Discussion

5.1 δD and d-excess reflect climate processes and moisture source transitions

Our timeseries data of δD follow expected spatial patterns with the most depleted values occurring in the Upper Arun site draining from the high-elevation Tibetan Plateau and the most enriched values located in the low-elevation Sabha Khola (Hren et al., 2009). All sites have a notable depletion in δD at the onset of the monsoon followed by stabilization from mid-July onwards. This pattern likely reflects an intensification of the ISM rainfall (the amount effect) as the region transitions to peak monsoon season (Balestrini et al., 2016;

Meese et al., 2018; Rozanski et al., 1993; Kumar et al., 2010). The d-excess data reflect a distinct transition in moisture source from WWD to ISM with increasing values through May followed by a sharp decrease and stabilization through October. This general pattern has been described in other parts of the Himalaya and is attributed to the melting of WWD-derived snowpack (with high d-excess values) at the onset of the monsoon before the catchments are flushed with ISM rainfall (Meese et al., 2018; van der Veen et al., 2018; Voss et al., 2018).

5.2 Dissolved ion concentrations elucidate temporal variability in source waters

Each sample sites' dissolved ion concentration reflects an integrated value of its source waters and the seasonal variation of these sources over a hydrologic year. When we combine our results of total dissolved cations with the SO_4^{2-}:Na^+ and Ca^{2+}:Na^+ ion ratios several critical patterns emerge for each watershed. The Sabha Khola's high total dissolved cation and Ca^{2+}:Na^+ ratio at the onset of the monsoon (May and June) followed by a decline through the monsoon is likely indicative of a groundwater-dominated basin that is mixing with ISM rainfall that is known to have low solute concentrations. The high SO_4^{2-}:Na^+ and Ca^{2+}:Na^+ values in the Barun Khola are predicted for a glacier-dominated catchment. The decline in these values through mid-August reflects mixing with snowmelt and rainfall (which have low dissolved ion concentrations), and the subsequent increase from August to the end of the timeseries implies greater contributions of glacier-melt to Barun Khola discharge. The similarities and differences between the Upper Arun and Lower Arun sites provides critical insights to source water changes as the Arun River crosses from the Tibetan Plateau into the Himalayan lowlands. The timeseries of total dissolved cation for the Lower Arun site is notably dampened and temporally delayed compared to the Upper Arun, which is

likely driven by mixing with tributaries that have lower dissolved ion concentrations, i.e. tributaries similar to the Barun Khola and Sabha Khola. The increase in SO_4^{2-}:Na^+ and Ca^{2+}:Na^+ ion ratios throughout the timeseries in both the Upper and Lower Arun sites suggests increased contributions from glacial melt from the Tibetan headwaters and from glacierized tributaries mixing with the Arun River as a result of high temperatures throughout the summer.

5.3 Cross-site comparisons imply seasonal influence of tributaries contributing to the Arun

A comparison of the geochemical and isotopic patterns across the Arun River sites reveals the time-variable influence of Himalayan tributaries on the Arun River. From May through August, the dampening of the dissolved ion concentrations and SO_4^{2-}:Na^+ values in the Lower Arun site relative to the Upper Arun site implies mixing with low-elevation, ISM-rain dominated tributaries. Indeed, the Lower Arun and Sabha Khola SO_4^{2-}:Na^+ values appear to match during this time period. After August, the Lower Arun's SO_4^{2-}:Na^+ and Ca^{2+}:Na^+ values match and track with the Upper Arun as well as the Barun Khola, which suggests a diminishing influence from the ISM and rain-fed tributaries on Arun River discharge and an increasing influence from glacierized tributaries as the Arun flows through the Himalayan belt. These patterns validate previous studies that assess the temporal variability of source waters across the Himalaya (Bookhagen & Burbank, 2010; Immerzeel & Bierkens, 2012; Racoviteanu et al., 2013; Smith & Bookhagen, 2018; Wilson et al., 2015).

6 Conclusions

This study offers new geochemical and isotopic data to assess the seasonally-variable hydroclimatic processes controlling discharge in the Arun River. Specifically, our timeseries

data illustrate the following processes. First, δD and d-excess values reveal a distinct transition from WWD- to ISM-sourced precipitation from May through mid-June followed by a dominance of ISM rainfall through August. Second, variation in SO_4^{2-}:Na^+ and Ca^{2+}:Na^+ ion ratios indicate that ISM rainfall contributes the bulk of discharge in the Arun basin through August at which point glacier melt begins to increasingly contribute to streamflow. Third, the differences between the Upper and Lower Arun sites imply that both high- and low-elevation tributaries in the Himalaya contribute significantly to streamflow through their relative contributions vary seasonally. Our data imply that low-elevation groundwater and rain sourced catchments (i.e. the Sabha Khola) have a greater contribution before and during the monsoon while glacierized catchments (i.e. the Barun Khola) begin to contribute more in the late and post-monsoon season.

7 Next Steps

This study adds to a growing body of literature focused on Himalayan water supply and highlights the utility of geochemical and isotopic data to assess regional hydrologic and climate process that control water resources in the eastern Himalaya. The following two chapters will probe the variation of these geochemical and isotopic data at a finer spatial scale and explore the utility of the tracers to provide a quantitative assessment of discrete water resources in the Arun watershed. Specifically, this paper found strong seasonal moisture controls on the isotopic composition of meteoric water. Chapter Three will investigate the role of elevation and precipitation patterns on local δD, δ^{18}O, and d-excess values to determine how these values vary among snow, glacier, rain, and groundwater sources and, ultimately, are reflected in river water. This chapter also identifies specific

dissolved ion ratios that correlate with source waters and may be used to assess seasonal water budgets. Chapter Four will assess the utility of these geochemical and isotopic tracers and apply them in a mixing model analysis to provide a quantitative assessment of the Barun and Sabha Khola water budgets during low-flow periods before and after the monsoon when the influence from ISM rainfall is minimal.

Chapter III. Variation of deuterium excess in surface waters across a 5000-m elevation gradient in eastern Nepal

1 Introduction

Stable isotopes of oxygen and hydrogen ($\delta^{18}O$ and δD) and their spatiotemporal variation in surface water provide a unique tracer to characterize contributions of different water sources, including seasonal precipitation, snowmelt, and glacial melt (Aggarwal et al., 2006; Gat, 2010; Kendall & McDonnell, 2012). Differences in $\delta^{18}O$ and δD values emerge from fractionations occurring during water-vapor transport and precipitation, which are correlated to altitude, latitude, precipitation intensity, and distance from the moisture source. In addition, post-deposition fractionation from evaporation in soil and sublimation in snow fields can modify the isotopic composition of surface and groundwaters (Dansgaard, 1964; Joel R Gat, 2010). In high mountain regions, distinguishing the $\delta^{18}O$ and δD values of different water sources that contribute to stream flow is complicated by the extreme effects of topographic rise, seasonal changes in water-vapor sources, melting of snow fields and glaciers, and difficulties in accessing high-altitude regions. The differences in $\delta^{18}O$ and δD values among sources contributing to streamflow can be exploited to investigate the spatiotemporal patterns of water supply in the Himalaya and to characterize regional climatic processes.

In the Himalaya, the combination of decreasing temperatures and increasing rainout with increasing elevation accentuates fractionation processes and results in water that is isotopically heavy. This relationship, reported as $\delta^{18}O$ and δD lapse rates, ranges in surface water in Himalayan rivers from -0.45 to -4.4 ‰ km^{-1} for $\delta^{18}O$ and -8.3 to -33.0 ‰ km^{-1} for

δD, but these estimates largely draw on surface water samples from streams in low and mid elevations less than 5000 m (Florea et al., 2017; Hren et al., 2009; Meese et al., 2018; Poage & Chamberlain, 2001; Racoviteanu et al., 2013; van der Veen et al., 2018; Varay et al., 2017; Wilson et al., 2015). High-elevation samples are sparse but essential to accurately characterize mountain-sourced surface waters, especially in regions with significant contributions from isotopically heavy snow and glacial melt. River water is commonly used to construct δ^{18}O and δD lapse rates; however, river water does not represent the "true" precipitation δ^{18}O and δD values, but instead reflects an integrated signal of upstream processes and source waters that vary seasonally. Critically, δ^{18}O and δD lapse rates derived from mountainous regions are often used in paleoclimate and regional climate modeling (Caves et al., 2015; Poage & Chamberlain, 2001). These analyses often depend on the δ^{18}O and δD values preserved in minerals in the sedimentary record, which may be influenced by seasonal variations in moisture source and assume a linear relationship between δ^{18}O or δD and altitude.

In addition to elevation, the distinct moisture regimes in the Himalaya – the Indian Summer Monsoon (ISM) and Winter Westerly Disturbances (WWD) – control surface water and precipitation isotopic signatures due to the source, path, and precipitation intensity of the two storm systems. The ISM originates in the Bay of Bengal and Indian Ocean and moves across the Indian subcontinent before intersecting with the Himalayan orographic barrier (Bookhagen & Burbank, 2010). WWD moisture originates in the Mediterranean, Black, and Caspian Seas and follows a continental path across the Middle East and Central Asia before reaching the western edge of the Himalaya (Barry, 2008; Cannon et al., 2015; Lang & Barros, 2004). The bulk of ISM precipitation falls as rain from June to September while

WWD precipitation is deposited as snowpack from December to April (Barry, 2008; Bookhagen & Burbank, 2010; Lang & Barros, 2004).

Deuterium excess (d-excess) is a tool to measure kinetic fractionation effects related to humidity, moisture recycling, and post-deposition processes, including sublimation(Dansgaard, 1964; Froehlich et al., 2002; Pfahl & Sodemann, 2014). Broadly, deuterium excess relates the proportion of ^{18}O and ^{2}H contained in water. These proportions are controlled by the physical conditions at the source of precipitation (i.e. humidity, air temperature, and sea surface temperature) as well as the conditions during water vapor transport (i.e. mixing and evaporation of different sources) (Froehlich et al., 2002). Given the different conditions at the origin and storm pathways of the ISM versus WWD precipitation, the two moistures regimes can be expected to have distinct deuterium excess signatures. In the Himalaya, precipitation from the ISM is marked by low deuterium excess values while WWD-sourced precipitation has relatively high deuterium excess values (Balestrini et al., 2016; Bershaw et al., 2012; Hren et al., 2009; Jeelani et al., 2013; Pande et al., 2000). Previous studies of surface water isotope signatures in the Himalaya largely sampled in the post-monsoon season and reflect a dominant ISM moisture source, and little is known about the temporal evolution of surface water oxygen and hydrogen stable isotope values driven by seasonal moisture source variation, particularly the influence of seasonal snowmelt (Grujic et al., 2018; Hren et al., 2009; Meese et al., 2018; van der Veen et al., 2018; Varay et al., 2017).

This study, based in the Arun River basin in eastern Nepal, captures the temporal and spatial variability in $\delta^{18}O$ and δD values of river water driven by seasonal ISM and WWD moisture sources as well as the influence of different melt waters. It targets the pre- and post-monsoon seasons, which represent base flow conditions when Himalayan rivers are not

flushed with runoff from the ISM, in order to assess the importance of snow melt, glacial melt, and groundwater on river water $\delta^{18}O$ and δD values. Accordingly, we analyze data from water samples sourced from tributaries with varying amounts of snowmelt, glacial melt, and groundwater. This study contributes to a growing understanding of the sources and timing of water contributions at low and mid elevations and offers $\delta^{18}O$ and δD data from elevations above 5000 m, where few samples have been collected previously. In the past, models of $\delta^{18}O$ and δD depletion at high elevation relied on linear regression models to extrapolate isotope values from low and mid elevations. We show that there are strong nonlinear changes in the $\delta^{18}O$ and δD values of water contributions to the Arun River catchment driven by high-elevation surface water influenced by snow and glacial melt waters as well as variability in seasonal moisture source.

2 Study Site

The Arun Valley receives precipitation from both the ISM and WWD and exhibits one of the steepest elevation gradients in the eastern Himalaya (200 m to 8480 m in altitude). The 33,000-km^2 Arun River contains ~15% glacierized area and is estimated to receive ~25% of annual streamflow from WWD-sourced snowmelt and ~70% from ISM-sourced rainfall (Bookhagen & Burbank, 2010; RGI Consortium, 2017). We collected data from two sub-basins of the Arun River: the Barun Khola and the Sabha Khola (Fig. 1). The Barun Khola is a 468-km^2 watershed with a mean catchment elevation of 4758 meters above sea level (masl) and ~30% glaciated area (Fig. 1a). The confluence of the Barun Khola with the Arun River is at Barun Bazaar. The Sabha Khola is a 549-km^2 nonglacierized watershed with a mean elevation of 1503 masl (Fig. 1b). The confluence of the Sabha Khola and Arun

River is located near Tumlingtar. Combined, the Barun and Sabha Kholas span from 200 m to 8480 m at the summit of Mt. Makalu. The relief of the region allows for dense sampling over a wide range of elevations while minimizing changes in latitude and longitude. High elevation regions in the Himalaya are known to have different moisture regimes and seasonal changes in water source driven by ISM and WWD precipitation as well as melt-water inputs from snow and glaciers (Immerzeel et al., 2013; Mölg et al., 2014; Smith & Bookhagen, 2018). The spatiotemporal variation in oxygen and hydrogen isotope values in the Barun and Sahba Kholas allow us to explore the elevation fingerprint on $\delta^{18}O$ and δD values as well as the potential applications of these isotopic tracers to parse surface water sources. Based on previous studies from the region, we anticipate that the Barun Khola will exhibit isotopically depleted $\delta^{18}O$ and δD values as well as higher deuterium excess values relative to the Sabha Khola due to its higher average catchment elevation, greater contributions from WWD-derived snowmelt, and seasonal glacier melt. As such, this 6000-m elevation gradient highlights variability in river water $\delta^{18}O$ and δD lapse rates that may be driven by "catchment effects" related to mixing water sources and as well as elevation effects (Dutton et al., 2005).

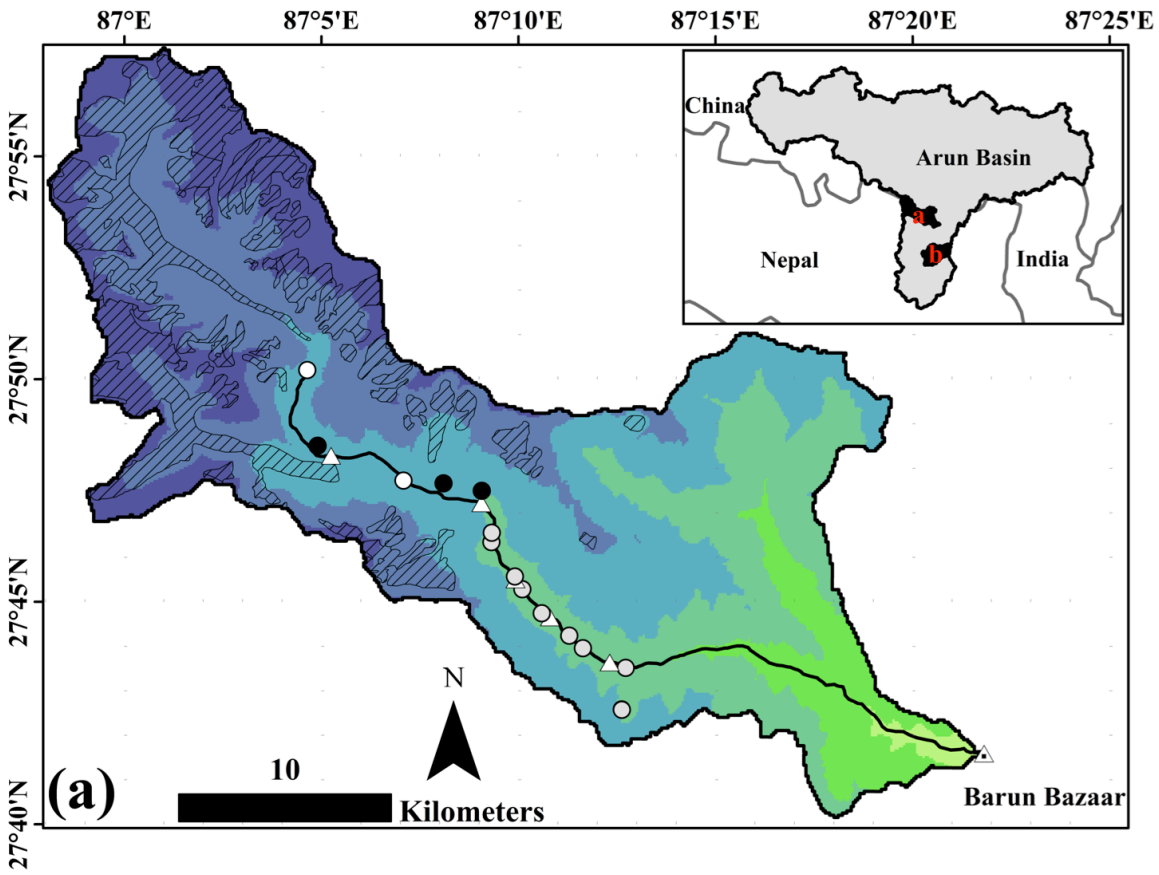
87°E
87°5'E
87°10'E
87°15'E
87°20'E
87°25'E
27°55'N
27°50'N
27°45'N
27°40'N
China
Arun Basin
Nepal
India
a
b
N
10
Kilometers
(a)
Barun Bazaar

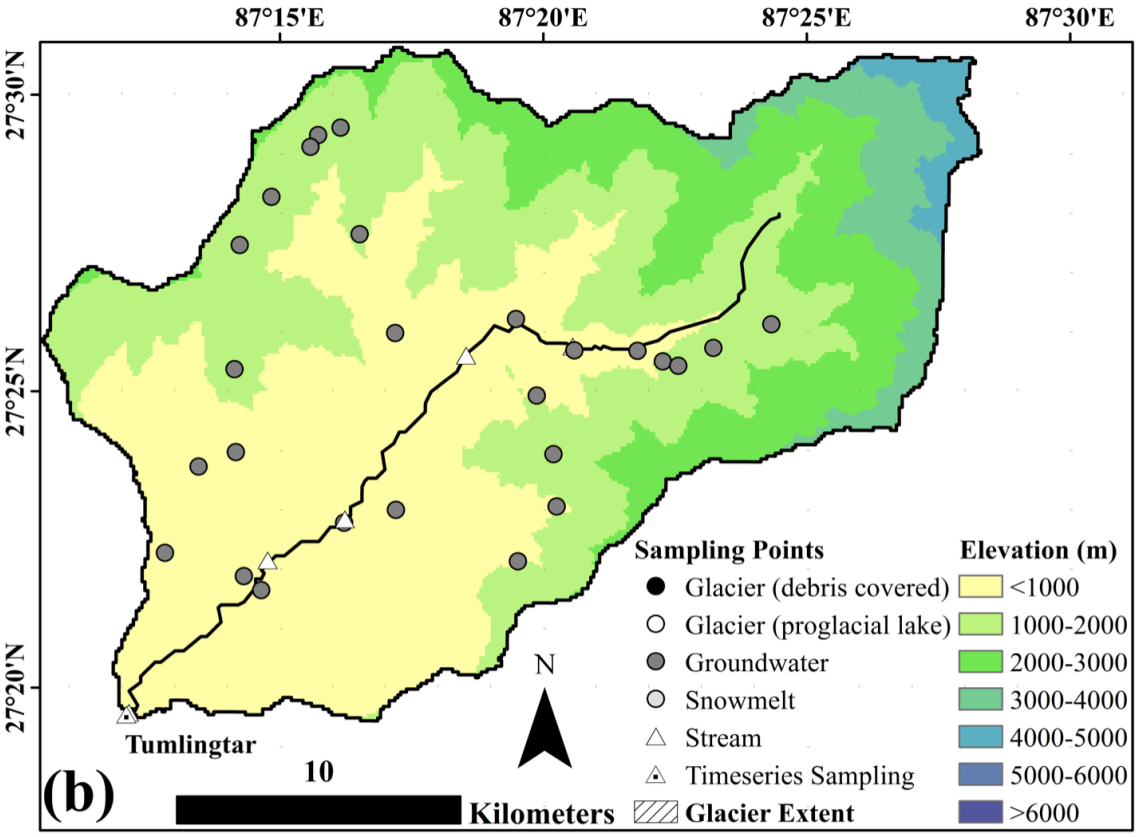
87°15'E
87°20'E
87°25'E
87°30'E
27°30'N
27°25'N
27°20'N
Tumlingtar
N
10
Kilometers
(b)
Sampling Points
Glacier (debris covered)
Glacier (proglacial lake)
Groundwater
Snowmelt
Stream
Timeseries Sampling
Glacier Extent
Elevation (m)
<1000
1000-2000
2000-3000
3000-4000
4000-5000
5000-6000
>6000

Figure 1. Map of the Barun Khola and Sabha Khola, two sub-basins of the Arun watershed located in eastern Nepal (see map inset). Glacier extent is from the Randolf Glacier Inventory derived from Global Land Ice Measurements from Space (GLIMS)(RGI Consortium, 2017). Synoptic samples were collected in the Barun and Sabha Kholas (a and b, respectively) in the pre- and post-monsoon seasons. Time-series samples were collected at the confluence of the Barun and Sabha Khola with the Arun River at Barun Bazaar and Tumlingtar, as labeled. The dominant water source for each drainage area is indicated by the shading of the circles. Main stem river samples are indicated with a triangle.

3 Data and Methods

We used a synoptic sampling approach to characterize spatial variation in $\delta^{18}O$ and δD values in the Sabha and Barun Kholas during two field campaigns (Baraer et al., 2009; Mark et al., 2005; Wilson et al., 2015). A pre-monsoon sampling was conducted during April and May 2016 with repeat sampling at the same locations during October and November 2016 (see data repository for list of samples). The shoulder periods of the monsoon were targeted to characterize river isotopic composition under base-flow conditions when glacier and snowmelt as well as groundwater are important contributors to river discharge. During the summer season, orographic effects on ISM rainfall dominate river discharge and its isotopic composition, but access for sampling is greatly restricted. When possible, river samples were collected from the main stem of the Barun Khola and Sabha Khola every 200-m of elevation gain (N = 28; 13/season). Samples were also collected from surface water drainages that contained extensive snowpack (N = 22; 11/season), proglacial lakes (N = 4; 2/season), debris-covered glaciers (N = 6; 3/season), as well as groundwater-

sourced springs/wells and surface-water tributaries draining from forested and agriculture-dominated areas (N = 56; 28/season). Snowmelt and glacial melt samples were collected as close to the snow line or glacial terminus as possible, and therefore represent an integrated value of melt sources upstream of the sample collection point. Groundwater-sourced samples (labeled collectively as groundwater in Fig. 1) were collected from springs/wells as well as surface water tributaries sourced exclusively from rainfall-fed subsurface flow. Groundwater samples collected from springs/wells likely reflect shallow subsurface groundwater from the vadose zone with lower residence times relative to groundwater samples collected from surface water tributaries, which likely represent an integrated shallow and deep groundwater source. Local Nepali schoolteachers were trained to collect time-series samples at the confluence of the Barun and Sabha Kholas with the Arun River at Barun Bazaar and Tumlingtar, respectively. Samples were collected every 4 days from late April/early May through October 2016 (N = 41 for the Sabha Khola; N = 45 for Barun Khola).

Two sets of water samples were collected from each site. Each sample was filtered through 0.45-µm glass filters into 30-mL polyethylene Nalgene bottles that were rinsed three times with filtered water. Bottles were filled completely to produce a positive meniscus, sealed tightly, and wrapped with tape to prevent the formation of air bubbles and possible evaporation before laboratory analysis. Bottles were stored in a dark place until the completion of the field season and then stored in a refrigerator at 4°C at UC Santa Barbara. During the pre- and post-monsoon synoptic sampling campaigns, additional field duplicates were collected every 10 samples for error analysis.

Samples were analyzed for $\delta^{18}O$ and δD at the German Research Center for

Geosciences (GFZ) Organic Surface Geochemistry Lab with a Picarro L-2140i Laser Spectrometer. Isotope values for $\delta^{18}O$, δD, and deuterium excess are reported in delta notation as parts per thousand as related to their deviation from Vienna Standard Mean Ocean Water (VSMOW). Precision for $\delta^{18}O$ and δD measurements was ± 0.03 $^{0}/_{00}$ and ± 0.3 $^{0}/_{00}$, respectively. Analytical uncertainties for the oxygen and hydrogen stable isotope measurements are reported as standard deviation of triplicate measurements in the data repository. Deuterium excess was calculated for each sample as $d = \delta D - 8*\delta^{18}O$ (Dansgaard, 1964). Data for individual samples are listed in Table 1.

The mean catchment elevation of the drainage area contributing to each sample location was calculated using NASA's Shuttle Radar Topography Mission (SRTM) global 1 arc second dataset for Asia (SRTMGL1; NASA JPL, 2013). The drainage area was defined using the watershed toolbox with ESRI's ArcGIS based on GPS coordinates of the samples recorded during the field campaigns. To supplement the isotope interpretation, snow extent was calculated for the pre- and post-monsoon seasons. Two Landsat 8 OLI images with minimal cloud cover were selected from the beginning (March 24th, 2016) and end (November 11th, 2016) of the synoptic sampling campaigns. Regions of interest were selected for each image to conduct a supervised classification using Maximum Likelihood classification. The classification output was validated and adjusted manually to ensure accurate representation of snow extent. Weekly averaged land-surface temperatures for the Barun Khola were calculated from the MODIS/Terra Land Surface Temperature Daily Global 1-km gridded data (MOD11A1) product for the duration of the time-series data (April through November 2016) to provide further insight to climate processes during the study period (Wan, 2015). Days with extensive cloud cover where less than 10% of pixels in the

study basins were visible are excluded from the analysis. Daily rainfall data were averaged over the Barun Khola and Sahba Khola basins with precipitation data from the U.S. Geological Survey and UC Santa Barbara Climate Hazards Group Infrared Precipitation with Stations (CHIRPS) dataset (Funk et al., 2015).

4 Results

4.1 Oxygen and hydrogen isotope values and lapse rates

River sample $\delta^{18}O$ and δD values in the Barun Khola and Sabha Khola show a distinct elevation fingerprint with a clear depletion effect that strengthens at higher elevations (Figs. 2 and 3). In both the Barun and Sabha Kholas, $\delta^{18}O$ and δD values in the post-monsoon season are isotopically heavy relative to the pre-monsoon season. On average, water samples collected in the Sabha Khola watershed are notably lighter in isotopic values relative to the Barun Khola (see Appendix B for data repository). In the Barun Khola, the post-monsoon $\delta^{18}O$ and δD lapse rates of the river samples (-6.0±0.4 $^{0}/_{00}$ km^{-1} and -49.8±3.2 $^{0}/_{00}$ km^{-1}, respectively) are slightly weaker than the pre-monsoon signal (-6.7±1.4 $^{0}/_{00}$ km^{-1} and -54.8±12.0 $^{0}/_{00}$ km^{-1}). In contrast, the pre-monsoon $\delta^{18}O$ and δD lapse rates in the Sabha Khola (-1.3±0.3 $^{0}/_{00}$ km^{-1} and -8.0±2.8 $^{0}/_{00}$ km^{-1}) are weaker than the post-monsoon lapse rates (-1.4±0.1 $^{0}/_{00}$ km^{-1} and -9.5±1.0 $^{0}/_{00}$ km^{-1}). The gap from 3000-4000 m is a consequence of inaccessible terrain in the lower reaches of the Barun Khola. When all river samples are combined, the lapse rates for the $\delta^{18}O$ and δD are -2.2±0.2 $^{0}/_{00}$ km^{-1} and -17.4±2.0 $^{0}/_{00}$ km^{-1} in the pre-monsoon season and -2.4±0.2 $^{0}/_{00}$ km^{-1} and -19.0±1.4 $^{0}/_{00}$ km^{-1} in the post-monsoon season.

The regressions comparing $\delta^{18}O$ and δD to altitude are statistically significant ($p <$

0.01), and the coefficients of determination (r^2) of the ordinary least squares (OLS) regressions strengthen between the pre- and post-monsoon seasons. The lapse rates of $\delta^{18}O$ and δD from glacial melt and groundwater show a significant ($p<0.1$) relationship with altitude whereas samples from snowmelt are inconclusive ($p>0.1$) (see inset Figs. 2 and 3). The low r^2 and p-values in the snowmelt samples are indicative of greater variability, which may reflect sublimation processes influencing these samples (Table 2).

Ordinary Least Squares Regression	**δ18O isotope lapse rate ($^0/_{00}$ km^{-1})**	**δD isotope lapse rate ($^0/_{00}$ km^{-1})**	**Deuterium excess lapse rate ($^0/_{00}$ km^{-1})**
Sabha Khola (<3000m) Pre-Monsoon	y = -1.3x [km] – 4.0 r^2=0.83; p<0.1	y = -8.0x [km] – 21.8 r^2=0.74; p<0.1	y = 2.0x [km] + 10.7 r^2=0.98; p<0.001
Sabha Khola (<3000m) Post-Monsoon	y= -1.4x [km] – 5.3 r^2=0.99; p<0.001	y = -9.5x [km] - 32.4 r^2=0.97; p<0.01	y = 1.5x [km] + 10.2 r^2=0.64; p=0.103
Barun Khola (>4000m) Pre-Monsoon	y = -6.6x [km] + 22.2 r^2 = 0.79; p<0.01	y = -54.8x [km] + 204.9 r^2=0.78; p<0.01	y = -2.3x [km] + 27.2 r^2=0.52; p<0.1
Barun Khola (>4000m) Post-Monsoon	y = -6.0x [km] – 16.7 r^2=0.98; p<0.0001	y = -49.8x [km] + 157.8 r^2=0.98; p<0.0001	y = -1.9x [km] + 24.0 r^2=0.90; p<0.001
All Samples Pre-Monsoon	y = -2.2x [km] - 2.1 r^2=0.89; p<0.0001	y = -17.4x [km] – 2.1 r^2=0.87; p<0.0001	y = -0.0x [km] + 14.7 r^2=0.00; p=0.825
All Samples Post-Monsoon	y = -2.4x [km] – 3.3 r^2=0.95; p<0.0001	y = -19.0x [km] – 13.0 r^2=0.95; p<0.0001	y = 0.1x [km] + 13.0 r^2=0.02; p=0.636
Weighted Least Squares Regression	**δ18O isotope lapse rate ($^0/_{00}$ km^{-1})**	**δD isotope lapse rate ($^0/_{00}$ km^{-1})**	**Deuterium excess lapse rate ($^0/_{00}$ km^{-1})**
Sabha Khola (<3000m) Pre-Monsoon	y = -1.2x [km] – 4.0 r^2=0.79; p<0.1	y = -7.9x [km] – 21.9 r^2=0.68; p<0.1	y = 2.0x [km] + 10.7 r^2=0.98; p<0.01
Sabha Khola (<3000m) Post-Monsoon	y = -1.4x [km] - 5.3 r^2=0.99; p<0.001	y = -9.5x [km] – 32.5 r^2=0.97; p<0.01	y = 1.5x [km] +10.2 r^2=0.59; p=0.127
Barun Khola (>4000m) Pre-Monsoon	y = -13.3x [km] + 60.3 r^2=0.96; p<0.0001	y = -113.1x [km] +533.1 r^2=0.96; p<0.0001	y = -6.5x [km] + 50.8 r^2=0.93; p<0.001
Barun Khola (>4000m) Post-Monsoon	y = -7.9x [km] + 27.5 r^2=0.99; p<0.0001	y = -50.0x [km] +158.7 r^2=0.97; p<0.0001	y = -1.9x [km] + 23.9 r^2=0.88; p<0.001
All Samples Pre-Monsoon	y = -1.9x [km] – 2.8 r^2=0.95; p<0.0001	y = -15.1x [km] - 8.0 r^2=0.94; p<0.0001	y = 0.0x [km] + 14.6 r^2=0.02; p=0.619
All Samples Post-Monsoon	y = -2.4x [km] - 3.4 r^2=0.97; p<0.0001	y = -19.0x [km] – 14.1 r^2=0.97; p<0.0001	y = 0.1x [km] + 12.9 r^2=0.04; p=0.522

Table 2. Summary of ordinary least squares and weighted regression calculations used to derive stable isotope lapse rates.

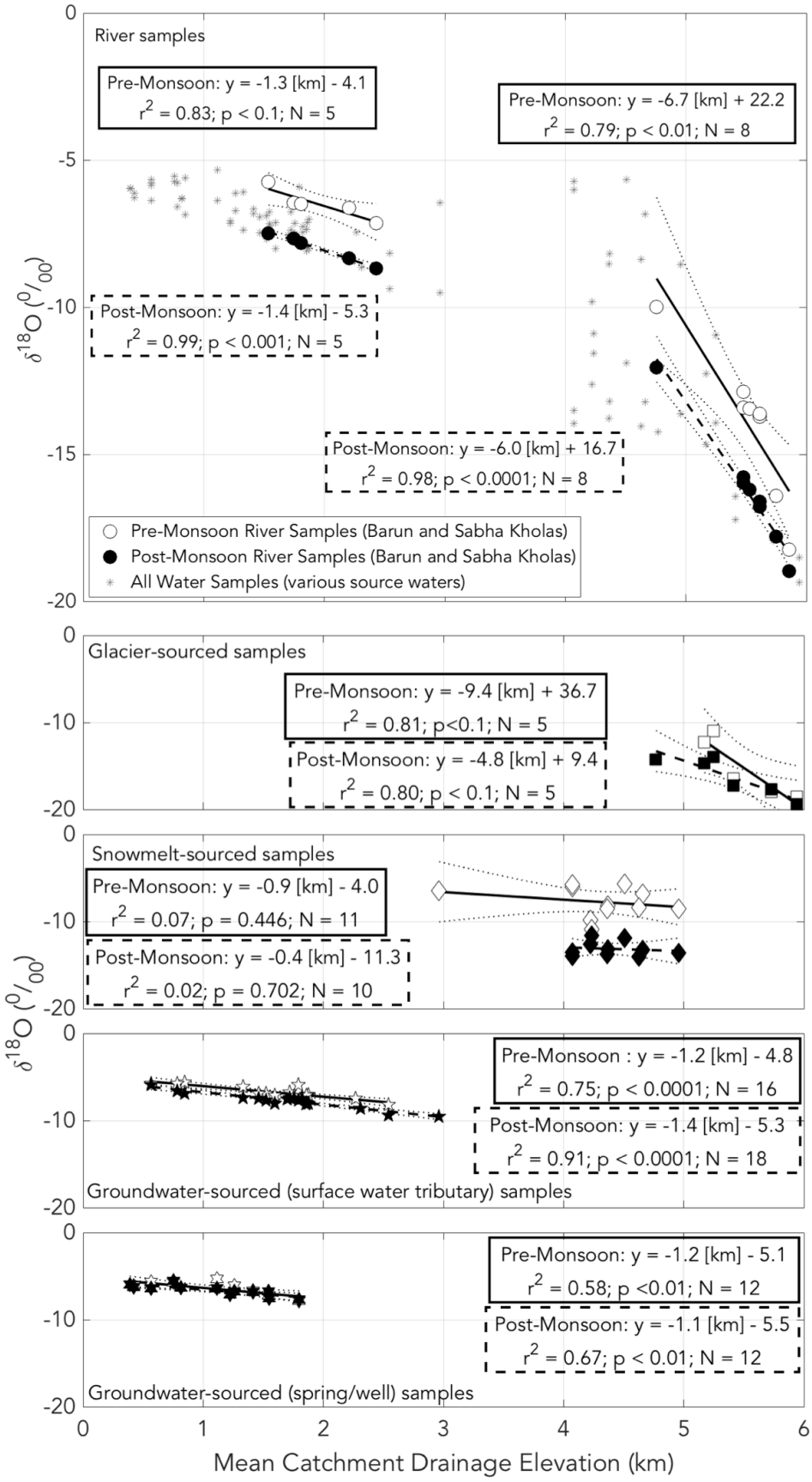
River samples
Pre-Monsoon: y = -1.3 [km] - 4.1
r2 = 0.83; p < 0.1; N = 5
Pre-Monsoon: y = -6.7 [km] + 22.2
r2 = 0.79; p < 0.01; N = 8
Post-Monsoon: y = -1.4 [km] - 5.3
r2 = 0.99; p < 0.001; N = 5
Post-Monsoon: y = -6.0 [km] + 16.7
r2 = 0.98; p < 0.0001; N = 8
Pre-Monsoon River Samples (Barun and Sabha Kholas)
Post-Monsoon River Samples (Barun and Sabha Kholas)
All Water Samples (various source waters)
Glacier-sourced samples
Pre-Monsoon: y = -9.4 [km] + 36.7
r2 = 0.81; p<0.1; N = 5
Post-Monsoon: y = -4.8 [km] + 9.4
r2 = 0.80; p < 0.1; N = 5
Snowmelt-sourced samples
Pre-Monsoon: y = -0.9 [km] - 4.0
r2 = 0.07; p = 0.446; N = 11
Post-Monsoon: y = -0.4 [km] - 11.3
r2 = 0.02; p = 0.702; N = 10
Pre-Monsoon : y = -1.2 [km] - 4.8
r2 = 0.75; p < 0.0001; N = 16
Post-Monsoon: y = -1.4 [km] - 5.3
r2 = 0.91; p < 0.0001; N = 18
Groundwater-sourced (surface water tributary) samples
Pre-Monsoon: y = -1.2 [km] - 5.1
r2 = 0.58; p <0.01; N = 12
Post-Monsoon: y = -1.1 [km] - 5.5
r2 = 0.67; p < 0.01; N = 12
Groundwater-sourced (spring/well) samples
δ18O (0/00)
Mean Catchment Drainage Elevation (km)

Figure 2. Comparison of pre- and post-monsoon $\delta^{18}O$ in the Barun Khola and Sabha Khola relative to the mean catchment elevation of the drainage areas of the samples. OLS regressions represent the $\delta^{18}O$ lapse rates for each kilometer of elevation gain. Analytical uncertainty of stable isotope measurements (y-error bars) are smaller than the data points. 95% confidence intervals of the OLS regressions are indicated with dotted lines. Grey asterisks (top panel) represent all water samples collected, which are then partitioned by the dominant source contributing to that sample (bottom panel) to calculate the individual lapse rates for each water source type. Mean catchment drainage elevations are calculated for each sample using NASA's SRTMGL1 data product.

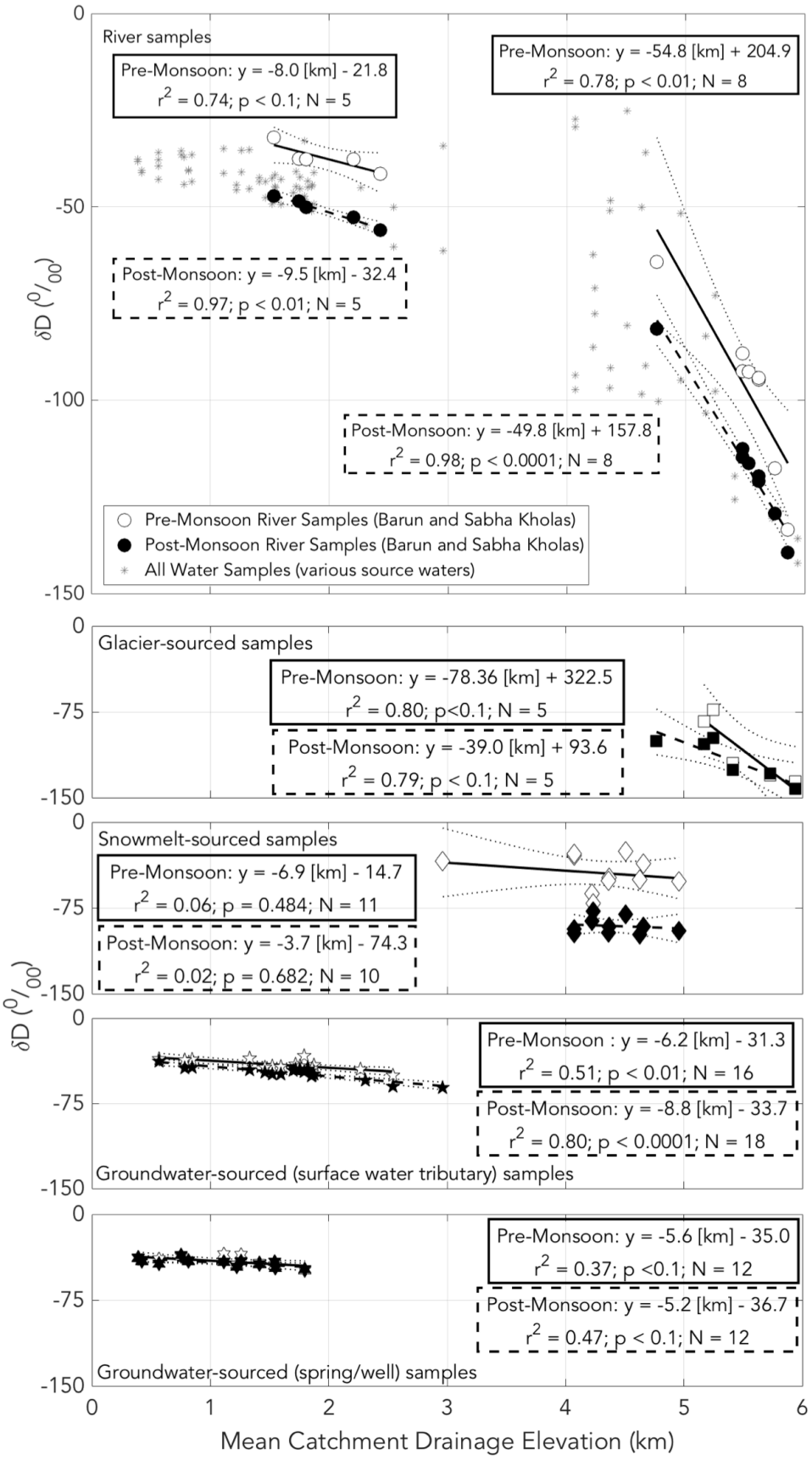
River samples
Pre-Monsoon: y = -8.0 [km] - 21.8
r2 = 0.74; p < 0.1; N = 5
Post-Monsoon: y = -9.5 [km] - 32.4
r2 = 0.97; p < 0.01; N = 5
Pre-Monsoon: y = -54.8 [km] + 204.9
r2 = 0.78; p < 0.01; N = 8
Post-Monsoon: y = -49.8 [km] + 157.8
r2 = 0.98; p < 0.0001; N = 8
Pre-Monsoon River Samples (Barun and Sabha Kholas)
Post-Monsoon River Samples (Barun and Sabha Kholas)
All Water Samples (various source waters)
Glacier-sourced samples
Pre-Monsoon: y = -78.36 [km] + 322.5
r2 = 0.80; p<0.1; N = 5
Post-Monsoon: y = -39.0 [km] + 93.6
r2 = 0.79; p < 0.1; N = 5
Snowmelt-sourced samples
Pre-Monsoon: y = -6.9 [km] - 14.7
r2 = 0.06; p = 0.484; N = 11
Post-Monsoon: y = -3.7 [km] - 74.3
r2 = 0.02; p = 0.682; N = 10
Pre-Monsoon : y = -6.2 [km] - 31.3
r2 = 0.51; p < 0.01; N = 16
Post-Monsoon: y = -8.8 [km] - 33.7
r2 = 0.80; p < 0.0001; N = 18
Groundwater-sourced (surface water tributary) samples
Pre-Monsoon: y = -5.6 [km] - 35.0
r2 = 0.37; p <0.1; N = 12
Post-Monsoon: y = -5.2 [km] - 36.7
r2 = 0.47; p < 0.1; N = 12
Groundwater-sourced (spring/well) samples
δD (‰)
Mean Catchment Drainage Elevation (km)

Figure 3. Comparison of pre- and post-monsoon δD in the Barun Khola and Sabha Khola relative to the mean catchment elevation of the drainage areas of the samples. OLS regressions represent the δD lapse rates for each kilometer of elevation gain. Analytical uncertainty of stable isotope measurements (y-error bars) are smaller than the data points. 95% confidence intervals of the OLS regressions are indicated with dotted lines. Grey asterisks (top panel) represent all water samples collected, which are then partitioned by the dominant source contributing to that sample (bottom panels) to calculate the individual lapse rates for each water source type. Mean catchment drainage elevations are calculated for each sample using NASA's SRTMGL1 data product.

Deuterium excess values also exhibit a distinct elevation relationship (Fig. 4). They are positively correlated in mean catchment elevations up to ~3000 m and then switch to a negative correlation after ~4000 m. In the pre-monsoon season, the deuterium excess lapse rate of the river samples is -2.3±0.9 $^{0}/_{00}$ km^{-1} in the Barun Khola (with mean catchment drainage elevations ranging from 4000 m to 6000 m) and 2.0±0.2 $^{0}/_{00}$ km^{-1} in the Sabha Khola (with mean catchment elevations between 350 m and 3000 m). In the post-monsoon season, the elevation influence weakens to -1.9±0.3 $^{0}/_{00}$ km^{-1} in higher elevation catchments and 1.5±0.6 $^{0}/_{00}$ km^{-1} in lower elevation catchments. Groundwater-sourced samples (both from springs/wells and surface tributaries) exhibit a significant relationship between deuterium excess and elevation (p-values <0.1); however, snow and glacial melt-sourced samples have no significant relationship.

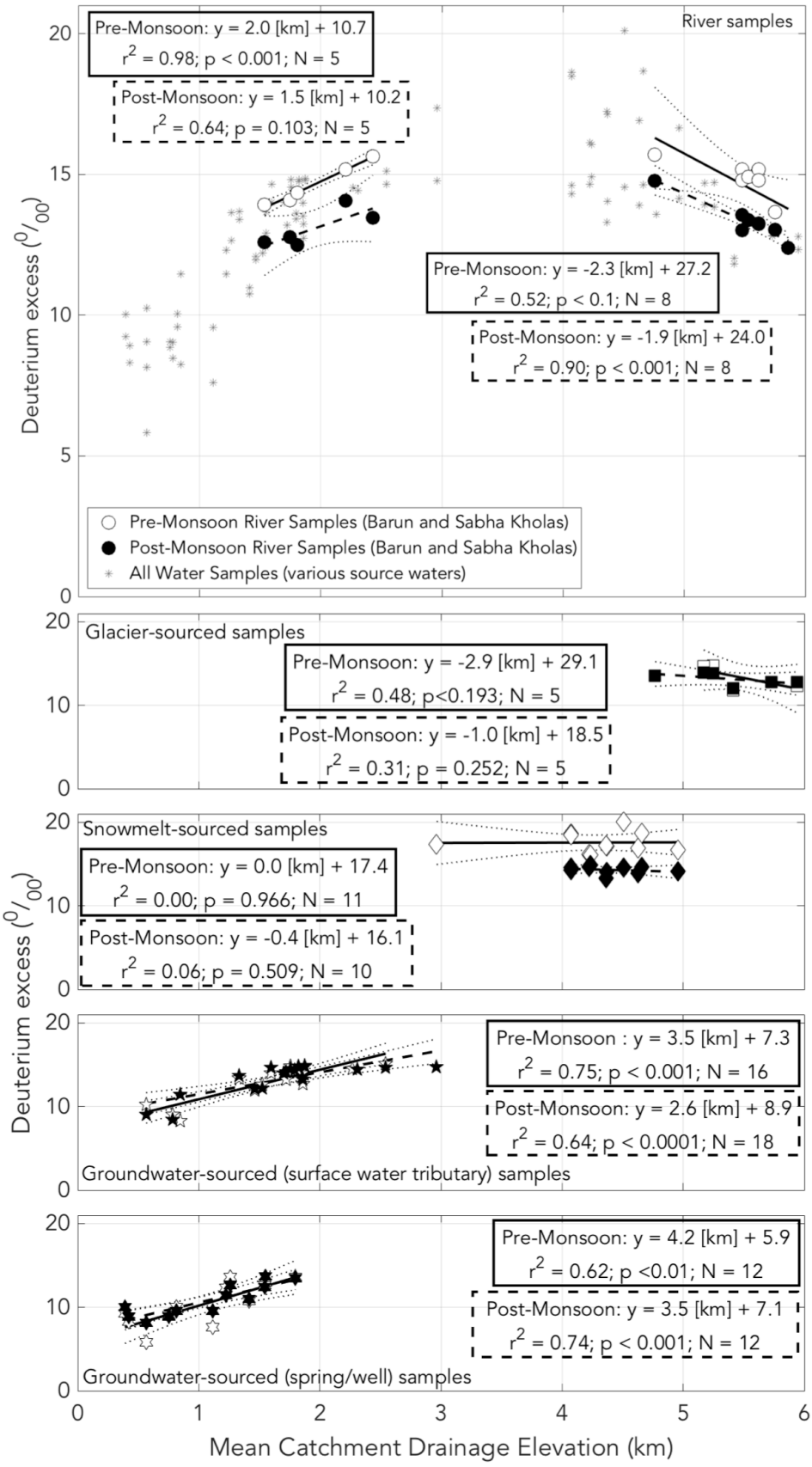
River samples
Pre-Monsoon: y = 2.0 [km] + 10.7
r2 = 0.98; p < 0.001; N = 5
Post-Monsoon: y = 1.5 [km] + 10.2
r2 = 0.64; p = 0.103; N = 5
Pre-Monsoon: y = -2.3 [km] + 27.2
r2 = 0.52; p < 0.1; N = 8
Post-Monsoon: y = -1.9 [km] + 24.0
r2 = 0.90; p < 0.001; N = 8
Pre-Monsoon River Samples (Barun and Sabha Kholas)
Post-Monsoon River Samples (Barun and Sabha Kholas)
All Water Samples (various source waters)
Glacier-sourced samples
Pre-Monsoon: y = -2.9 [km] + 29.1
r2 = 0.48; p<0.193; N = 5
Post-Monsoon: y = -1.0 [km] + 18.5
r2 = 0.31; p = 0.252; N = 5
Snowmelt-sourced samples
Pre-Monsoon: y = 0.0 [km] + 17.4
r2 = 0.00; p = 0.966; N = 11
Post-Monsoon: y = -0.4 [km] + 16.1
r2 = 0.06; p = 0.509; N = 10
Pre-Monsoon : y = 3.5 [km] + 7.3
r2 = 0.75; p < 0.001; N = 16
Post-Monsoon: y = 2.6 [km] + 8.9
r2 = 0.64; p < 0.0001; N = 18
Groundwater-sourced (surface water tributary) samples
Pre-Monsoon: y = 4.2 [km] + 5.9
r2 = 0.62; p <0.01; N = 12
Post-Monsoon: y = 3.5 [km] + 7.1
r2 = 0.74; p < 0.001; N = 12
Groundwater-sourced (spring/well) samples
Deuterium excess (0/00)
Mean Catchment Drainage Elevation (km)

Figure 4. Comparison of pre- and post-monsoon deuterium excess in the Barun Khola and Sabha Khola relative to the mean catchment elevation of the drainage areas of the samples. OLS regressions represent the deuterium excess lapse rates for each kilometer of elevation gain. Analytical uncertainty of stable isotope measurements (y-error bars) are smaller than the data points. 95% confidence intervals of the OLS regressions are indicated with dotted lines. Grey asterisks (top panel) represent all water samples collected, which are then partitioned by the dominant source contributing to that sample (bottom panels) to calculate the individual lapse rates for each water source type. Mean catchment drainage elevations are calculated for each sample using NASA's SRTMGL1 data product.

To further elucidate the relationship between precipitation moisture source and deuterium excess, we compare the change in snow-covered area of the drainage basins for samples in the pre- and post-monsoon seasons with the difference in deuterium excess across seasons (Fig. 5). Since snow in the region is largely sourced from WWD we would expect a large change in deuterium excess values across seasons indicative of a moisture source transition from WWD- to ISM-sourced precipitation. Indeed, there is a clear relationship between loss of snowpack and decreased deuterium excess values from the pre- to post-monsoon seasons

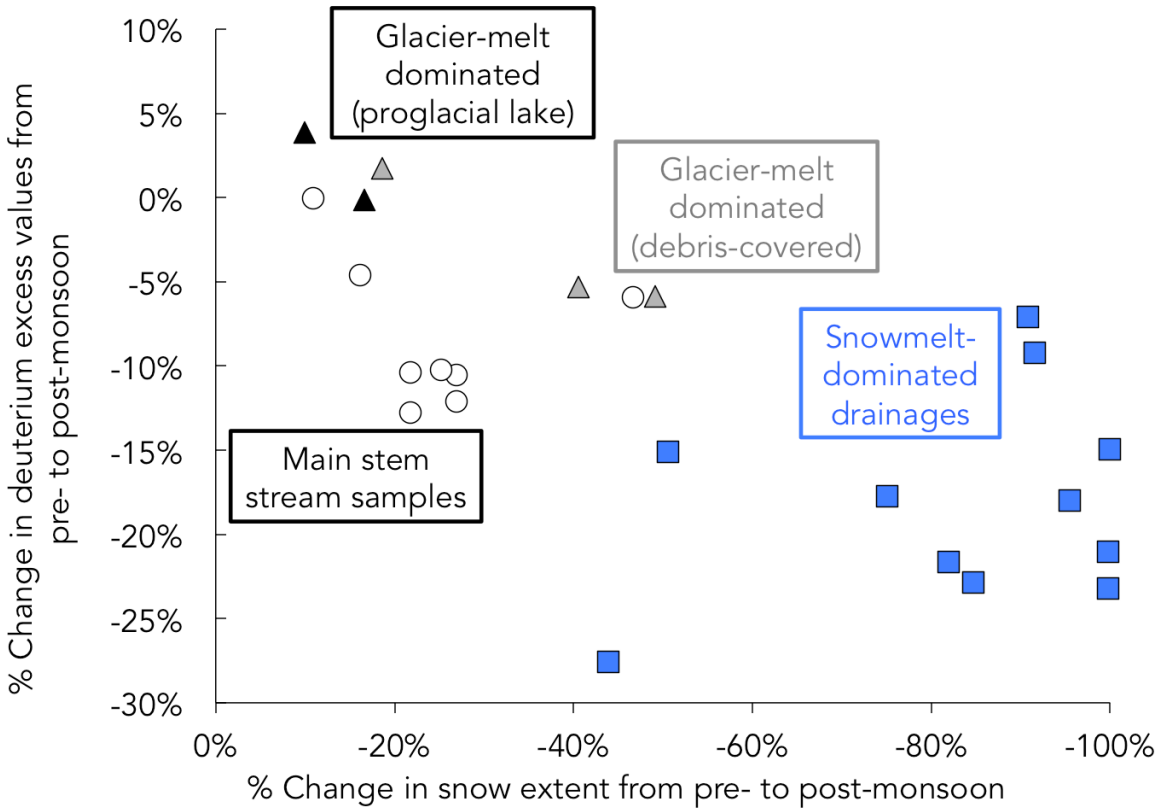

Figure 5. Comparison of the change in snow covered area with deuterium excess values for samples collected in the pre- and post-monsoon seasons. Change in snow was calculated based on the difference in snow extent from Landsat 8 OLI imagery between 24 March and 11 November 2016 for the contributing drainage areas of each sample. Samples are classified based on the dominant water source type for the drainage area in the pre-monsoon season.

4.2 Temporal variation in deuterium excess

Deuterium excess exhibits a distinct temporal signal from late April to October in both the Barun Khola and Sabha Khola (Fig. 6). From late April to early June, during the onset of the monsoon, deuterium excess values increase until 4 June 2016 at which point they decline until 14 July 2016 and stabilize for the duration of the time series. Deuterium excess

values in the Sabha Khola are lower than the Barun Khola throughout the time series with the exception of a large drop in deuterium excess values in the Barun Khola in early September. Temperatures in the Barun Khola, which best represent high-elevation regions where snowmelt may be occurring, are relatively high and stable until early June, then decrease until mid July with a sudden increase in temperatures in late August. The surface temperature declines through September and remains stable, but relatively low, until mid October. The rainfall data indicate sparse rainfall during May and more continuous rainfall from June to September that then diminish in October.

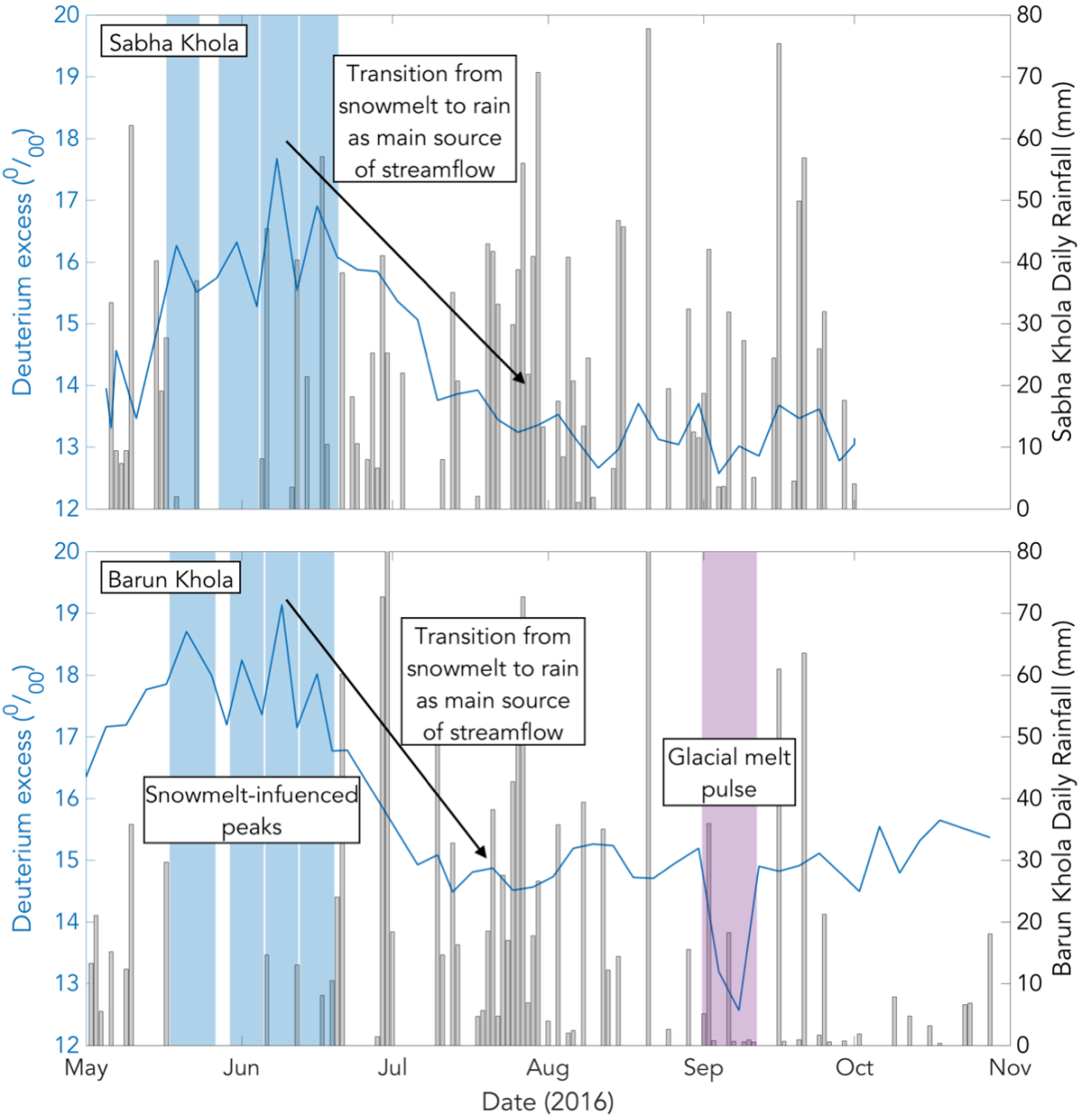

Figure 6. Temporal variation of daily rainfall and 4-day deuterium excess values sampled at the mouth of the Barun Khola and Sabha Khola from late April through October 2016. Rainfall data from CHIRPS are averaged over the Barun and Sabha Khola basins, respectively. deuterium excess values in the Barun and Sabha Kholas, increase through May, peak in June and decline through September. The peaks in May and June represent an increasing contribution of WWD-sourced snow from melting at the onset of the monsoon

(higher deuterium excess values) followed by a transition to ISM-sourced rainfall (lower deuterium excess values) during the summer season. The decline deuterium excess in the Barun Khola in early September is indicative of a glacial melt pulse following peak temperatures in August (see Figure S1). These events are marked with shaded boxes and labeled accordingly.

5 Discussion

5.1 $\delta^{18}O$ and δD lapse rates are strongly controlled by elevation and water sources

Through targeted sampling in low- and high-elevation watersheds replicated across the pre- and post-monsoon seasons, we find nonlinear trends in $\delta^{18}O$ and δD stable isotope lapse rates of river samples that are strongly controlled by elevation and mixing of source waters (i.e. snowmelt, glacial melt, and groundwater). The seasonal transition in precipitation from WWD snowmelt to ISM rainfall acts as an additional control on $\delta^{18}O$ and δD lapse rates. Given the terrain of the region, samples collected in the Barun Khola encompassed a nearly 4-km vertical range over a 33-km horizontal path while Sabha Khola samples covered a 1.2-km elevation rise within a 25-km path. This dense sampling approach should minimize the influence of variables other than elevation, but when we compare the pre- and post-monsoon data there is evidence that stable isotope lapse rates are highly variable across seasons, suggesting controls beyond elevation. River water $\delta^{18}O$ and δD values represent an integrated signal of contributing sub-drainages and tributaries, which are sourced from snowmelt, glacial melt, and groundwater. In the Barun Khola, the weakening lapse rates in river samples from the pre- to post-monsoon season are similar to the weakening signal and depletion of $\delta^{18}O$ and δD values in the glacier- and snowmelt-sourced

samples (Figs. 2 and 3). Snowmelt-sourced samples have a relatively lower $\delta^{18}O$- and δD-elevation relationship and less variability across the pre- to post-monsoon season compared to the glacier and river samples, which is likely because these samples are sourced from a single moisture source each season. The transition in $\delta^{18}O$ and δD values as well as the isotope-altitude relationship in the river samples reflects a shift in the relative contributions of snowmelt and glacial melt to river discharge as well as a broader shift from WWD-sourced precipitation in the spring to ISM-sourced water in the fall after most or all snowpack has melted (Taylor Smith & Bookhagen, 2018).

In the lower-elevation sites in the Sabha Khola, where there is no glacial contribution and snowmelt is minimal, the $\delta^{18}O$ and δD lapse rates increase from the pre- to post-monsoon season, which may reflect a transition from deeper subsurface flow in the pre-monsoon season to recent elevation-controlled ISM rainfall inputs in the post-monsoon season. This transition is reflected in the $\delta^{18}O$ and δD lapse rates of the two types of groundwater samples. Samples collected from groundwater-fed surface water tributaries, which likely integrate shallow and deeper groundwater, have more variation across seasons and reflect the isotopic signature of recent ISM rainfall more than the spring/well samples, which likely drain from the shallow vadose zone and are influenced by evaporation-driven fractionation. Notably, the $\delta^{18}O$ and δD lapse rates of the groundwater samples and the Sabha Khola river samples are similar, which implies an overlap in source waters between the Sabha Khola and local groundwater. The $\delta^{18}O$ and δD lapse rates in both the Sabha and Barun Kholas validate the "catchment effect" described in Dutton et al. (2005) and filled their articulated need posed by Dutton et al. (2005) to investigate the potential non-linearity of $\delta^{18}O$ and δD lapse rates at high elevations.

Our isotope lapse rates most closely align with van der Veen et al. (2018), whose data also exhibit nonlinear δD lapse rates that strengthen around 4000-m elevation in the western Himalaya, and Racoviteanu et al. (2013), whose study includes high-elevation snow samples from the eastern Himalaya (Fig. 7 and details in Table 3). Varay et al. (2017) demonstrate a strengthening of δ^{18}O and δD lapse rates from the pre- to post-monsoon season in the low-elevation Tons and Yamuna watersheds in the western Himalaya while the δ^{18}O and δD lapse rate in the higher elevation Sutlej basin remains relatively stable across seasons. In general, studies from the west and central Himalaya report δ^{18}O and δD lapse rates that are notably weaker than those found in our study. We attribute the differences in δ^{18}O and δD lapse rates to the paucity of high-elevation data, the spatial coverage of our sampling approach, the west-to-east gradient in snow coverage and snow water equivalents (Immerzeel et al., 2009; Smith & Bookhagen, 2018), as well increased contribution of δ^{18}O- and δD-depleted glacier and snowmelt to surface water at high-elevation sites. These factors emerge as clear controls on δ^{18}O and δD lapse rates when we compare studies across the Himalayan front (Fig. 7). Broadly, we know that sites in the western Himalaya have stronger WWD influence than the east, whereas the eastern Himalaya sites have a stronger ISM influence than the west. This relative influence of WWD versus ISM precipitation is reflected in regional patterns of δ^{18}O and δD lapse rates (Fig. 7) with the steepest lapse rates occurring in large basins with relatively greater snowpack from the WWD and drainage areas that include headwaters in the Tibetan Plateau, where the ISM influence is weaker than the WWD. Indeed, several other studies note that δ^{18}O and δD lapse rates derived from surface waters in high-altitude regions are strongly influenced by complex precipitation patterns driven by varying influence of the ISM versus WWD, post-depositional processes in snowpack, and seasonal glacial melt (Hren

et al., 2009; Poage & Chamberlain, 2001). Our data document strong non-linear $\delta^{18}O$ and δD lapse rates in the eastern Himalaya, a region with reduced WWD influence compared to the western Himalaya, where non-linear lapse rates have also been suggested (van der Veen et al., 2018).

Reference	**Region**	**Season**	**δ18O and δD stable isotope lapse rates ($^{0}/_{00}$ km^{-1})**	**Range of elevations sampled (m)**	**Type of surface water sampled**
Mark and Mckenzie (2007)	Andes	dry season	-7	3600-4100	nonglacierized springs
Rohrmann et al. (2014)	Andes	wet season	-0.2 to -1.7	340-4836	stream
Varay et al. (2017)	West Himalaya	pre- and post-monsoon	-0.45 to -1.9	500-4200	stream
Hren et al. (2009)	Himalaya	pre- and post-monsoon	-2.9	300-5200	stream
Racoviteanu et al. (2013)	Central/East Himalaya	post-monsoon	-0.6 to -1.1 (river) -4.4 (snow)	500-6400 5300-6400	stream; snow
Wilson et al. (2016)	Central Himalaya	pre- and post-monsoon	-0.9	1500-4100	stream
Hoffmann et al. (2016)	East Himlaya	post-monsoon	-8.3*	700-4900	stream
van der Veen (2015)	West Himalaya	pre- and post-monsoon	-0.7 to -1.5 / -8.8* -1.6 to -3.9 / -32.7* -1.3 to -2.2 / -8.8 to -17.4*	1000-4100 4100-5400 1000-5400	stream
Voss et al. (this study)	East Himalaya	pre- and post-monsoon	-1.3 to -1.4 / -8.0 to -9.5* -6.0 to -6.6 / -49.8 to -54.8* -2.2 to -2.4 / -17.4 to -19.0*	350-3000 4000-6000 350-6000	stream; snow; glacier; springs

*δD lapse rate

Table 3. Summary of stable isotope lapse rates and corresponding sampling approaches from other high mountain isotope studies in the Andes and Himalaya.

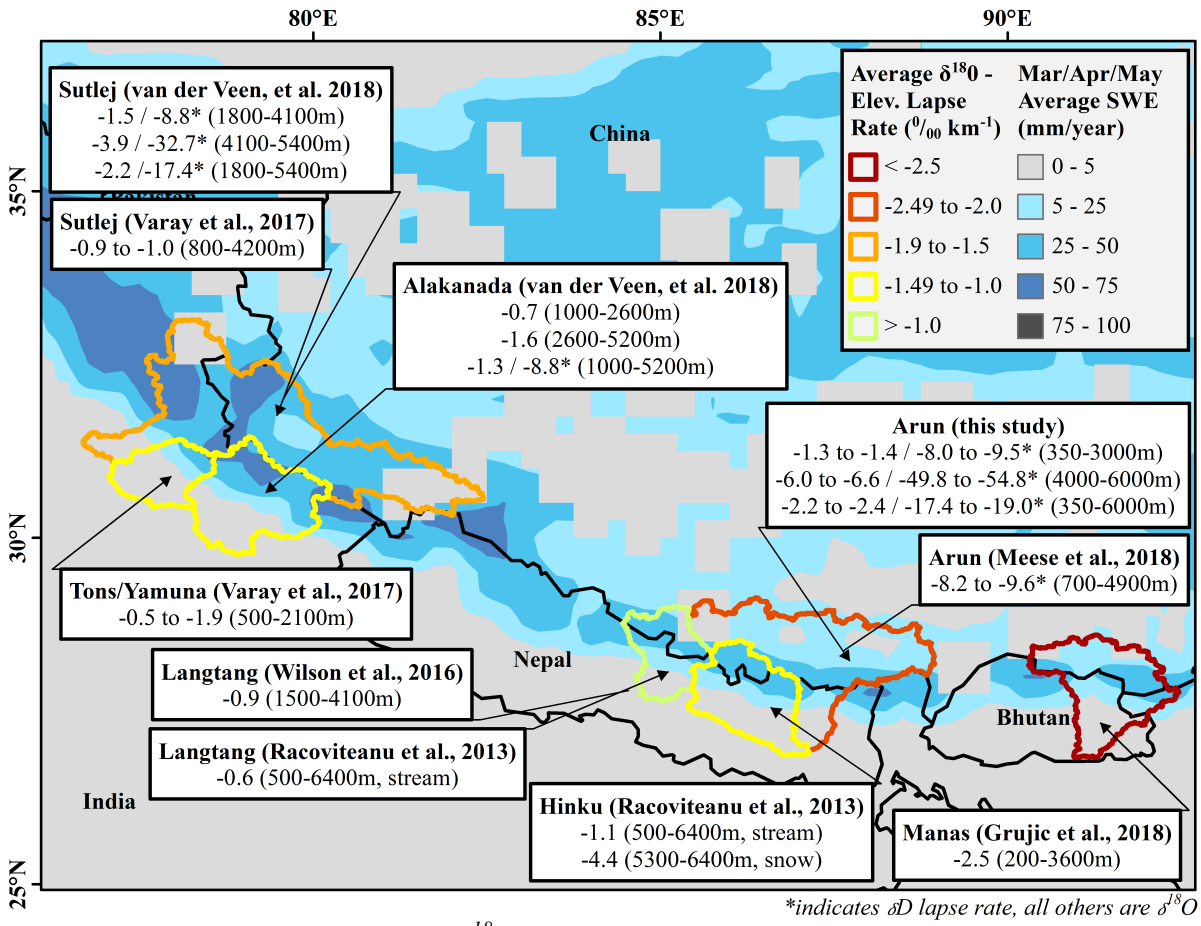

Figure 7. Comparison of reported $\delta^{18}O$ and δD isotope lapse rates across major watersheds in the Himalaya and average snow water equivalent (SWE) in the pre-monsoon (March, April, May) season from 1987 to 2009. δD lapse rates are indicated with an asterisk. $\delta^{18}O$ and δD isotope lapse rates are referenced accordingly with additional information in Table 2. The magnitude of the average $\delta^{18}O$ lapse rate covering the widest range of elevations is indicated by the watershed boundary colors as labeled in the legend. SWE averages are derived from passive microwave data from the special sensor microwave imager as reported in Smith & Bookhagen, (2018) and courtesy of T. Smith.

$\delta^{18}O$ and δD lapse rates are used as inputs to paleoclimate and modern climate reconstructions; however, as indicated by our results, there are significant differences in the

magnitude of the $\delta^{18}O$ and δD lapse rates across seasons, which is likely driven by transitions between the ISM and WWD precipitation regimes. Paleoclimate reconstructions often rely on pedogenic stable oxygen ($\delta^{18}O$) values for the analysis and assume linear lapse rates along an elevation gradient. Florea et al. (2017) argue that groundwater more accurately reflects the "true" precipitation $\delta^{18}O$ and δD lapse rate; however, our study indicates that even groundwater $\delta^{18}O$ and δD values are not fully conservative and reflect distinct seasonal transitions in moisture source. This seasonal variability is reinforced in Bershaw et al. (2012), who note that $\delta^{18}O$ and δD values reflect distinct precipitation sources and local meteorological processes along elevation transects of the Himalayan and the Tibetan Plateau. Our results support concerns raised by Hren et al. (2009) that the assumption of linear $\delta^{18}O$ and δD lapse rates will lead to misinterpretation of paleoclimatic or paleoenvironmental change. We suggest that the sensitivity of $\delta^{18}O$ and δD lapse rates to seasonal precipitation patterns can be used to improve the application of $\delta^{18}O$ and δD lapse rates in paleoclimate and modern climate analyses.

5.2 Deuterium excess as a tracer for seasonal moisture source transitions

Deuterium excess emerges as a useful tool to investigate the variation in $\delta^{18}O$ and δD values driven by precipitation patterns and seasonal moisture source transitions. Altitude controls on deuterium excess (Fig. 4) may reflect two distinct processes: (1) increased evaporation and moisture recycling in lower elevations and (2) post-depositional processes, such as sublimation, in the higher elevation regions (Taylor Smith & Bookhagen, 2018). Average deuterium excess values for WWD-sourced water are relatively high (>15 $^{0}/_{00}$) whereas ISM-sourced water averages are lower (~8-12 $^{0}/_{00}$) (Gat & Carmi, 1970; Hren et al., 2009). The pre-monsoon samples in the Barun Khola that drain snowmelt-dominated basins

(mean catchment elevations between 4000-5000 m) align with average WWD deuterium excess values whereas the post-monsoon samples more closely resemble the ISM (Fig. 4), indicating a distinct transition and mixing of moisture sources across seasons (Jeelani et al., 2013). Furthermore, the melting and refreezing of snow accentuates the elevated deuterium excess values found in drainage basins dominated by snowmelt as compared to basins dominated by glacial melt (Cooper, 1998; Taylor et al., 2002). As expected, the majority of deuterium excess values from samples collected in the Sabha Khola in both the pre- and post-monsoon seasons fall within the average range of ISM deuterium excess values with the exception of river samples collected from the headwaters of the Sabha Khola, which have snowpack from WWD precipitation and exhibit elevated deuterium excess values compared to the rest of the basin.

There is a clear correlation between loss of snowpack from pre- to post-monsoon season and decreased deuterium excess values (Fig. 5), which provides further evidence of a transition in moisture sourced from continental-sourced WWD precipitation (with relatively high deuterium excess values) in the pre-monsoon season to marine-sourced ISM precipitation in the post-monsoon season (with relatively lower deuterium excess values). Glacier melt samples exhibit almost no variation in deuterium excess values across seasons, reinforcing our hypothesis that high deuterium excess is an indicator specific to WWD-sourced precipitation in the region. River samples, which integrate snowmelt, glacial melt, and groundwater sources, decrease from the pre- to post-monsoon season, indicating shift in discharge sourced from WWD-sourced snowmelt to ISM-sourced rainfall. These results complement previous studies across the Himalaya that found similar patterns in deuterium excess linked to precipitation moisture sources in the Himalaya. In a broad survey across the

Himalaya and Tibetan Plateau, Hren et al. (2009) notes that deuterium excess values are strongly correlated to elevation and longitude, providing a distinct tracer for water vapor transported from the Bay of Bengal, Indian Ocean, and westerly-derived continental sources. Van der Veen et al. (2018) notes a transition in deuterium excess lapse rates at ~4200 m in the Sutlej River in the western Himalaya (a shift from ~1.5 $^{0}/_{00}$ km^{-1} below 4200 m to -3.0 $^{0}/_{00}$ km^{-1} above 4200 m) that correlates to increased snowpack in the high-elevation regions of the watershed. The deuterium excess breakpoint does not exist in the Alaknanda basin, about 350 km to the east of the Sutlej, which receives less snowpack and is a lower-elevation catchment. Considered in tandem with the spatial variability of WWD-derived snowpack across the Himalaya (Fig. 7), these results predict increased seasonal variation in deuterium excess and isotope values as we move westward along the Himalayan front.

Building from the results of our synoptic sampling campaign, the time-series data (Fig. 6) show increasing deuterium excess values at the onset of the monsoon, indicating increased contributions from high deuterium excess, continental-sourced WWD snowpack to river discharge, and is associated with surface temperatures greater than 0°C. Snow melt dominates the water budget until early June at which point the contributing source to streamflow transitions to lower deuterium excess, marine-sourced ISM rainfall, eventually stabilizing around mid-July when ISM rainfall dominates the water supply in both catchments. Both the Barun and Sabha Khola time-series data include peaks in deuterium excess at the onset of the monsoon in May and June (Fig. 6). Two processes could explain these peaks. First, the rivers may be flushed with snowmelt at the onset of the monsoon driven by a combination of increasing temperature and rain-on-snow melting events (Smith & Bookhagen, 2018; Wulf et al., 2012). Second, the peaks could indicate mixing with pre-

monsoon rainfall events which, based on Balestrini et al. (2016)'s study in the Khumbu region, may have elevated deuterium excess values. This is particularly true in the Sabha Khola, where deuterium excess values in early monsoon rainfall events could be further elevated due to high humidity, increased evaporation, and moisture recycling with local water vapor. Either of these processes alone or a combination of the two could drive the peaks in deuterium excess at the monsoon onset. The decline in deuterium excess values in the Barun Khola in early September is most likely associated with a pulse of low deuterium excess glacial melt water following high temperatures throughout August (see Fig. S1).

6 Conclusions

Our results indicate that $\delta^{18}O$ and δD lapse rates strengthen in the high-elevation eastern Himalaya regions. The $\delta^{18}O$ and δD lapse rates derived from river water are controlled by the relative influence of source waters (groundwater, snowmelt, and glacial melt) as well as regional climate processes, particularly seasonal variability precipitation sourced from the ISM and WWD, and as such are temporally variable on interannual time scales. Our data indicate that $\delta^{18}O$ and δD lapse rates derived from river water draining from catchments with mean elevations greater than 4 km are 5-7 times more negative than the $\delta^{18}O$ and δD lapse rates calculated from river water samples with basin elevations below 3 km. These results may influence the interpretation of paleoclimate and paleoelevation records, and reinforce the need for additional high-elevation sampling campaigns from areas with high relief in the Himalaya.

As evidenced in the time-series data, the unique seasonal variability of oxygen and hydrogen isotopes can be exploited to track individual hydro-metrological events (see also

Balestrini et al. (2016) in the Khumbu and van der Veen et al. (2018) in northwest India). Additional studies from other regions of the Himalaya that capture the variability in the strength of the ISM or WWD and incorporate sampling sites from rivers with varying contributions from snowmelt, glacial melt, groundwater, and rainfall are needed to further validate the spatiotemporal patterns described here.

By targeting low-flow periods before and after the monsoon, we derive new insights on the utility of isotopic tracers to assess base flow from meltwaters and groundwater contributing to Himalayan Rivers. In small- and mid-sized catchments, such as the Barun Khola and Sabha Khola, rivers are ungauged and in-situ meteorological data are nonexistent. Our data highlight the timing of snowmelt events and can be used to broadly assess the potential impacts of glacial retreat, seasonal and interannual variability in snowpack, and regional shifts in the intensity and timing of the ISM and WWD on the composition of Himalayan rivers (Bolch et al., 2012; Cannon et al., 2015; Malik et al., 2016). These results contribute to a growing body of work from the Himalaya and Andes (see Hill et al., (2018)) that utilize oxygen and hydrogen stable isotope tracers, particularly deuterium excess, to define the spatiotemporal indicators of rain, snow and glacial meltwaters, and groundwater to assess seasonal fluxes in high mountain rivers.

Chapter IV. Deciphering source-water contributions to streamflow during the winter-dry season in the eastern Himalaya using geochemical and isotopic tracers

1 Introduction

Rivers sourced from the Himalaya provide a critical water supply for South Asia (Beniston, 2003; Immerzeel et al., 2010). Different water sources – snowmelt, glacial melt, groundwater, and rain – contribute to discharge, but the timing and relative magnitude of these contributions varies both seasonally and geographically. Broadly, we know that rainfall from the Indian Summer Monsoon (ISM) dominates river discharge from June to September and that rainfall contributions to streamflow decrease along an east-to-west transect (Bookhagen & Burbank, 2010; Malik et al., 2016). Snowpack from Winter Westerly Disturbances (WWD) is a critical source to streamflow from December to April and its influence increases along an east-to-west gradient (Barry, 2008; Bookhagen & Burbank, 2010; Lang & Barros, 2004; Smith et al., 2017; Smith & Bookhagen, 2018). Glacier melt is variable and is dependent on a variety of factors, including elevation, debris-cover, and the relative influence of WWDs (Alford & Armstrong, 2010; Bajracharya et al., 2015; Bolch et al., 2012; Rounce et al., 2015; Scherler et al., 2011). In general, glacial melt contributions to streamflow increase from east-to-west across Himalayan catchments and supplement streamflow in low-flow periods before and after the monsoon (Immerzeel et al., 2010; Miller et al., 2012; Wulf et al., 2016). Groundwater also accounts for a portion of the water budget; however, the relative importance compared to other sources is largely unknown and dependent on the scale of the catchment, residence time of the groundwater, and the season (Andermann et al., 2012).

The contributions of these sources to Himalayan rivers changes on annual timescales (i.e. rainfall contributions are dependent on a strong or weak monsoon) and on decadal scales due to climate change. Glacier retreat is accelerating in most parts of High Mountain Asia (HMA) although there is a more complex pattern in the Karakoram region (Alford & Armstrong, 2010; Bolch et al., 2012; Brun et al., 2017; Lutz et al., 2014). Proglacial lakes are expanding and may provide a consistent supply of glacial melt to rivers; however, our understanding of the climatic and physical controls on glacial lake discharge is limited (Nie et al., 2017). The timing of the ISM and WWD storm systems is increasingly variable and the intensity of precipitation events is strengthening (Annamalai et al., 2013; Bookhagen, 2010; Cannon et al., 2015; Malik et al., 2016; Turner & Annamalai, 2012). Snowpack is declining (again, with the exception of the Karakoram region) with rapid melt events in the early monsoon season that increase flood risk and decrease the reliability of snowpack to supply water during low-flow periods (Smith et al., 2017). These combined changes affect Himalayan rivers in two major ways: first, the timing and magnitude of low and high flow periods is increasingly variable; and second, the occurrence of hazards – particularly floods, landslides, and glacial lake outburst floods – is rising (Barnett et al., 2005; ICIMOD, 2011; Petley et al., 2007). High-altitude regions dominated by glacier- and snow-fed headwaters may contribute to river discharge more substantially in shoulder periods before and after the monsoon while lower-elevation catchments where groundwater and rainfall are dominant likely flush river systems during the monsoon period.

The topographic and climatic complexity of HMA precluded many studies of small- and mid-sized watersheds in the region. This finer scale analysis is necessary for two reasons. First, these basins are more sensitive to climate change; a small perturbation in

snowpack extent or monsoon timing may have dramatic effects on streamflow in a small catchment. Second, water management decisions related to hydropower development, irrigation expansion, or natural hazard mitigation are made at this scale (Beniston, 2003). Yet, the water budgets of small- and mid-sized basins are poorly understood because they are often remote, ungauged, and difficult to access. Methodologies using hydrologic models are inadequately constrained due to a lack of traditional ground-based meteorological and hydrologic observational data. Remote-sensing methodologies are limited in their utility to decipher source waters, particularly to separate glacier melt from snowmelt, due to the coarse spatial resolution and complications from fine-scale processes, such as snow redistribution from avalanches and wind or the local energy balance that drives melt and sublimation (Litt et al., 2019; Stigter et al., 2017). To quantify the seasonal and temporal fluxes of smaller catchments, extensive technical infrastructure would be needed, ranging from glacier monitoring to groundwater assessments. This infrastructure does not exist and is difficult to maintain in remote Himalayan catchments.

Several recent studies explore the water budgets of small- and mid-sized basins by using geochemical and isotopic tracers to characterize and estimate snowmelt, glacial melt, rainfall, and groundwater contributions to streamflow (Maurya et al., 2011; Meese et al., 2016; Racoviteanu et al., 2013; van der Veen et al., 2018; Voss et al., 2018; Williams et al., 2016; Wilson et al., 2015). Broadly, the approach exploits the natural variation of solute concentrations as well as δD and δ^{18}O values in rainfall, snowmelt, glacial melt, and groundwater to quantify the relative contribution of each component within a watershed. Differences in ion concentrations can be attributed to weathering and ion exchange within soil and bedrock, and indicate the residence time or flow path of a specific water source,

whereas isotopic differences are mostly controlled by elevation and precipitation moisture source. The geochemical fingerprints of snowmelt, glacial melt, groundwater, or rainfall are distinct and provide a useful method to disentangle water budgets in high mountain catchments (Frenierre & Mark, 2014).

Our study builds on the aforementioned body of literature to assess HMA water supply. This study offers a baseline analysis of the seasonal variation of source waters in the Barun Khola and Sabha Khola, two tributaries to the Arun River, a watershed in eastern Nepal. Specifically, we characterize drainages fed by seasonal snowmelt, glacial melt, and groundwater by their dissolved ion concentrations, δD, and δ^{18}O values. We then explore the applicability of these tracers to estimate the relative contributions of individual sources that contribute to streamflow using the hydrochemical basin characterization model (HBCM; Baraer et al., (2009)). The data presented here are unique in two ways. First, we synthesize geochemical *and* isotopic tracers to partition seasonal snowmelt, debris-covered glacial melt, proglacial lake melt, and groundwater. Second, the dense spatial and temporal coverage of our data allows us to explore the hydrologic and climatic processes that control source water contributions to discharge. We identify specific combinations of dissolved ions and isotopes to separate (1) snow versus glacial melt waters and (2) water sourced from monsoon rain versus winter snowpack. We address gaps in knowledge related to the timing and magnitude of snowmelt and glacial melt as well as the relative input of subsurface groundwater to river discharge.

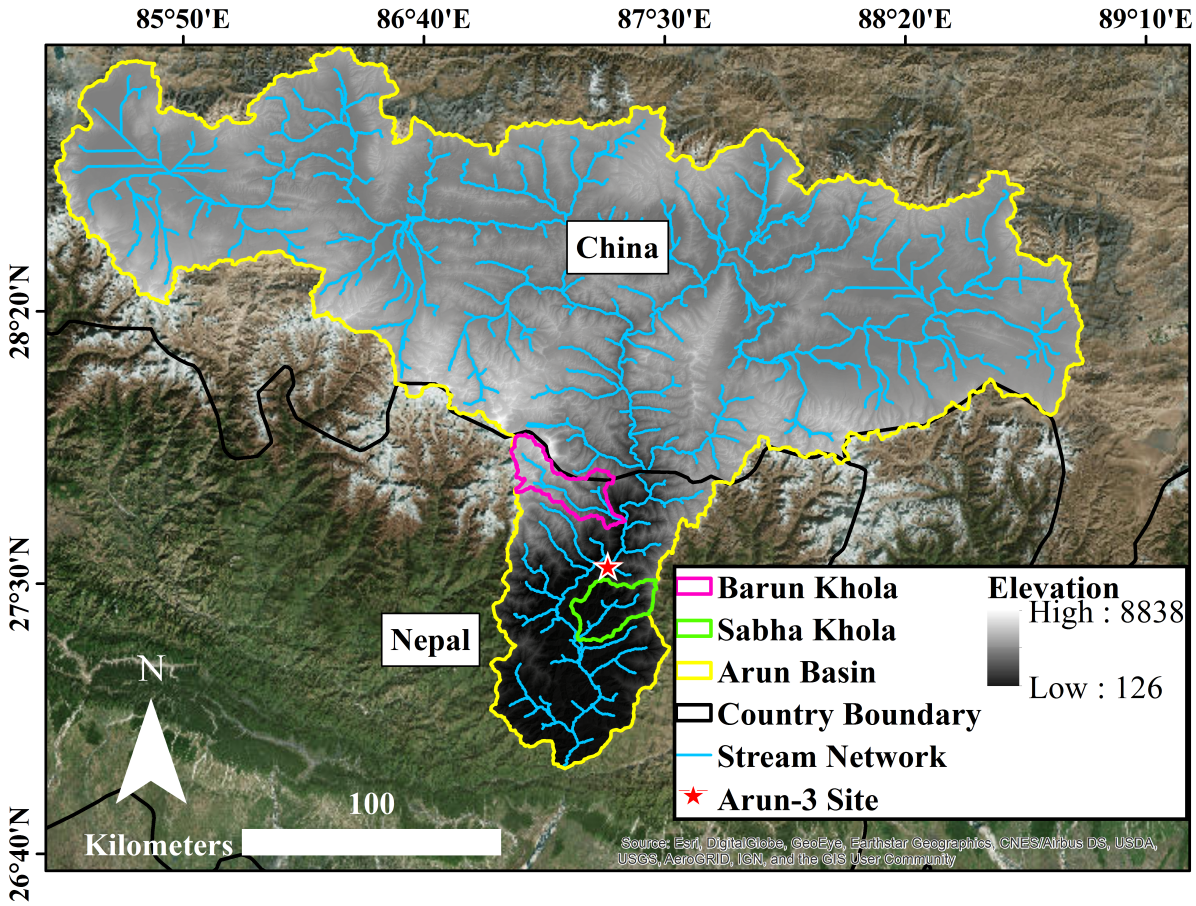

Figure 1. Regional map of the Arun watershed located in the eastern Himalaya with headwaters in Tibet draining into eastern Nepal. The paired catchments analyzed in this study – the high-elevation Barun Khola and low-elevation Sabha Khola – are highlighted accordingly. Elevation data are derived from NASA's Shuttle Radar Topography Mission (SRTM) global 1 arc second dataset for Asia (NASA JPL, 2013).

2 Paired Catchment Approach: Characteristics of the Barun and Sabha Kholas

The eastern Himalaya provide a unique setting to assess the spatiotemporal variation of rainfall, snowmelt, glacier melt, and subsurface flow contributions to streamflow. The region is influenced by both the ISM and WWDs, contains significant glacierized areas, and offers a mix of vegetation coverage, including terraced agriculture, dense forest, and alpine

grasslands. The 33,000 km^2 Arun River contains ~15% glacierized area and is estimated to receive ~25% of annual streamflow from snowmelt and ~70% from rainfall (Bookhagen & Burbank, 2010; RGI Consortium, 2017). Approximately 85% of the Arun River is located in the Tibetan Plateau, and consequently, the headwaters of the Arun are climatically distinct from the downstream portion of the river that drains through the Himalaya in Nepal. The Tibetan portion of the Arun lies in the rainshadow of the Himalaya and likely derives most of its streamflow from snow and glacial melt (Gonga-Saholiariliva et al., 2016; Meese et al., 2018). To control for a single climate regime, this study targets the Barun Khola and Sabha Khola, two tributaries in the downstream, Nepal-side of the Arun River (Figure 1). The Barun Khola is a ~468 km^2 glacierized sub-catchment with a mean catchment elevation of 4758 masl and ~30% glaciated area while the Sabha Khola is a 549 km^2 lower elevation catchment (mean elevation 1503 masl) that receives some seasonal snowpack and has undergone extensive land use change from agricultural terracing. The paired catchment approach allows us to investigate the varying contributions from glacier melt, seasonal snowmelt, and groundwater that are driven by the physical attributes of the two watersheds while maintaining similar seasonal precipitation patterns.

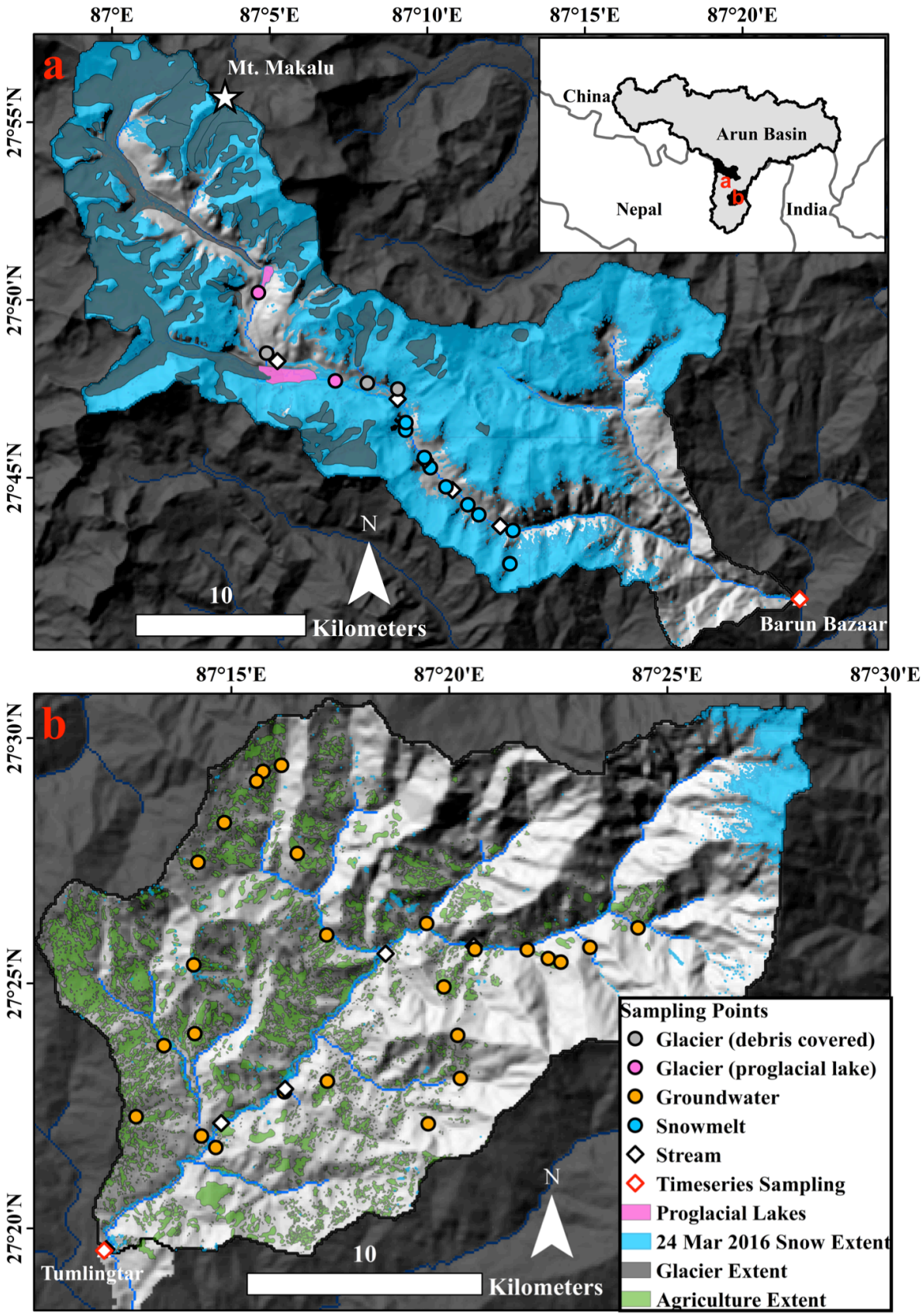
a
Mt. Makalu
China
Arun Basin
Nepal
India
a
b
87°E
87°5'E
87°10'E
87°15'E
87°20'E
27°55'N
27°50'N
27°45'N
N
10
Kilometers
Barun Bazaar
b
87°15'E
87°20'E
87°25'E
87°30'E
27°30'N
27°25'N
27°20'N
N
10
Kilometers
Tumlingtar
Sampling Points
Glacier (debris covered)
Glacier (proglacial lake)
Groundwater
Snowmelt
Stream
Timeseries Sampling
Proglacial Lakes
24 Mar 2016 Snow Extent
Glacier Extent
Agriculture Extent

Figure 2. Map of the Barun Khola and Sabha Khola (a and b, respectively). Glacier extent is from the Randolf Glacier Inventory derived from Global Land Ice Measurements from Space (GLIMS) (RGI Consortium, 2017). Agriculture extent is estimated from Landsat imagery and cross-validated with manual adjustments in Google Earth. Snow extent for 24 March 2016 is derived from a Landsat OLI 8 image. Samples are classified based on the dominant type of source water (snowmelt, glacial melt, groundwater) found within the drainage area contributing to the respective sample.

The Barun Khola exhibits a steep elevation gradient ranging from ~1000-m asl to over 8000-m asl at the summit of Mount Makalu. Along this transition, the land cover shifts from dense forest in the lower elevations (~1000-m to 3500-m) to subalpine shrubs and grasslands (~3500-m to 4800-m) and finally to barren alpine (above 4800-m)(Zomer et al., 2001). The average hillslope angle in the Barun Khola is at 30° and the region has frequent landslides, high erosion rates, and thin soil cover (Olen et al., 2015). The complex land cover limits the potential for subsurface flow. Two glacial lakes, one of which is rapidly expanding as the Lower Barun Glacier melts, dominate the headwaters of the Barun Khola and may pose a risk for a glacial lake outburst flood (Rounce et al., 2016). These physical characteristics render the Barun Khola an ideal sub-basin to partition the geochemical and isotopic signatures of glacier melt and seasonal snowmelt (Figure 2a).

The Sabha Khola differs from the Barun in two major ways: first, it is not glaciated; and second, the landscape is significantly altered from land use change to support local agriculture. The Sabha Khola drains a similarly sized area, but the catchment has a lower mean elevation than the Barun Khola that ranges from 200-m at Tumlingtar to 4600-m at the

headwater ridgelines. The average hillslope angle in the Sabha is 26° with many hillsides terraced to support local subsistence agriculture. Approximately 12% (64 km^2) of the watershed is cropland - predominantly rice, millet, and cardamom - that is clustered in the lower regions of the watershed (see Figure 1b). While the Sabha and Barun Kholas are controlled by the same regional precipitation patterns, the Sabha Khola receives substantially less seasonal snowpack from WWDs and greater rainfall during the ISM than the Barun Khola. Snowpack in the Sabha Khola is limited to the headwaters. The physical characteristics of the Sabha Khola allow us to parse the relative influence of seasonal snowpack versus rainfall-derived subsurface flow on discharge (Figure 2b).

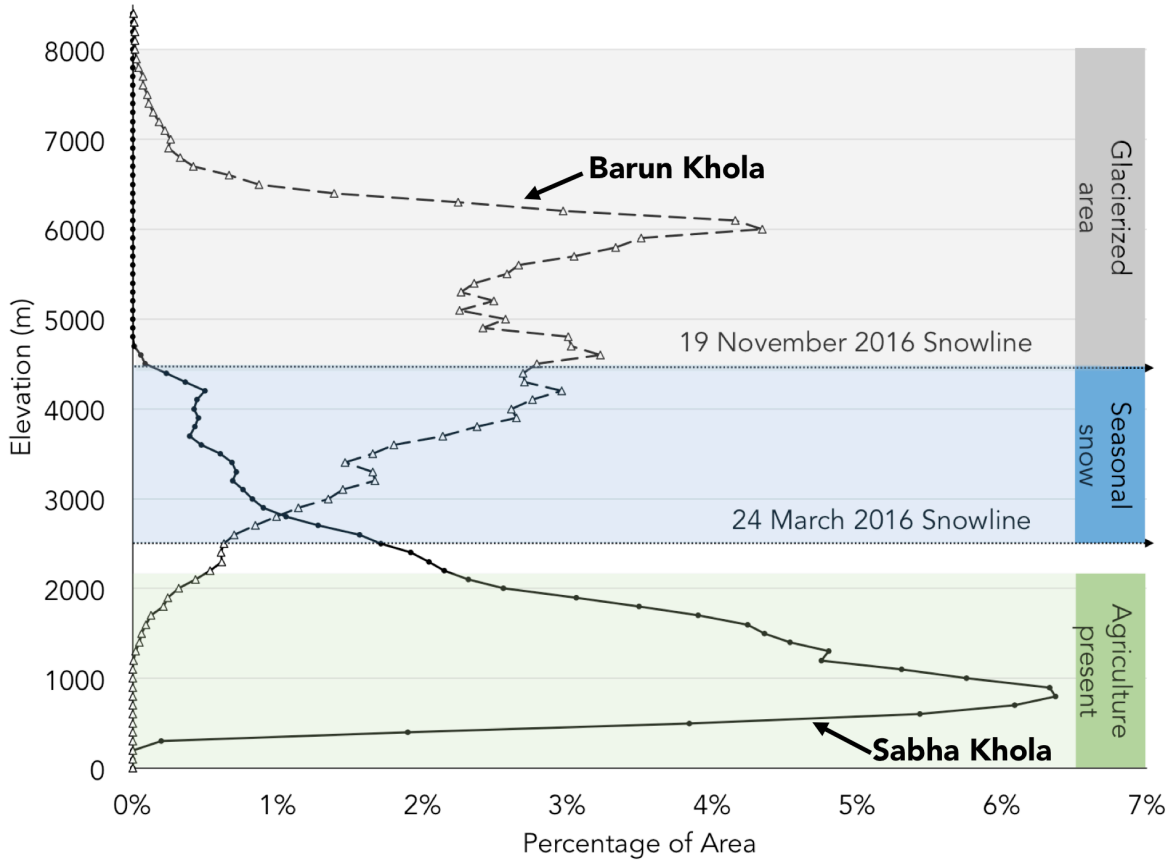

Figure 3. Hypsometric plot of the Barun Khola and Sabha Khola with bins in 100-m increments and land cover transition. Elevation bins were derived from the Shuttle Radar

Topography Mission 1-arc second global void-filled data product accessed from U.S. Geological Survey. Glacier elevations are estimated from the Randolf Glacier Inventory derived from Global Land Ice Measurements from Space (GLIMS) (RGI Consortium, 2017). Agriculture elevations are estimated from Landsat imagery and cross-validated with manual adjustments in Google Earth and field-based observations. Snowlines are estimated with Landsat 8 OLI imagery on 24 March and 11 November 2016, to provide estimates for snow extent before and after the monsoon.

3 Data and Methods

3.1 Hydrochemical Basin Characterization Method (HBCM)

Mixing models have been used in high mountain catchments in both the Himalaya and the Andes to determine the relative contributions of snowmelt, glacial melt, groundwater, and rain to river discharge (Baraer et al., 2009; Mark et al., 2005; Wilson et al., 2015). We apply the hydrochemical basin characterization method (HBCM) developed by Baraer et al., (2009), which uses the following mass balance equation to exploit the distinct geochemical and isotopic signatures of river sources to determine the relative contributions of each source to streamflow:

$$C_{tot_j} = \frac{\sum_{i=1}^{n} \left(C_{i_j} Q_i \right) + \varepsilon_j}{Q_{tot}}$$

C_{totj} and C_{ij} indicate the relative concentration or proportion of a tracer (j) at a mixing point for one of the total n identified potential end members (i); Q_{tot} and Q_i represent the total discharge at the mixing point (if discharge data are available) or the proportional contribution of the tracer i; and, ε_j, which is ideally near zero and corresponds to the residual error that

results from the accumulation of inaccuracies and uncertainties associated with the data and model. Assumptions of the HBCM model include: (1) unknown, additional sources are not included; (2) the geochemical tracers are conservative; (3) there is significant differentiation (>5%) among the various tracers to accurately represent individual source waters; and, (4) tracer concentrations are spatially constant or treated as different components. Tracers were selected using a principal component analysis (PCA) and bivariate plot interpretation, both of which reflects the geologic and landscape controls on dissolved ion concentrations. The HBCM model tests all possible combinations of tracers in a quasi-Monte Carlo approach and reports the 20 results with the lowest residual errors (additional details of the model are described in Baraer et al., (2015)). Here we assess all model results using 2- to 7-tracer combinations that exhibited less than 2% residual error. We report the mean and standard deviation of the mixing model results to provide an uncertainty estimate that arises from different combinations of tracers.

Unlike the end-member mixing analysis developed in Christophersen & Hooper (1992) and Hooper (2003), the HBCM allows spatial variation in the end-members and tracers and uses the raw dissolved ion concentration values (in mg L^{-1}) as inputs to the linear mixing model equations. The mass-balance equation is applied at each main stem sample taken along the Barun Khola and Sabha Khola, offering a spatial transect of source water contributions from the headwaters to confluence with the Arun River (see Figure S1 for mixing model schematic). The headwaters are calculated first and considered an input to the next downstream mixing point. This "moving window" mixing continues until the final mixing point at the confluence with the Arun River is calculated. We investigate the utility of individual tracers to characterize source water types and their applicability at each mixing

point of the Sabha and Barun Kholas by calculating (1) the frequency that an individual tracer is used as an input and (2) that it produces a result with less than 2% residual error in different mixing combinations. This assessment allows us to determine which tracers are sufficiently different among source waters as well as which tracers produce robust mixing model results.

3.2 Geochemical and Isotopic Sampling Approach

Water samples were collected in the pre- and post-monsoon seasons from drainages fed by seasonal snowmelt, debris-covered glacier melt, proglacial lake meltwaters, and groundwater (N = 114; 57/season) following a synoptic sampling approach (see Figure 1 for geographic locations; Baraer et al., 2009; Mark et al., 2005; Wilson et al., 2015). Samples were collected in the same hydrologic year in the dry season immediately before the monsoon (April/May 2016) and resampled after the monsoon (October/November 2016) to minimize the influence of recent rainfall events. These shoulder periods represent low-flow periods when river discharge is likely sourced from snowmelt, glacial melt, and groundwater rather than dominated by ISM rainfall.

When possible, river samples were collected from the main stem of the Barun Khola and Sabha Khola every 200-m of elevation gain (N = 28; 13/season). Samples were also collected from surface water drainages that contained extensive snowpack (N = 22; 11/season), proglacial lakes (N = 4; 2/season), debris-covered glaciers (N = 6; 3/season), as well as groundwater-sourced springs/wells and surface-water tributaries draining from forested and agriculture-dominated areas (N = 56; 28/season). Snowmelt and glacial melt samples were collected as close to the snow line or glacial terminus as possible, and therefore represent an integrated value of melt sources upstream of the sample collection point.

Groundwater-sourced samples (labeled collectively as groundwater in Fig. 1) were collected from springs/wells as well as surface water tributaries sourced exclusively from rainfall-fed subsurface flow. Groundwater samples collected from springs/wells likely reflect shallow subsurface groundwater from the vadose zone with lower residence times relative to groundwater samples collected from surface water tributaries, which likely represent an integrated shallow and deep groundwater source.

Two sets of water samples were collected from each site. Each sample was filtered through 0.45-µm glass filters into 30-mL polyethylene Nalgene bottles that were rinsed three times with filtered water. Bottles were filled completely to produce a positive meniscus, sealed tightly, and wrapped with tape to prevent the formation of air bubbles and possible evaporation before laboratory analysis. Bottles were stored in a dark place until the completion of the field season and then stored in a refrigerator at 4°C at UC Santa Barbara. Additional field duplicates were collected every 10 samples for error analysis.

Samples were analyzed for $\delta^{18}O$ and δD at the German Research Center for Geosciences (GFZ) Organic Surface Geochemistry Lab with a Picarro L-2140i Laser Spectrometer. Precision for $\delta^{18}O$ and δD measurements was $\pm 0.03\ ^{0}/_{00}$ and $\pm 0.3\ ^{0}/_{00}$, respectively. Analytical uncertainties for the oxygen and hydrogen stable isotope measurements are reported as standard deviation of triplicate measurements in the data repository. Deuterium excess was calculated for each sample as $d = \delta D - 8*\delta^{18}O$ (Dansgaard, 1964). Samples were also analyzed for Ca^{2+}, Mg^{2+}, Na^{+}, K^{+}, Si, Cl^{-}, and SO_4^{2-}. Major cations (Ca^{2+}, Mg^{2+}, Na^{+}, K^{+}, Si) were analyzed at the University of California Santa Barbara's TEMPO research facilities at the Materials Research Lab with a Thermo iCAP 6300 inductively coupled plasma spectrometer. The detection limit for each solute was <0.1

mg L^{-1} with precision for Ca^{2+}, K^{+}, Mg^{2+}, Na^{+}, and Si measurements of +/- 0.03 mg L^{-1}, 0.10 mg L^{-1}, 0.01 mg L^{-1}, 0.09 mg L^{-1}, and 0.03 mg L^{-1}, respectively. Major anions (Cl^{-}, SO_4^{2-}) were measured at Stanford University's Environmental Measurements Lab with a Dionex DX-500 Ion Chromatography (IC) System. The detection limit was <0.5 mg L^{-1} with precision for Cl^{-}, SO_4^{2-} measurements of +/- 0.11 mg L^{-1} and 0.33 mg L^{-1}, respectively. All ion data are reported in milligrams per liter (mg L^{-1}) and δD and δ^{18}O isotope data are reported in delta notation as parts per thousand as related to their deviation from Vienna Mean Standard Ocean Water (VSMOW).

4 Results

4.1 Seasonal variation of geochemical data

Dissolved ion concentrations act as indicators of water flow paths and ion exchange that results from interactions with soil or bedrock (see raw data in Appendix C Tables S1 and S2). Cation solute concentrations, especially silica, and Cl^{-} are highest in groundwater-sourced drainages. Glacial melt-dominated drainages, particularly those sampled from debris-covered glaciers, have markedly high SO_4^{2-} concentrations. Seasonal snowmelt-dominated drainages are uniformly low in their anion and cation concentrations. These patterns hold across seasons, and solute concentrations are generally lower in the post-monsoon season.

4.2 Seasonal variation in isotopic data

δD and δ^{18}O values in the Barun Khola and Sabha Khola follow expected depletion and enrichment patterns based on elevation and evaporation processes. In both the pre- and post-monsoon seasons, isotope values from samples collected in the Barun Khola match

closely with the Global Meteoric Water Line (GWML: $\delta D = 8*\delta^{18}O + 10$) with slopes around 8. Samples collected in the Sabha Khola, on the other hand, have slopes of 5.6 and 6.1 in the pre- and post-monsoon seasons, respectively (Figure 3). δD and $\delta^{18}O$ values are most depleted in the high-elevation glacierized drainages and relatively enriched in the groundwater-dominated drainages. D-excess values are highest in the snowmelt-dominated drainages during the pre-monsoon seasons and decrease in the post-monsoon season. D-excess values in the other samples remain roughly constant across seasons.

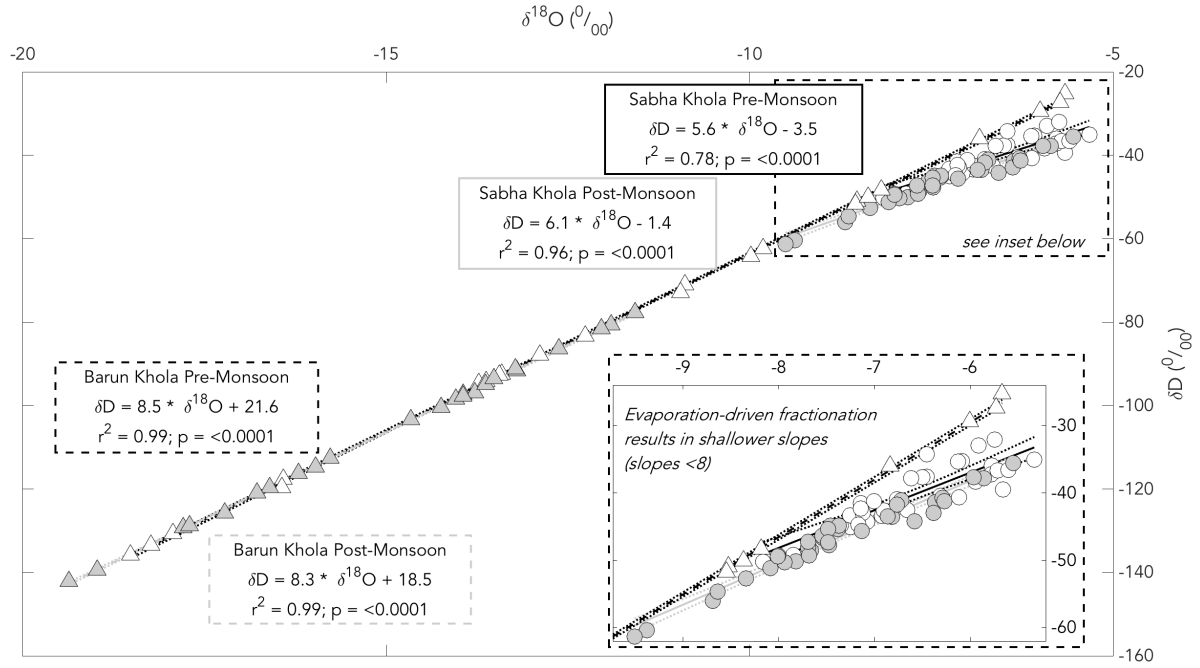

Figure 4. δD and $\delta^{18}O$ meteoric water line relationships in the pre- and post-monsoon season for both the Sabha and Barun Khola. Sabha Khola samples are indicated with circles whereas Barun Khola samples are marked with triangles. The Global Meteoric Water Line (GMWL) is estimated as $\delta D = 8*\delta^{18}O + 10$. Confidence bounds reflect 95% confidence intervals for ordinary least-squares linear regressions. Deviations from the GMWL are indicative of local processes driving isotope values. Specifically, the weaker slopes in the

Sabha Khola (5.6 in the pre-monsoon and 6.1 in the post-monsoon) are indicative of evaporation-driven fractionation.

4.3 Source water partitioning using HBCM mixing model in the Barun and Sabha Kholas

The combination of dissolved ion concentrations, δD, δ^{18}O, and d-excess values render a distinct geochemical fingerprint for each water source and satisfy the assumptions needed to apply the HBCM mixing model. We applied the HBCM mass balance equation to the pre- and post-monsoon stream samples in the Barun Khola and to the pre-monsoon samples in the Sabha Khola (see Appendix C Figures S1 for mixing model schematic). In the Barun Khola, we estimated the source water contributions at six mixing points along a longitudinal transect of the river at elevations of 4700 m, 4000 m, 3600 m, 3500 m, 3300 m, and 1200 m at the confluence with the Arun River. In the Sabha Khola, we estimated source contributions at five mixing points: 733 m, 520 m, 416 m, 414 m, and 312 m. We report the mean estimated contribution of different source waters and standard error for all mixing model results with less than 2% residual error in Table 1.

Barun Khola Spring (Pre-Monsoon)				
Mixing Point	**Mixing Point Elevation (m)**	**Glacier melt (proglacial lake)**	**Glacier melt-dominated (debris covered)**	**Seasonal snowmelt-dominated**
Headwaters (K52)	4700	92% ±1%	8% ± 1%	0%
Upper Valley (K48)	4000	74% ± 5%	26% ± 9%	0%
Mid Valley (K46)	3600	53% ± 6%	31% ± 10%	16% ± 1%
Low Valley (K40)	3500	47% ± 7%	29% ± 11%	24% ± 4%
Low Valley (K38)	3300	46% ± 7%	28% ± 11%	26% ± 4%
Arun Confluence (K60)	1200	36% ± 9%	22% ± 13%	42% ± 12%
Barun Khola Fall (Post-Monsoon)				
Mixing Point	**Mixing Point**	**Glacier melt (proglacial lake)**	**Glacier melt-dominated**	**Rainfall-influenced/**

	Elevation (m)		(debris covered)	subsurface flow
Headwaters (K85)	4700	81% ± 6%	19% ± 6%	0%
Upper Valley (K81)	4000	77% ± 8%	23% ± 9%	0%
Mid Valley (K77)	3600	56% ± 8%	39% ± 9%	5% ± 0%
Low Valley (K72)	3500	48% ± 13%	33% ± 13%	19% ± 9%
Low Valley (K70)	3300	46% ± 13%	32% ± 14%	21% ± 10%
Arun Confluence (K91)	1200	36% ± 14%	26% ± 15%	38% ± 13%

Sabha Khola Spring (Pre-Monsoon)			
Mixing Point	**Mixing Point elevation (m)**	**Seasonal snowmelt-dominated (headwaters)**	**Groundwater-dominated**
Headwaters (K13)	733	50% ± 1%	50% ± 1%
Upper Valley (K23)	520	38% ± 2%	62% ± 4%
Mid Valley (K6)	416	22% ± 4%	78% ± 8%
Low Valley (K4)	414	19% ± 8%	81% ± 15%
Arun Confluence (K62)	312	18% ± 8%	82% ± 16%

Table 1. Summary of results and potential contributions of different source waters to discharge at all mixing points (main stem samples) of the Barun and Sabha Kholas. The range of potential contributions reflects all HBCM model results for all possible combinations of isotopic and geochemical tracers (2- to 7-tracer combinations) with less than 2% residual error.

The mixing model results for the Barun Khola are illustrated in Figure 5. During the pre-monsoon period, 92% ±1% of streamflow at the headwaters is composed of glacial melt from proglacial lakes with the remaining 8% ± 1% sourced from drainages dominated by debris-covered glaciers. Moving downstream, the contribution of seasonal snowmelt increases until the final mixing point at the confluence with the Arun River where 36% ± 9% of streamflow is sourced from proglacial lake melt water, 22% ± 13% from drainages with debris-covered glaciers, and 42% ± 12% from drainages with seasonal snowmelt. In the

post-monsoon period, the elevation pattern remains the same with contributions from glacial melt greatest in the headwaters of the Barun Khola and contributions from precipitation-influenced drainages increasing downstream. In the post-monsoon season, the overall contribution from proglacial lake melt water decreased to 36% ± 14%, debris-covered glacier melt increased to 26% ± 15%, and drainages that contained snowpack in the pre-monsoon season but are now rainfall-influenced remain roughly the same (38% ± 13%).

In the Sabha Khola, we apply the HBCM in the pre-monsoon season when the headwaters of the Sabha Khola contain extensive snowpack that is geochemically and isotopically distinct from the downstream groundwater-dominated drainages. In the post-monsoon season, once all the headwater snowpack has melted, differentiation among source waters in the Sabha Khola is inconclusive due to the homogenous geochemical make-up of the samples collected. In the pre-monsoon period, water sourced from the snowmelt-dominated headwaters contributes approximately 18% ± 8% of discharge at the confluence with the Arun River while groundwater-sourced drainages contribute the remaining 82% ± 16% (Figure 6). In the post-monsoon season, all seasonal snowpack in the Sabha Khola has melted we assume that 100% of discharge is sourced from deep groundwater or shallow subsurface flow recently recharged from ISM rainfall.

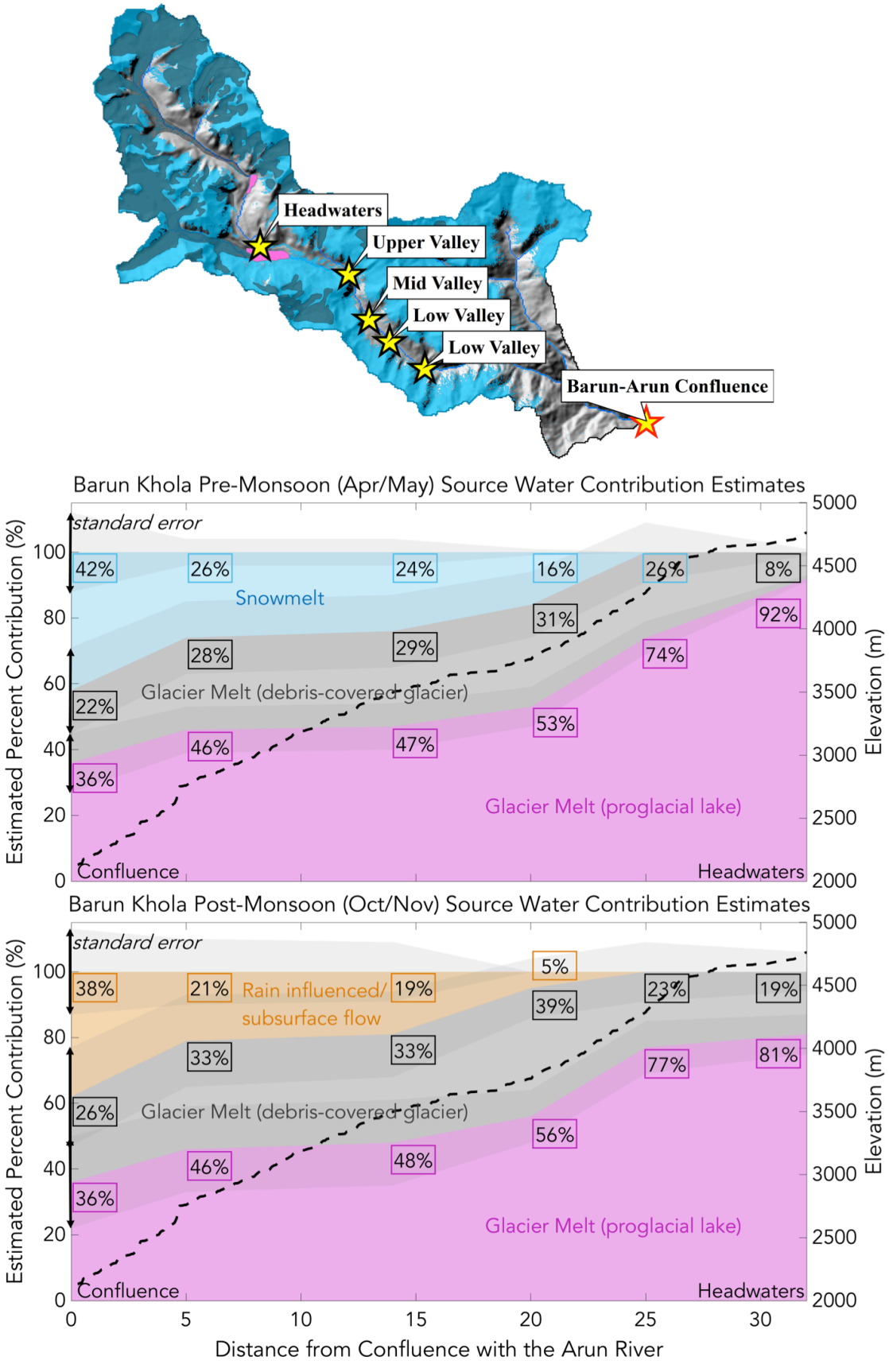
Headwaters
Upper Valley
Mid Valley
Low Valley
Low Valley
Barun-Arun Confluence
Barun Khola Pre-Monsoon (Apr/May) Source Water Contribution Estimates
standard error
42%
26%
24%
16%
26%
8%
Snowmelt
28%
29%
31%
74%
92%
Glacier Melt (debris-covered glacier)
22%
46%
47%
53%
36%
Glacier Melt (proglacial lake)
Confluence
Headwaters
Estimated Percent Contribution (%)
Elevation (m)
Barun Khola Post-Monsoon (Oct/Nov) Source Water Contribution Estimates
standard error
38%
21%
Rain influenced/
subsurface flow
19%
5%
39%
23%
19%
33%
33%
77%
81%
26%
Glacier Melt (debris-covered glacier)
46%
48%
56%
36%
Glacier Melt (proglacial lake)
Confluence
Headwaters
Estimated Percent Contribution (%)
Elevation (m)
Distance from Confluence with the Arun River

Figure 5. HBCM water budget estimates separation results for the April-May pre-monsoon (top) season and October-November post-monsoon (bottom) season in the Barun Khola. Source water types are designated based on the dominant source water in the drainage area for the respective sample. The percent contribution represents the results from the HBCM mixing model analysis with the lowest residual error (<2%) consistent across combinations of tracers.

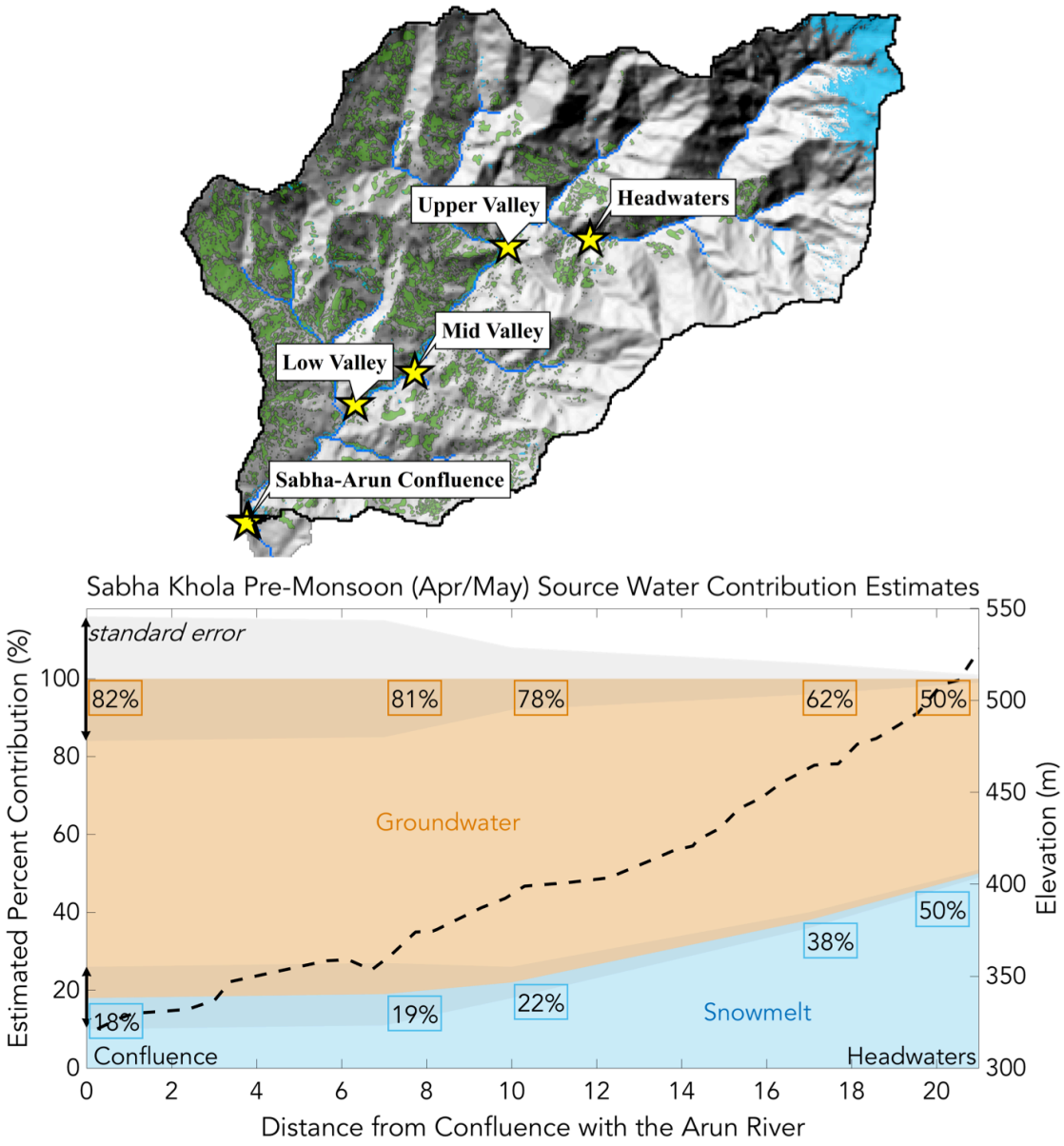

Figure 6. HBCM water budget estimates for the April-May pre-monsoon season in the Sabha Khola. Source water types are designated based on the dominant source water in the drainage area for the respective sample. The percent contribution represents the results from the HBCM mixing model analysis with the lowest residual error (<2%) consistent across combinations of tracers.

4.4 Utility of individual tracers applied in the mixing model

In the pre-monsoon season in the Barun Khola, SO_4^{2-} and δD were used as inputs to every mixing point and d-excess, Ca^{2+}, Mg^{2+}, Na^{+}, and K^{+} were used in at least half of the confluence points. That said, SO_4^{2-}, Mg^{2+}, and d-excess were the most frequently used tracers that produced reliable results (<2% residual error). In the post-monsoon season, δD and Ca^{2+} are used as inputs at all mixing points, but δD, Ca^{2+}, Mg^{2+}, and d-excess produce model results within the 2% residual error limits. In the Sabha Khola, d-excess is the only tracer used in every mixing point, and it is used in combination with δD, SO_4^{2-}, Mg^{2+}, and Na^{+} to produce mixing model results with less than 2% residual error.

5 Discussion

5.1 Dissolved ion concentrations, δD, and $\delta^{18}O$ as unique tracers for source waters

Glacier-sourced samples have high concentrations of solutes that reflect the chemical and mechanical weathering processes of glacier retreat, particularly ion exchange within proglacial lakes and interaction with debris on the glacier surface. In the Barun Khola, high concentrations of dissolved ions associated with glacial silt (Ca^{2+}, Mg^{2+}, K^{+}, SO_4^{2-}) are consistent with geochemical analyses of glaciers in other parts of the Himalaya (Tartari et al., 1998). Sulfate emerges as a valuable tracer for glacier-derived water due to increased sulfide oxidation during glacial retreat (Anderson, (2007); Salerno et al., (2016); see Figure S2). Samples from seasonal snowmelt have the lowest solute concentrations in both the pre- and post-monsoon seasons, indicating little ion exchange from interaction with bedrock or soils. In groundwater-sourced samples, variation in the concentrations of solutes is indicative of increased water residence time within the catchment and is influenced by the physical

landscape and land management practices across the basin (i.e. agriculture terracing). Samples collected at the bottom of hillslopes and draining from terraced areas have higher dissolved ion concentrations than the samples collected closer to ridgelines, suggesting greater ion exchange with soil and bedrock and, potentially, longer groundwater residence times. Dissolved ion concentrations in most samples decrease from the pre- to post-monsoon season and indicate mixing with ISM rainfall, which is known to have low solute concentrations in this region of the Himalaya (Balestrini et al., 2016).

δD and δ^{18}O data from the Barun and Sabha Kholas are strongly controlled by elevation and seasonal moisture source (Figure 3). Samples collected from the Sabha Khola exhibit an enriched isotopic signature discernable by a deviation in slope from the global meteoric water line (Figure 3 inset). A slope shallower than 8 indicates that evaporation-driven fractionation has occurred and is consistent with known fractionation processes associated with subsurface, groundwater resources (Gat, 2010; Hsieh et al., 1998). High d-excess values are correlated to snowmelt-dominated drainages in the pre-monsoon season in both the Barun Khola and Sabha Khola and match with average WWD-sourced precipitation values, rendering d-excess a useful tracer to track WWD-derived snowpack in both watersheds (Meese et al., (2018); van der Veen et al., (2018); see Appendix C Figure S3). In the post-monsoon season, after all seasonal snowpack has melted, the d-excess values of the snowmelt-sourced drainages align closely with known averages from ISM precipitation, indicating that these drainages are now sourced predominately from rainfall (Jeelani et al., 2013).

5.2 Water budgets in the pre- and post-monsoon seasons

Our analysis of the utility of the tracers indicates that d-excess is useful to

differentiate WWD-derived snowpack, SO_4^{2-} correlates to glacial melt, and other dissolved ions, mainly Ca^{2+}, Mg^{2+}, Na^{+}, indicate weathering processes and ion exchange linked to shallow subsurface or deeper groundwater. A principal component analysis of the water samples confirms that these attributes can effectively characterize and separate these distinct water sources (see Appendix C Figure S4).

In the Sabha Khola, we found that seasonal snow is a critical source in upstream portions of the catchment during the pre-monsoon season (contributing 50% ± 1%); however, subsurface groundwater is the prime contributor to discharge moving downstream and in the post-monsoon season. Critically, Smith & Bookhagen (2018) found that snowpack is declining in this region of the Himalaya. While discharge data do not exist for the Sabha Khola, our results indicate that streamflow in the headwaters of the basin is seasonally dependent on snowmelt. A decline in snowpack may increase the variability of discharge in the dry season and poses a potential risk that requires consideration in local water management decisions.

In the Barun Khola, the role of glacial melt is strongest in the headwaters and decreases moving downstream toward the Barun-Arun River confluence. This spatial pattern is consistent with a glacierized catchment (Racoviteanu et al., 2013); however, the overall contribution of glacial melt relative to seasonal snowmelt is greater than what we initially hypothesized. Surprisingly, our results suggest that the overall contribution of glacial melt to streamflow remains relatively stable across seasons, which diverges from previous studies that found greater snowmelt contributions in the pre-monsoon and a transition to glacial melt during the warmer post-monsoon season (Bolch et al., 2012; Bookhagen & Burbank, 2010). We find that drainages with debris-covered glaciers contribute more in the post-monsoon

season, which may indicate increased melting as a result of higher temperatures throughout the summer season.

To explore the sensitivity of our mixing model to the "water type" classifications that we assigned to each drainage area, we calculated the contribution of each sample as well as cumulative contributions between each mixing point (see Appendix C Figure S5 and S6). In general, the spatial patterns of the contributing areas remain constant across the seasons with the glacierized headwaters contributing nearly half of river discharge and the lower reaches of the basin with extensive seasonal snowpack contributing about a third. While we acknowledge that the drainage area contributing to each sample likely contains a mixture of sources, the differentiation in the geochemical and isotopic data is distinct and we are confident in our assigned classifications as well as the mixing model results (see Appendix C for PCA result in Figure S4).

5.3 Spatial scale impacts on Himalayan water budget partitioning

The preponderance of water budget analyses in HMA rely on remotely-sensed data and hydrologic modeling to assess larger river basins (i.e. the whole of the Arun watershed or the entire Ganges or Brahmaputra river basins). Notably, results from small- and mid-sized basin studies, including this one, produce different estimates of snow and glacial melt contributions than those reported in the regional, larger-scale analyses. Using a similar methodology, Wilson et al., (2015) assessed the central Himalayan Langtang watershed and estimated a glacier melt contribution of 36% in the pre-monsoon season and 22% in the post-monsoon season. Racoviteanu et al., (2013) used an ice ablation model and a simple two-component mixing model with δD and δ^{18}O values and calculated glacier melt contributions to in the post-monsoon season for the Langtang Valley (68%), Betrawti (10%), Trushili

(5%), Hinku (21%), and Dudh Koshi (7%). Further east, Williams et al., (2016) assessed Bhutan's Chamkar Chhu River and estimated that glacial melt contributes 14% and 31% of streamflow in the early- and post-monsoon seasons, respectively.

At a larger scale, assessments using remote-sensing data and hydroclimatic energy balance models produce notably different estimates of source contributions to river discharge. Bookhagen & Burbank (2010) found that snowmelt accounts for ~50% of streamflow in the western Himalaya (where the ISM is weaker) and less than 20% in the central and eastern Himalaya (where the ISM is stronger) on an annual timescale; but, in the early-monsoon season snowmelt may contribute over 40% of streamflow in the central and eastern Himalaya. Armstrong et al., (2018) quantified water budgets for the upper regions (above 2000-m) of the Syr Darya, Amu Darya, Indus, Ganges, and Brahmaputra River basins and report snow contributions between 65%-72% of annual streamflow in all of the basins with the exception of the Ganges (43%), and glacial melt contributions of less than 3% with the exception of the Amu Darya (8%). The study describes glacier melt peaking in the late summer (July and August); however, even during this season, the overall contribution of glacial melt remains relatively small (<10% of total discharge). While the seasonal and spatial patterns described in Bookhagen & Burbank (2010) and Armstrong et al., (2018) are similar, the estimated proportions of snowmelt and rainfall contributing to discharge are much greater than the results from the small- and mid-sized basin studies described above.

When we compare these studies, spatial scale and temporal variation emerge as defining controls on Himalayan source waters. Kaser et al., (2010) explains that glacier melt is a critical water source for high-elevation watersheds in arid regions with minimal influence from the ISM, especially compared to larger basins draining in the lowlands of the Himalaya.

Similarly, Racoviteanu et al., (2013) posits that the influence of glacial melt on discharge is directly proportional to the glacier coverage in a basin. Additionally, the emergence of glacial lakes adds complexity to these hydrologic systems because seasonal variability in the outflow from glacial lakes is poorly understood, as is the potential of these lakes to act as a buffer to discharge from headwater regions. Our results imply that proglacial lakes may act as a stable source to streamflow across seasons in high-elevation, glacierized catchments.

6 Conclusions

This study indicates that a combination of *both* isotopic and dissolved ion data are necessary to fully distinguish between potential source waters in the Himalaya, especially to separate glacial melt from snowmelt. We find that glacial melt is a significant component of the water budget in both the pre- and post-monsoon seasons in high-elevation headwaters whereas seasonal snowpack contributes nearly 40% of streamflow in the pre-monsoon season. Recent studies indicate that snowpack in eastern HMA is declining and, combined with retreating glaciers, we anticipate these changes may present new strains on water supply, particularly in high-elevation catchments or in low-elevation headwaters where snow is an essential source during the pre-monsoon season (Smith & Bookhagen, 2018). Additional analyses of small- and mid-sized basins are needed to provide a basin-specific context for local water management. This study contributes a critical perspective of water resources in small tributaries in the eastern Himalaya and can be used in tandem with regional studies to assess the baseline spatiotemporal variability of water resources along the Himalayan front.

Chapter V. Conclusions

This study was motivated by the urgent need to quantify water resources in the Himalaya and to enhance our understanding of the baseline hydroclimatic factors that control river systems in the region. Specifically, we were interested in evaluating the main sources of water that contribute to streamflow in the Arun watershed and to assess how these sources vary seasonally and across spatial scales. Our study site in the eastern Himalaya provided an ideal location to assess both the influence of the Indian Summer Monsoon and the Winter Westerly Disturbances, which contribute rain and snow, respectively, in discrete seasonal cycles. Additionally, the Arun watershed's unique physical landscape – extensive glacier coverage, headwaters in the Tibetan Plateau, agriculture terracing in low elevation regions – allowed us to constrain glacier melt and groundwater sources. We explored the applicability of geochemical and isotopic tracers to qualitatively and quantitatively explain hydrologic processes and water flowpaths in the Arun River system, and identified unique attributes associated with specific water sources that can be used across the Himalaya or, potentially, other high mountain regions. Collectively, the conclusions from this dissertation contribute to three overarching themes: (1) Himalayan water budgets; (2) tools for water resource assessments in remote and ungauged basins; and, (3) opportunities for and limitations of data-informed water management in High Mountain Asia.

5.1 Assessing Himalayan water budgets and considerations under climate change

Overall, our water budget and regional assessment of the hydroclimatic drivers in the Arun River (Chapters 2 and 4) compliment those of other small- and mid-sized basin studies across the Himalaya as well as regional remote-sensing analyses. We find that snowmelt contributes substantially in the pre-monsoon season (April to mid-June) before the Arun

Valley is flushed with rainfall from the ISM from June through September. Glacier melt contributions to the Arun River increase through summer and peak in the post-monsoon season (September to October) from increased melting in the Tibetan Plateau headwaters as well as high-elevation tributaries. In the Arun's glacierized tributaries, i.e. the Barun Khola, glacial melt is a key source contributing ~60% of river discharge in low-flow seasons before and after the monsoon. We also identify snowmelt as a vital source in non-glacierized basins, particularly in the headwaters of watersheds with extensive snowpack.

These results offer a foundational assessment of water resources in an eastern Himalaya watershed from which we can predict potential changes and tension points that will arise due to climate change. In particular, we identify two climate-driven trends that will impact the region's water availability: first, eastern Himalaya snowpack is diminishing and melt patterns are shifting (Barnett et al., 2005; Smith & Bookhagen, 2018); and second, glacier retreat is accelerating with proglacial lakes expanding across the region (Rounce et al., 2016). As snowpack declines and the timing of melt events becomes temporally condensed, tributaries that rely on snowmelt in the pre-monsoon season will likely see a decline in discharge. In the Arun watershed, many microhydropower plants are proposed in small tributaries that drain glacierized or snowpack-laden headwaters. Future variability in snowpack extent and the timing of melt events will inevitably alter the efficacy of the proposed microhydropower plants.

Additionally, the accelerated retreat of glaciers in the region poses two challenges. First, the rapid growth of large proglacial lakes poses a risk of glacial lake outbursts floods (GLOFs). In the Arun basin, the Lower Barun Lake is identified as a high risk lake (Rounce et al., 2016). Large hydropower plants proposed on the main stem of the Arun River,

specifically the Arun-3, are particularly vulnerable to GLOFs as evidenced by a recent event in 2017 that resulted in a debris flow that blocked flow of the Arun River for several days and transported large boulders down the river (Byers, 2017; Rest, 2012). In addition to new hazards, the second dilemma linked to glacial retreat is the potential loss of a stable water source, particularly in low-flow seasons outside of the monsoon and in tributaries with extensive glacier coverage. In the early stages of glacial retreat, the increased melt from will result in increased runoff throughout the Himalaya; however, the region will eventually cross a "peak water" threshold and glacial melt contributions to streamflow will decline (Lutz et al., 2014). This transition is trivial for the transboundary, continental river basins draining HMA – the Ganges, Bramaputra, and Indus – that are sourced predominantly from rainfall and snowpack (Armstrong et al., 2018). However, glacial retreat may ultimately exacerbate water stress in small- and mid-sized Himalayan that rely on meltwaters during low-flow, dry seasons.

5.2 Methodological approaches to assess water resources in ungauged basins

This dissertation effectively utilized geochemical and isotopic tracers to decipher seasonal moisture sources in the Himalaya, to separate snowmelt from glacial melt contributions to river discharge, and to explore the hydroclimatic processes that influence the composition of meteoric water. Our methodological approach is similar to other studies across the Himalayan belt and reinforces the effectiveness of these tools to characterize water resources in remote and ungauged basins, particularly in fine-scale assessments of small- and mid-sized watersheds where remote-sensing data may be limited due to its course resolution. In particular, we identify deuterium excess as an exceptional tracer to partition storm systems in the Himalaya and as a marker for seasonal snowmelt. We also pinpoint sulfate as a

reliable indicator for glacial melt. These two metrics have been used in other watersheds across the Himalaya and have the potential to be applied more extensively in the region to elucidate the varying contributions of snowmelt and glacial melt in river systems with diverse hydroclimatic controls, such as varying glacier coverage or influence from ISM versus WWD.

Our discussion of the differences between large- and small-scale water budget assessments in Chapter 4 alludes to an opportunity to integrate remote-sensing and field-based methodological approaches. Both approaches bypass the paucity of ground-based meteorological and hydrologic gauge data in the Himalaya; however, they differ in their scale of assessment. Remote-sensing data provide insights to regional processes as well as large-scale basins whereas field-based data are more localized and often evaluate process specific to an individual watershed. Combined, remote-sensing and field-based studies offer a more complete and accurate assessment of water resources in the Himalaya across spatial and temporal scales. This nuanced understanding of Himalayan water resources is critical to acknowledge when leveraging data from remote-sensing or field-based studies to inform water management decisions.

5.3 Implications for water management in Nepal and High Mountain Asia

The geopolitics of water management in HMA are marked by competition between India and China as well as individual nations' attempts to establish economic independence through energy, agriculture, and industrial security (Wirsing, 2013; Wirsing et al., 2012). Nepal, in particular, has ample water resources and is poised in a strategic location nestled between India and China. The Government of Nepal's prioritization of hydropower and road infrastructure, particularly via transboundary agreements with India and China, is an attempt

to (1) achieve economic independence, (2) establish political cooperation and goodwill between its neighboring superpowers, and (3) simultaneously reinforce state-building and security at home (Lord, 2014; Murton et al., 2016). Yet, the proposed management of Nepal's water resources is built on a tenuous foundation of hydrologic data that will only become more variable under a changing climate (Agrawala et al., 2003). For the proposed Arun-3 hydropower plant in particular, the results from this dissertation provide a broad assessment of water supply in the Arun River and its tributaries, which may offer a useful framework for large- and microhydropower planning throughout the basin.

As discussed in the previous section and Chapter 4, the results from this research highlight the importance of scale in matching hydrologic data with water management decisions. While large-scale analyses from remote-sensing studies provide essential information for regional or transboundary planning, field-based studies of local basins provide essential data to inform local water management decisions, particularly irrigation and hydropower planning. The scale of the management decision dictates which data are needed to appropriately inform the decision at hand; however, data-informed management is a challenge in remote and ungauged watersheds. This dissertation offers one approach to assess water resources in such scenarios and urges new synthesis between remote-sensing and field-based studies to characterize water availability across HMA.

5.4 Future Directions

This study explores the applicability of geochemical and isotopic tracers to describe the hydroclimatic processes and water budgets of rivers in high mountain regions. Future research to build on the results from this dissertation could be directed toward two priorities: (1) new data collection across HMA and (2) data synthesis among existing field-based and

remote-sensing studies. Specifically, Chapter Three identifies non-linear $\delta^{18}O$ and δD lapse rates that could be cross-validated in other high-altitude transects. Ideally, an assessment of the $\delta^{18}O$ and δD lapse rates would include both rainfall and river water samples. To complement the results from Chapter Four, additional studies that follow a similar methodological approach but strategically target watersheds from other regions of the Himalaya with varying influence from the ISM, WWD, glaciers, and groundwater would further constrain our knowledge of Himalayan water budgets. A concerted effort is needed to combine the relative water budget analyses described in this dissertation with volumetric estimates of discrete water sources (snowmelt, glacial melt, groundwater, rainfall) to accurately partition Himalayan river hydrographs. Since an expansive network of ground-based gauge and observational tools does not exist given the inaccessible terrain of the region, this is a priority that could be fulfilled with remote-sensing approaches.

5.5 Concluding remarks

The watersheds of HMA offer a unique "living laboratory" to explore water resources in remote and ungauged river basins while providing practical data to inform pressing water management decisions. Given the dynamic hydroclimatic and political conditions of the region, there is an urgent need for ongoing research to quantify the variability of rain, snow, glacier, and groundwater contributions to river discharge. Equally important, the communication of scientific results to the appropriate stakeholders at local, national, and regional levels is vital to steer data-informed management decisions and to build trust between decision-makers and scientists. This dissertation was rooted in collaboration with local community members in the Arun Valley, politicians from the Government of Nepal, and a range of international stakeholders, including nongovernmental organizations, regional

think tanks, and the U.S. Agency for International Development. While the scientific results of this study contribute to our knowledge of high mountain water resources, I hope that the overarching dissertation design, particularly the citizen science campaign, offers inspiration for future research to be intentional, ambitious, and inclusive in linking stakeholder and scientific priorities. As we strive for a sustainable water future, this type of active engagement among scientists, the public, and decision-leaders will be the springboard for innovative research and robust policy outcomes to tackle the grand challenges of our lifetime.

References

Aggarwal, P. K., Gat, J. R., & Froehlich, K. F. (2006). *Isotopes in the Water Cycle: Past, Present and Future of a Developing Science*. Springer Science & Business Media.

Agrawala, S., Raksakulthai, V., van Aalst, M., Larsen, P., Smith, J., & Reynolds, J. (2003). *Development And Climate Change In Nepal: Focus On Water Resources And Hydropower*. 64.

Alford, D., & Armstrong, R. (2010). The role of glaciers in stream flow from the Nepal Himalaya. *The Cryosphere Discussions*, *4*(2), 469–494. https://doi.org/10.5194/tcd-4-469-2010

Andermann, C., Longuevergne, L., Bonnet, S., Crave, A., Davy, P., & Gloaguen, R. (2012). Impact of transient groundwater storage on the discharge of Himalayan rivers. *Nature Geoscience*, *5*(2), 127–132. https://doi.org/10.1038/ngeo1356

Anderson, S. P. (2007). Biogeochemistry of Glacial Landscape Systems. *Annual Review of Earth and Planetary Sciences*, *35*(1), 375–399. https://doi.org/10.1146/annurev.earth.35.031306.140033

Annamalai, H., Hafner, J., Sooraj, K. P., & Pillai, P. (2013). Global Warming Shifts the Monsoon Circulation, Drying South Asia. *Journal of Climate*, *26*(9), 2701–2718. https://doi.org/10.1175/JCLI-D-12-00208.1

Armstrong, R. L., Rittger, K., Brodzik, M. J., Racoviteanu, A., Barrett, A. P., Khalsa, S.-J. S., … Armstrong, B. (2018). Runoff from glacier ice and seasonal snow in High Asia: separating melt water sources in river flow. *Regional Environmental Change*. https://doi.org/10.1007/s10113-018-1429-0

Bajracharya, S. R., Maharjan, S. B., Shrestha, F., Guo, W., Liu, S., Immerzeel, W., & Shrestha, B. (2015). The glaciers of the Hindu Kush Himalayas: current status and observed changes from the 1980s to 2010. *International Journal of Water Resources Development*, *31*(2), 161–173. https://doi.org/10.1080/07900627.2015.1005731

Balestrini, R., Delconte, C. A., Sacchi, E., Wilson, A. M., Williams, M. W., Cristofanelli, P., & Putero, D. (2016). Wet deposition at the base of Mt Everest: Seasonal evolution of the chemistry and isotopic composition. *Atmospheric Environment*, *146*, 100–112. https://doi.org/10.1016/j.atmosenv.2016.08.056

Baraer, M., McKenzie, J. M., Mark, B. G., Bury, J., & Knox, S. (2009). Characterizing contributions of glacier melt and groundwater during the dry season in a poorly gauged catchment of the Cordillera Blanca (Peru). *Advances in Geosciences*, *22*, 41–49. https://doi.org/10.5194/adgeo-22-41-2009

Baraer, Michel, McKenzie, J., Mark, B. G., Gordon, R., Bury, J., Condom, T., … Fortner, S. K. (2015). Contribution of groundwater to the outflow from ungauged glacierized catchments: a multi-site study in the tropical Cordillera Blanca, Peru. *Hydrological Processes*, *29*(11), 2561–2581. https://doi.org/10.1002/hyp.10386

Barnett, T. P., Adam, J. C., & Lettenmaier, D. P. (2005). Potential impacts of a warming climate on water availability in snow-dominated regions. *Nature*, *438*(7066), 303–309. https://doi.org/10.1038/nature04141

Barry, R. G. (2008). *Mountain Weather and Climate Third Edition* (3rd ed.). Retrieved from http://ebooks.cambridge.org/ref/id/CBO9780511754753

Beniston, M. (2003). Climatic Change in Mountain Regions: A Review of Possible Impacts. In H. F. Diaz (Ed.), *Climate Variability and Change in High Elevation Regions: Past,*

Present & Future (pp. 5–31). Retrieved from http://link.springer.com.proxy.library.ucsb.edu:2048/chapter/10.1007/978-94-015-1252-7_2

Bershaw, J., Penny, S. M., & Garzione, C. N. (2012). Stable isotopes of modern water across the Himalaya and eastern Tibetan Plateau: Implications for estimates of paleoelevation and paleoclimate. *Journal of Geophysical Research: Atmospheres*, *117*(D2), D02110. https://doi.org/10.1029/2011JD016132

Bolch, T., Kulkarni, A., Kääb, A., Huggel, C., Paul, F., Cogley, J. G., … Stoffel, M. (2012). The State and Fate of Himalayan Glaciers. *Science*, *336*(6079), 310–314. https://doi.org/10.1126/science.1215828

Bookhagen, B. (2010). Appearance of extreme monsoonal rainfall events and their impact on erosion in the Himalaya. *Geomatics, Natural Hazards and Risk*, *1*(1), 37–50. https://doi.org/10.1080/19475701003625737

Bookhagen, B., & Burbank, D. W. (2010). Toward a complete Himalayan hydrological budget: Spatiotemporal distribution of snowmelt and rainfall and their impact on river discharge. *Journal of Geophysical Research: Earth Surface*, *115*(F3), n/a–n/a. https://doi.org/10.1029/2009JF001426

Brun, F., Berthier, E., Wagnon, P., Kääb, A., & Treichler, D. (2017). A spatially resolved estimate of High Mountain Asia glacier mass balances from 2000 to 2016. *Nature Geoscience*, *10*(9), 668–673. https://doi.org/10.1038/ngeo2999

Burt, T. P., & Pinay, G. (2005). Linking hydrology and biogeochemistry in complex landscapes. *Progress in Physical Geography*, *29*(3), 297–316. https://doi.org/10.1191/0309133305pp450ra

Byers, A. (2017, July 27). High Water. *Atavist*. Retrieved from https://nepalitimes.atavist.com/high-water

Cannon, F., Carvalho, L. M. V., Jones, C., & Bookhagen, B. (2015). Multi-annual variations in winter westerly disturbance activity affecting the Himalaya. *Climate Dynamics*, *44*(1–2), 441–455. https://doi.org/10.1007/s00382-014-2248-8

Carpenter, C., & Zomer, R. (1996). Forest Ecology of the Makalu-Barun National Park and Conservation Area, Nepal. *Mountain Research and Development*, *16*(2), 135–148. https://doi.org/10.2307/3674007

Caves, J. K., Winnick, M. J., Graham, S. A., Sjostrom, D. J., Mulch, A., & Chamberlain, C. P. (2015). Role of the westerlies in Central Asia climate over the Cenozoic. *Earth and Planetary Science Letters*, *428*, 33–43. https://doi.org/10.1016/j.epsl.2015.07.023

Christophersen, N., & Hooper, R. P. (1992). Multivariate analysis of stream water chemical data: The use of principal components analysis for the end-member mixing problem. *Water Resources Research*, *28*(1), 99–107. https://doi.org/10.1029/91WR02518

Consortium, R. G. I. (2017). *Randolph Glacier Inventory 6.0*. https://doi.org/10.7265/N5-RGI-60

Cooper, L. W. (1998). Chapter 4 - Isotopic Fractionation in Snow Cover. In C. Kendall & J. J. McDonnell (Eds.), *Isotope Tracers in Catchment Hydrology* (pp. 119–136). https://doi.org/10.1016/B978-0-444-81546-0.50011-2

Dansgaard, W. (1964). Stable isotopes in precipitation. *Tellus*, *16*(4), 436–468. https://doi.org/10.1111/j.2153-3490.1964.tb00181.x

Dutton, A., Wilkinson, B. H., Welker, J. M., Bowen, G. J., & Lohmann, K. C. (2005). Spatial distribution and seasonal variation in 18O/16O of modern precipitation and river

water across the conterminous USA. *Hydrological Processes*, *19*(20), 4121–4146. https://doi.org/10.1002/hyp.5876

Faure, G. (1998). *Principles and applications of geochemistry : a comprehensive textbook for geology students*. Retrieved from http://espace.library.uq.edu.au/view/UQ:331441

Florea, L., Bird, B., Lau, J. K., Wang, L., Lei, Y., Yao, T., & Thompson, L. G. (2017). Stable isotopes of river water and groundwater along altitudinal gradients in the High Himalayas and the Eastern Nyainqentanghla Mountains. *Journal of Hydrology: Regional Studies*, *14*, 37–48. https://doi.org/10.1016/j.ejrh.2017.10.003

Frenierre, J. L., & Mark, B. G. (2014). A review of methods for estimating the contribution of glacial meltwater to total watershed discharge. *Progress in Physical Geography*, *38*(2), 173–200. https://doi.org/10.1177/0309133313516161

Froehlich, K., Gibson, J. J., & Aggarwal, P. K. (2002). *Deuterium excess in precipitation and its climatological significance*. Retrieved from http://inis.iaea.org/Search/search.aspx?orig_q=RN:34017972

Funk, C., Peterson, P., Landsfeld, M., Pedreros, D., Verdin, J., Shukla, S., … Michaelsen, J. (2015). The climate hazards infrared precipitation with stations—a new environmental record for monitoring extremes. *Scientific Data*, *2*, 150066. https://doi.org/10.1038/sdata.2015.66

Gat, J. R., & Carmi, I. (1970). Evolution of the isotopic composition of atmospheric waters in the Mediterranean Sea area. *Journal of Geophysical Research*, *75*(15), 3039–3048. https://doi.org/10.1029/JC075i015p03039

Gat, Joel R. (2010). *Isotope Hydrology: A Study of the Water Cycle*. Retrieved from http://www.worldscientific.com/worldscibooks/10.1142/p027

Gonga-Saholiariliva, N., Neppel, L., Chevallier, P., Delclaux, F., & Savéan, M. (2016). Geostatistical Estimation of Daily Monsoon Precipitation at Fine Spatial Scale: Koshi River Basin. *Journal of Hydrologic Engineering*, *21*(9), 05016017. https://doi.org/10.1061/(ASCE)HE.1943-5584.0001388

Grujic, D., Govin, G., Barrier, L., Bookhagen, B., Coutand, I., Cowan, B., … Najman, Y. (2018). Formation of a Rain Shadow: O and H Stable Isotope Records in Authigenic Clays From the Siwalik Group in Eastern Bhutan. *Geochemistry, Geophysics, Geosystems*, *0*(0). https://doi.org/10.1029/2017GC007254

Hill, A. F., Stallard, R. F., & Rittger, K. (2018). Clarifying regional hydrologic controls of the Marañón River, Peru through rapid assessment to inform system-wide basin planning approaches. *Elem Sci Anth*, *6*(1). https://doi.org/10.1525/elementa.290

Hooper, R. P. (2003). Diagnostic tools for mixing models of stream water chemistry. *Water Resources Research*, *39*(3), 1055. https://doi.org/10.1029/2002WR001528

Hren, M. T., Bookhagen, B., Blisniuk, P. M., Booth, A. L., & Chamberlain, C. P. (2009). δ18O and δD of streamwaters across the Himalaya and Tibetan Plateau: Implications for moisture sources and paleoelevation reconstructions. *Earth and Planetary Science Letters*, *288*(1–2), 20–32. https://doi.org/10.1016/j.epsl.2009.08.041

Hsieh, J. C. C., Chadwick, O. A., Kelly, E. F., & Savin, S. M. (1998). Oxygen isotopic composition of soil water: Quantifying evaporation and transpiration. *Geoderma*, *82*(1–3), 269–293. https://doi.org/10.1016/S0016-7061(97)00105-5

ICIMOD. (2011). *Glacial lakes and glacial lake outburst floods in Nepal* (p. 109). Retrieved from ICIMOD website: http://www.icimod.org/dvds/201104_GLOF/reports/final_report.pdf

Immerzeel, W. W., & Bierkens, M. F. P. (2012). Asia's water balance. *Nature Geoscience*, *5*, 841–842. https://doi.org/10.1038/ngeo1643

Immerzeel, W. W., Droogers, P., de Jong, S. M., & Bierkens, M. F. P. (2009). Large-scale monitoring of snow cover and runoff simulation in Himalayan river basins using remote sensing. *Remote Sensing of Environment*, *113*(1), 40–49. https://doi.org/10.1016/j.rse.2008.08.010

Immerzeel, W. W., Pellicciotti, F., & Bierkens, M. F. P. (2013). Rising river flows throughout the twenty-first century in two Himalayan glacierized watersheds. *Nature Geoscience*, *6*(9), 742–745. https://doi.org/10.1038/ngeo1896

Immerzeel, Walter W., Beek, L. P. H. van, & Bierkens, M. F. P. (2010). Climate Change Will Affect the Asian Water Towers. *Science*, *328*(5984), 1382–1385. https://doi.org/10.1126/science.1183188

Jeelani, Gh., Saravana Kumar, U., & Kumar, B. (2013). Variation of δ18O and δD in precipitation and stream waters across the Kashmir Himalaya (India) to distinguish and estimate the seasonal sources of stream flow. *Journal of Hydrology*, *481*, 157–165. https://doi.org/10.1016/j.jhydrol.2012.12.035

Jimenez Cisneros, B. E., Oki, T., Arnell, N. W., Benito, G., Cogley, J. G., Doll, P., … Mwakalila, S. S. (2014). 3 — Freshwater Resources. In *Climate Change 2014: Impacts, Adaptation, and Vulnerability. Part A: Global and Sectoral Aspects. Contributions of Working Group II to the Fifth Assessment Report of the Intergovernmental Panel on Climate Change* (p. 41). Cambridge University Press.

Kaser, G., Grosshauser, M., & Marzeion, B. (2010). Contribution potential of glaciers to water availability in different climate regimes. *Proceedings of the National Academy of Sciences*, *107*(47), 20223–20227. https://doi.org/10.1073/pnas.1008162107

Kendall, C., Doctor, D. H., & Young, M. B. (2014). 7.9 - Environmental Isotope Applications in Hydrologic Studies. In H. D. Holland & K. K. Turekian (Eds.), *Treatise on Geochemistry (Second Edition)* (pp. 273–327). https://doi.org/10.1016/B978-0-08-095975-7.00510-6

Kendall, C., & McDonnell, J. J. (2012). *Isotope Tracers in Catchment Hydrology*. Elsevier.

Lang, T. J., & Barros, A. P. (2004). Winter Storms in the Central Himalayas. *Journal of the Meteorological Society of Japan. Ser. II*, *82*(3), 829–844. https://doi.org/10.2151/jmsj.2004.829

Litt, M., Shea, J., Wagnon, P., Steiner, J., Koch, I., Stigter, E., & Immerzeel, W. (2019). Glacier ablation and temperature indexed melt models in the Nepalese Himalaya. *Scientific Reports*, *9*(1), 5264. https://doi.org/10.1038/s41598-019-41657-5

Lord, A. (2014). Making a 'Hydropower Nation': Subjectivity, Mobility, and Work in the Nepalese Hydroscape. *HIMALAYA, the Journal of the Association for Nepal and Himalayan Studies*, *34*(2). Retrieved from http://digitalcommons.macalester.edu/himalaya/vol34/iss2/13

Lutz, A. F., Immerzeel, W. W., Shrestha, A. B., & Bierkens, M. F. P. (2014a). Consistent increase in High Asia's runoff due to increasing glacier melt and precipitation. *Nature Climate Change*, *4*(7), 587. https://doi.org/10.1038/nclimate2237

Lutz, A. F., Immerzeel, W. W., Shrestha, A. B., & Bierkens, M. F. P. (2014b). Consistent increase in High Asia's runoff due to increasing glacier melt and precipitation. *Nature Climate Change*, *4*(7), 587–592. https://doi.org/10.1038/nclimate2237

Malik, N., Bookhagen, B., & Mucha, P. J. (2016). Spatiotemporal patterns and trends of Indian monsoonal rainfall extremes. *Geophysical Research Letters*, 2016GL067841. https://doi.org/10.1002/2016GL067841

Mark, B. G., McKenzie, J. M., & Gómez, J. (2005). Hydrochemical evaluation of changing glacier meltwater contribution to stream discharge: Callejon de Huaylas, Peru / Evaluation hydrochimique de la contribution évolutive de la fonte glaciaire à l'écoulement fluvial: Callejon de Huaylas, Pérou. *Hydrological Sciences Journal*, *50*(6), null-987. https://doi.org/10.1623/hysj.2005.50.6.975

Maurya, A. S., Shah, M., Deshpande, R. D., Bhardwaj, R. M., Prasad, A., & Gupta, S. K. (2011). Hydrograph separation and precipitation source identification using stable water isotopes and conductivity: River Ganga at Himalayan foothills. *Hydrological Processes*, *25*(10), 1521–1530. https://doi.org/10.1002/hyp.7912

Meese, B., Bookhagen, B., Olen, S. M., Barthold, F., & Sachse, D. (2018). The effect of Indian Summer Monsoon rainfall on surface water δD values in the central Himalaya. *Hydrological Processes*.

Meese, B., Feakins, S., Bookhagen, Bodo, Olen, Stephanie, Adhikari, D. P., Mainali, J., & Sachse, D. (2016). Ecologic, climatic, and geomorphic drivers of terrestrial organic matter transport in the trans-Himalayan Arun River catchment, E. Nepal. *In Review*.

Miller, J. D., Immerzeel, W. W., & Rees, G. (2012). Climate Change Impacts on Glacier Hydrology and River Discharge in the Hindu Kush–Himalayas. *Mountain Research and Development*, *32*(4), 461–467. https://doi.org/10.1659/MRD-JOURNAL-D-12-00027.1

Mölg, T., Maussion, F., & Scherer, D. (2014). Mid-latitude westerlies as a driver of glacier variability in monsoonal High Asia. *Nature Climate Change*, *4*(1), 68–73. https://doi.org/10.1038/nclimate2055

Murton, G., Lord, A., & Beazley, R. (2016). "A handshake across the Himalayas:" Chinese investment, hydropower development, and state formation in Nepal. *Eurasian Geography and Economics*, *57*(3), 403–432. https://doi.org/10.1080/15387216.2016.1236349

NASA JPL. (2013). *NASA Shuttle Radar Topography Mission Global 1 arc second* [Data set]. https://doi.org/10.5067/MEaSUREs/SRTM/SRTMGL1.003

National Research Council. (2012). *Himalayan Glaciers: Climate Change, Water Resources, and Water Security*. Retrieved from http://www.nap.edu/catalog/13449

Nie, Y., Sheng, Y., Liu, Q., Liu, L., Liu, S., Zhang, Y., & Song, C. (2017). A regional-scale assessment of Himalayan glacial lake changes using satellite observations from 1990 to 2015. *Remote Sensing of Environment*, *189*, 1–13. https://doi.org/10.1016/j.rse.2016.11.008

Olen, S. M., Bookhagen, B., Meese, B., Sachse, D., Adhikari, D. P., & Strecker, M. R. (2015). Understanding erosion rates in the Himalayan orogen: A case study from the Arun Valley. *Journal of Geophysical Research: Earth Surface*, *120*(10), 2014JF003410. https://doi.org/10.1002/2014JF003410

Pande, K., Padia, J. T., Ramesh, R., & Sharma, K. K. (2000). Stable isotope systematics of surface water bodies in the Himalayan and Trans-Himalayan (Kashmir) region. *Journal of Earth System Science*, *109*(1), 109–115. https://doi.org/10.1007/BF02719154

Petley, D. N., Hearn, G. J., Hart, A., Rosser, N. J., Dunning, S. A., Oven, K., & Mitchell, W. A. (2007). Trends in landslide occurrence in Nepal. *Natural Hazards*, *43*(1), 23–44. https://doi.org/10.1007/s11069-006-9100-3

Pfahl, S., & Sodemann, H. (2014). What controls deuterium excess in global precipitation? *Climate of the Past*, *10*(2), 771–781. https://doi.org/10.5194/cp-10-771-2014

Poage, M. A., & Chamberlain, C. P. (2001). Empirical Relationships Between Elevation and the Stable Isotope Composition of Precipitation and Surface Waters: Considerations for Studies of Paleoelevation Change. *American Journal of Science*, *301*(1), 1–15. https://doi.org/10.2475/ajs.301.1.1

Price, M., Byers, A. C., Friend, D., Kohler, T., & Price, L. W. (Eds.). (2013). *Mountain Geography: Physical and Human Dimensions* (1st ed.). Retrieved from http://www.jstor.org/stable/10.1525/j.ctt46n4cj

Racoviteanu, A. E., Armstrong, R., & Williams, M. W. (2013). Evaluation of an ice ablation model to estimate the contribution of melting glacier ice to annual discharge in the Nepal Himalaya. *Water Resources Research*, *49*(9), 5117–5133. https://doi.org/10.1002/wrcr.20370

Rest, M. (2012). Generating power: debates on development around the Nepalese Arun-3 hydropower project. *Contemporary South Asia*, *20*(1), 105–117. https://doi.org/10.1080/09584935.2011.646071

Rounce, D. R., Quincey, D. J., & McKinney, D. C. (2015). Debris-covered glacier energy balance model for Imja–Lhotse Shar Glacier in the Everest region of Nepal. *The Cryosphere*, *9*(6), 2295–2310. https://doi.org/10.5194/tc-9-2295-2015

Rounce, David R., McKinney, D. C., Lala, J. M., Byers, A. C., & Watson, C. S. (2016). A new remote hazard and risk assessment framework for glacial lakes in the Nepal Himalaya. *Hydrology and Earth System Sciences; Katlenburg-Lindau*, *20*(9), 3455–3475. http://dx.doi.org/10.5194/hess-20-3455-2016

Rounce, David R., Watson, C. S., & McKinney, D. C. (2017). Identification of Hazard and Risk for Glacial Lakes in the Nepal Himalaya Using Satellite Imagery from 2000–2015. *Remote Sensing*, *9*(7), 654. https://doi.org/10.3390/rs9070654

Rozanski, K., Araguás-Araguás, L., & Gonfiantini, R. (1993). Isotopic Patterns in Modern Global Precipitation. In P. K. Swart, K. C. Lohmann, J. Mckenzie, & S. Savin (Eds.), *Climate Change in Continental Isotopic Records* (pp. 1–36). Retrieved from http://onlinelibrary.wiley.com/doi/10.1029/GM078p0001/summary

Salerno, F., Rogora, M., Balestrini, R., Lami, A., Tartari, G. A., Thakuri, S., … Tartari, G. (2016). Glacier Melting Increases the Solute Concentrations of Himalayan Glacial Lakes. *Environmental Science & Technology*, *50*(17), 9150–9160. https://doi.org/10.1021/acs.est.6b02735

Saravana Kumar, U., Kumar, B., Rai, S. P., & Sharma, S. (2010). Stable isotope ratios in precipitation and their relationship with meteorological conditions in the Kumaon Himalayas, India. *Journal of Hydrology*, *391*(1), 1–8. https://doi.org/10.1016/j.jhydrol.2010.06.019

Scherler, D., Bookhagen, B., & Strecker, M. R. (2011). Spatially variable response of Himalayan glaciers to climate change affected by debris cover. *Nature Geoscience*, *4*(3), 156–159. https://doi.org/10.1038/ngeo1068

Smith, T., Bookhagen, B., & Rheinwalt, A. (2017). Spatiotemporal patterns of High Mountain Asia's snowmelt season identified with an automated snowmelt detection

algorithm, 1987–2016. *The Cryosphere*, *11*(5), 2329–2343. https://doi.org/10.5194/tc-11-2329-2017

Smith, Taylor, & Bookhagen, B. (2018). Changes in seasonal snow water equivalent distribution in High Mountain Asia (1987 to 2009). *Science Advances*, *4*(1), e1701550. https://doi.org/10.1126/sciadv.1701550

Stigter, E. E., Wanders, N., Saloranta, T. M., Shea, J. M., Bierkens, M. F. P., & Immerzeel, W. W. (2017). Assimilation of snow cover and snow depth into a snow model to estimate snow water equivalent and snowmelt runoff in a Himalayan catchment. *The Cryosphere*, *11*(4), 1647–1664. https://doi.org/10.5194/tc-11-1647-2017

Tartari, G. A., Tartari, G., & Mosello, R. (1998). Limnology of high altitude lakes in the Mt Everest Region (Nepal). *Memorie Dell' Istituto Italiano Di Idobiologia*, 51–76.

Taylor, S., Feng, X., Williams, M., & McNamara, J. (2002). How isotopic fractionation of snowmelt affects hydrograph separation. *Hydrological Processes*, *16*(18), 3683–3690. https://doi.org/10.1002/hyp.1232

Torres, M. A., Moosdorf, N., Hartmann, J., Adkins, J. F., & West, A. J. (2017). Glacial weathering, sulfide oxidation, and global carbon cycle feedbacks. *Proceedings of the National Academy of Sciences*, 201702953. https://doi.org/10.1073/pnas.1702953114

Turner, A. G., & Annamalai, H. (2012). Climate change and the South Asian summer monsoon. *Nature Climate Change*, *2*(8), 587–595. https://doi.org/10.1038/nclimate1495

van der Veen, I., Hassenruck, H. J., Smith, T., Deal, E., Wichura, H., Strecker, M. R., … Sachse, D. (2018). Identifying seasonal snowmelt in the western Himalaya using stable isotopes of modern surface waters and remote sensing. *Hydrological Processes*, *in review*.

Varay, L. S., Rai, S. P., Singh, S. K., & Jain, V. (2017). Estimation of snow and glacial melt contribution through stable isotopes and assessment of its impact on river morphology through stream power approach in two Himalayan river basins. *Environmental Earth Sciences*, *76*(23), 809. https://doi.org/10.1007/s12665-017-7142-3

Viviroli, D., Dürr, H. H., Messerli, B., Meybeck, M., & Weingartner, R. (2007). Mountains of the world, water towers for humanity: Typology, mapping, and global significance. *Water Resources Research*, *43*(7), W07447. https://doi.org/10.1029/2006WR005653

Vörösmarty, C. J., Green, P., Salisbury, J., & Lammers, R. B. (2000). Global Water Resources: Vulnerability from Climate Change and Population Growth. *Science*, *289*(5477), 284–288. https://doi.org/10.1126/science.289.5477.284

Voss, K. A., Bookhagen, B., Sachse, D., & Chadwick, O. A. (2018). Variation of deuterium excess in surface waters across a 5000-m elevation gradient in the east-central Himalaya. *Hydrology and Earth System Sciences Discussions*, 1–20. https://doi.org/10.5194/hess-2018-534

Williams, M. W., Wilson, A., Tshering, D., Thapa, P., & Kayastha, R. B. (2016). Using geochemical and isotopic chemistry to evaluate glacier melt contributions to the Chamkar Chhu (river), Bhutan. *Annals of Glaciology*, *57*(71), 339–348. https://doi.org/10.3189/2016AoG71A068

Wilson, A. M., Williams, M. W., Kayastha, R. B., & Racoviteanu, A. (2015). Use of a hydrologic mixing model to examine the roles of meltwater, precipitation and

groundwater in the Langtang River basin, Nepal. *Annals of Glaciology*. https://doi.org/10.3189/2016AoG71A067

Wirsing, R. G. (2013). Melting the Geopolitical Ice in South Asia. *Asia Policy*, *16*(1), 19–25. https://doi.org/10.1353/asp.2013.0029

Wirsing, R., Jasparro, C., & Stoll, D. (2012). *International Conflict over Water Resources in Himalayan Asia*. Springer.

Wulf, H., Bookhagen, B., & Scherler, D. (2012). Climatic and geologic controls on suspended sediment flux in the Sutlej River Valley, western Himalaya. *Hydrol. Earth Syst. Sci.*, *16*(7), 2193–2217. https://doi.org/10.5194/hess-16-2193-2012

Wulf, Hendrik, Bookhagen, B., & Scherler, D. (2016). Differentiating between rain, snow, and glacier contributions to river discharge in the western Himalaya using remote-sensing data and distributed hydrological modeling. *Advances in Water Resources*, *88*, 152–169. https://doi.org/10.1016/j.advwatres.2015.12.004

Z. Wan, S. H. (2015). *MOD11A1 MODIS/Terra Land Surface Temperature/Emissivity Daily L3 Global 1km SIN Grid V006*. https://doi.org/10.5067/MODIS/MOD11A1.006

Zomer, R. J., Ustin, S. L., & Carpenter, C. C. (2001). Land Cover Change Along Tropical and Subtropical Riparian Corridors Within the Makalu Barun National Park and Conservation Area, Nepal. *Mountain Research and Development*, *21*(2), 175–183. https://doi.org/10.1659/0276-4741(2001)021[0175:LCCATA]2.0.CO;2

Appendix A.

Name	Date	δ18O (‰)	Std. Dev. δ18O (‰)	δD (‰)	Std. Dev. δD (‰)	d18-excess (‰)	Sum of dissolved ions (mg L^{-1})	Na^+ (mg L^{-1})	Std. Dev. Na^+ (mg L^{-1})	K^+ (mg L^{-1})	Std. Dev. K^+ (mg L^{-1})	Mg^{2+} (mg L^{-1})	Std. Dev. Mg^{2+} (mg L^{-1})	Ca^{2+} (mg L^{-1})	Std. Dev. Ca^{2+} (mg L^{-1})	Si (mg L^{-1})	Std. Dev. Si (mg L^{-1})	Cl^- (mg L^{-1})	SO_4^{2-} (mg L^{-1})
Upper Arun 1	Apr-16	-11.8	0.0	-81.4	0.1	13.0	30.6	7.1	0.0	1.7	0.0	2.6	0.0	16.0	0.1	3.2	0.0		
Upper Arun 2	Apr-16	-11.8	0.0	-81.6	0.2	12.8	47.5	6.4	0.1	1.4	0.0	2.6	0.0	15.9	0.1	3.2	0.0	2.8	15.1
Upper Arun 3	May-16	-11.8	0.0	-81.8	0.1	12.6	29.3	6.3	0.0	1.5	0.0	2.6	0.0	15.8	0.0	3.2	0.0		
Upper Arun 4	May-16	-11.7	0.0	-80.4	0.3	13.4	49.3	5.8	0.0	1.5	0.0	2.5	0.0	17.1	0.1	3.2	0.0	3.8	14.8
Upper Arun 5	May-16	-12.1	0.0	-84.2	0.1	13.0	42.8	6.3	0.0	1.4	0.0	2.6	0.0	15.6	0.1	3.3	0.0	2.7	10.3
Upper Arun 6	May-16	-11.4	0.0	-77.4	0.1	13.9	40.1	5.4	0.0	1.4	0.0	2.3	0.0	14.0	0.1	3.0	0.0	2.4	11.1
Upper Arun 7	May-16	-10.4	0.0	-68.2	0.1	14.7	27.8	4.8	0.0	1.3	0.0	2.0	0.0	12.3	0.0	2.8	0.0	0.7	3.2
Upper Arun 8	May-16	-8.9	0.2	-55.1	0.6	15.9	28.3	3.4	0.0	1.2	0.0	1.5	0.0	10.0	0.0	2.5	0.0	1.5	8.2
Upper Arun 9	May-16	-10.2	0.0	-65.6	0.1	15.6	32.0	3.8	0.0	1.1	0.0	1.8	0.0	11.4	0.0	2.5	0.1	1.6	9.8
Upper Arun 10	May-16	-10.8	0.0	-72.9	0.1	13.9	37.3	4.6	0.0	1.3	0.0	2.1	0.0	13.1	0.1	2.8	0.0	1.9	11.5
Upper Arun 11	Jun-16	-9.3	0.0	-58.4	0.1	15.8	26.8	3.2	0.0	1.0	0.0	1.5	0.0	9.5	0.0	2.5	0.0	1.2	7.9
Upper Arun 12	Jun-16	-10.5	0.0	-69.7	0.1	14.6	35.6	5.0	0.0	1.2	0.0	1.8	0.0	11.6	0.0	2.7	0.0	3.1	9.6
Upper Arun 13	Jun-16	-8.0	0.0	-46.5	0.1	17.4	23.5	2.2	0.0	0.9	0.0	1.1	0.0	9.6	0.0	1.9	0.0	1.1	6.7
Upper Arun 14	Jun-16	-10.1	0.0	-65.8	0.1	15.2	26.3	3.7	0.0	1.6	0.0	1.7	0.0	11.1	0.0	2.4	0.0	0.7	5.0
Upper Arun 15	Jun-16	-9.0	0.0	-55.9	0.1	16.1	24.5	4.6	0.0	0.7	0.0	1.3	0.0	10.7	0.0	1.9	0.0	0.7	3.7
Upper Arun 16	Jun-16	-9.5	0.0	-60.1	0.1	15.8	24.2	2.4	0.0	1.1	0.0	1.3	0.0	9.6	0.0	2.2	0.0	1.1	5.9
Upper Arun 17	Jun-16	-9.7	0.0	-61.5	0.1	15.7	22.2	1.9	0.0	0.8	0.0	1.1	0.0	8.5	0.0	2.1	0.0	0.7	6.3
Upper Arun 18	Jul-16	-16.4	0.0	-119.4	0.2	11.9	84.9	5.5	0.0	1.1	0.0	4.3	0.0	24.8	0.1	2.7	0.0	4.6	41.9
Upper Arun 19	Jul-16	-16.4	0.0	-119.5	0.2	11.7	83.2	8.4	0.0	0.3	0.0	4.3	0.0	24.8	0.0	2.5	0.0	3.1	39.8
Upper Arun 20	Jul-16	-16.6	0.0	-120.9	0.1	11.8	61.8	6.5	0.0	0.4	0.0	4.2	0.0	24.7	0.1	2.4	0.0	1.7	21.3
Upper Arun 21	Jul-16	-16.3	0.0	-118.4	0.0	11.8	59.7	6.4	0.1	0.5	0.0	4.1	0.1	24.4	0.1	2.5	0.0	1.7	19.6
Upper Arun 22	Jul-16	-16.1	0.0	-117.4	0.1	11.7	83.4	6.7	0.0	0.9	0.0	4.2	0.0	30.0	0.1	2.4	0.0	1.9	37.3
Upper Arun 23	Jul-16	-17.3	0.0	-126.7	0.1	11.7	100.7	14.6	0.0	5.0	0.0	4.7	0.0	28.6	0.1	2.4	0.0	3.7	40.4
Upper Arun 24	Jul-16	-16.9	0.0	-123.8	0.1	11.6	93.7	8.4	0.0	0.7	0.0	4.6	0.0	26.4	0.1	2.8	0.0	6.4	43.8
Upper Arun 25	Aug-16	-16.1	0.0	-117.0	0.1	11.9	73.1	5.0	0.0	0.9	0.0	4.1	0.0	24.2	0.1	2.4	0.0	1.2	35.3
Upper Arun 26	Aug-16	-16.0	0.0	-116.8	0.1	11.2	70.7	5.7	0.0	1.0	0.0	4.1	0.0	24.3	0.1	2.5	0.0	2.4	30.6
Upper Arun 27	Aug-16	-16.0	0.0	-117.2	0.1	11.1	82.8	6.5	0.1	1.0	0.0	4.3	0.0	25.0	0.2	2.4	0.0	3.6	39.3
Upper Arun 28	Aug-16	-16.3	0.0	-119.5	0.1	11.2	99.0	11.7	0.0	0.4	0.0	4.8	0.0	26.4	0.1	2.6	0.0	6.6	46.6
Upper Arun 29	Aug-16	-11.2	0.0	-76.6	0.1	13.0	45.3	3.1	0.0	2.4	0.0	2.6	0.0	14.3	0.0	6.4	0.0	1.3	14.3
Upper Arun 30	Aug-16	-14.7	0.0	-105.1	0.1	12.2	54.8	2.6	0.0	3.3	0.0	4.4	0.0	21.0	0.1	7.1	0.0	1.4	15.1
Upper Arun 31	Aug-16	-13.3	0.0	-94.7	0.1	11.3	41.5	3.4	0.0	1.0	0.0	1.9	0.0	13.0	0.0	1.6	0.0	0.9	19.8
Upper Arun 32	Aug-16	-14.9	0.0	-106.7	0.1	12.7	40.4	2.7	0.0	0.7	0.0	2.1	0.0	13.5	0.0	2.3	0.0	0.9	18.1
Upper Arun 33	Sep-16	-14.5	0.0	-103.5	0.1	12.4	45.4	4.3	0.0	2.2	0.0	3.5	0.0	16.0	0.1	6.0	0.0	0.8	12.8
Upper Arun 34	Sep-16	-14.5	0.0	-103.9	0.1	12.4	33.5	5.2	0.0	0.6	0.0	2.6	0.0	16.2	0.0	2.6	0.0	0.5	5.9
Upper Arun 35	Sep-16	-14.6	0.0	-104.6	0.1	12.1	49.8	4.4	0.0	0.8	0.0	2.7	0.0	16.9	0.0	2.9	0.0	1.2	21.0
Upper Arun 36	Sep-16	-14.4	0.0	-103.3	0.2	12.1	43.4	3.4	0.0	1.0	0.0	2.8	0.0	17.4	0.0	2.7	0.0	0.9	14.5
Upper Arun 37	Sep-16	-14.5	0.0	-103.4	0.1	12.6	50.9	4.1	0.0	0.6	0.0	2.8	0.0	17.6	0.0	2.7	0.0	1.2	21.3
Upper Arun 38	Sep-16	-14.5	0.0	-103.7	0.1	12.3	50.0	3.6	0.1	0.8	0.0	2.8	0.0	17.6	0.1	2.7	0.0	1.4	21.1
Upper Arun 39	Sep-16	-14.6	0.0	-104.0	0.1	12.8	43.0	4.4	0.0	0.7	0.0	2.3	0.0	14.7	0.0	2.4	0.0	1.1	17.3
Upper Arun 40	Oct-16	-14.3	0.0	-100.8	0.2	13.2	36.8	3.0	0.0	0.7	0.0	2.1	0.0	13.1	0.1	2.4	0.0	0.9	14.0
Upper Arun 41	Oct-16	-14.6	0.0	-102.9	0.1	13.7	32.9	2.2	0.0	0.8	0.0	1.8	0.0	11.6	0.1	2.0	0.0	0.8	13.0
Upper Arun 42	Oct-16	-8.0	0.0	-49.5	0.2	14.4	20.9	4.8	0.0	0.7	0.0	0.7	0.0	5.9	0.0	6.5	0.0	0.3	2.0
Upper Arun 43	Oct-16	-14.0	0.0	-99.8	0.2	12.2	47.3	4.0	0.0	0.9	0.0	2.7	0.0	16.8	0.0	2.8	0.0	1.5	18.0
Upper Arun 44	Oct-16	-14.0	0.0	-100.3	0.2	11.8	53.9	4.1	0.0	1.2	0.0	2.8	0.0	17.6	0.0	2.9	0.0	3.2	21.5
Upper Arun 45	Oct-16	-13.9	0.0	-99.3	0.1	11.7	51.1	4.7	0.0	1.0	0.0	2.9	0.0	18.0	0.1	3.0	0.0	2.0	19.6
Lower Arun 1	5-May	-9.8	0.0	-65.1	0.3	13.6	34.9	3.8	0.0	1.3	0.0	1.6	0.0	11.8	0.0	3.2	0.0	1.6	10.9
Lower Arun 2	6-May	-10.1	0.0	-66.9	0.1	13.5	37.7	4.1	0.0	1.4	0.0	1.9	0.0	13.5	0.0	3.5	0.0	1.6	11.9
Lower Arun 3	7-May	-9.6	0.0	-63.2	0.1	13.9	35.5	3.9	0.0	1.4	0.0	1.8	0.0	12.5	0.0	3.5	0.0	1.4	10.9
Lower Arun 4	11-May	-9.4	0.0	-61.5	0.1	14.0	35.3	3.8	0.0	1.3	0.0	1.7	0.0	12.9	0.0	3.2	0.0	1.4	10.4
Lower Arun 5	15-May	-6.3	0.0	-34.5	0.1	16.2	24.3	2.1	0.0	1.1	0.0	1.1	0.0	10.2	0.0	2.3	0.0	0.2	6.6
Lower Arun 6	19-May	-8.4	0.0	-52.3	0.1	15.1	31.4	3.1	0.0	1.3	0.0	1.6	0.0	11.4	0.0	3.3	0.0	1.1	9.7
Lower Arun 7	23-May	-8.9	0.0	-56.2	0.1	15.1	31.3	3.0	0.0	1.4	0.0	1.5	0.0	11.6	0.0	3.3	0.0	1.0	9.5
Lower Arun 8	27-May	-8.4	0.0	-51.8	0.1	15.7	27.7	2.4	0.0	1.2	0.0	1.3	0.0	10.6	0.0	2.9	0.0	0.8	7.8
Lower Arun 9	31-May	-8.5	0.0	-52.6	0.1	15.6	27.0	2.7	0.0	1.1	0.0	1.3	0.0	9.7	0.0	3.0	0.0	0.9	7.8
Lower Arun 10	4-Jun	-9.1	0.0	-58.6	0.1	14.5	30.6	3.1	0.0	1.3	0.0	1.5	0.0	10.9	0.0	3.2	0.0	1.0	9.0
Lower Arun 11	8-Jun	-4.9	0.0	-21.3	0.4	17.9	27.8	3.7	0.0	1.8	0.0	1.0	0.0	10.9	0.1	2.0	0.0	2.2	5.6
Lower Arun 12	12-Jun	-8.5	0.0	-52.1	0.1	15.9	28.8	2.3	0.0	1.5	0.0	1.3	0.0	11.8	0.1	3.3	0.0	0.8	7.3
Lower Arun 13	16-Jun	-6.7	0.0	-37.2	0.1	16.7	32.1	4.4	0.0	0.9	0.0	1.1	0.0	10.8	0.0	3.0	0.0	2.1	9.2
Lower Arun 14	20-Jun	-8.0	0.0	-48.3	0.1	15.8	23.8	1.9	0.0	1.1	0.0	1.1	0.0	9.9	0.0	3.0	0.0	0.6	5.7
Lower Arun 15	24-Jun	-7.5	0.0	-44.9	0.1	15.3	25.8	3.9	0.0	0.9	0.0	1.0	0.0	10.9	0.0	2.7	0.0	0.9	4.8
Lower Arun 16	28-Jun	-8.9	0.0	-55.6	0.1	15.8	26.6	4.1	0.0	1.0	0.0	1.2	0.0	11.0	0.0	3.1	0.0	0.9	4.9
Lower Arun 17	2-Jul	-10.4	0.0	-68.2	0.1	15.3	27.8	3.9	0.0	1.2	0.0	1.1	0.0	11.8	0.1	2.9	0.0	0.8	5.6
Lower Arun 18	6-Jul	-11.3	0.0	-75.7	0.1	14.4	29.7	2.9	0.0	0.7	0.0	1.2	0.0	12.6	0.0	2.8	0.0	1.0	7.7
Lower Arun 19	10-Jul	-11.4	0.0	-76.4	0.1	14.5	30.8	3.6	0.0	0.8	0.0	1.2	0.0	12.4	0.0	2.9	0.0	2.0	7.9
Lower Arun 20	14-Jul	-11.8	0.0	-80.6	0.2	13.9	42.3	5.3	0.0	0.4	0.0	1.7	0.0	16.8	0.1	3.1	0.0	2.2	12.2
Lower Arun 21	18-Jul	-12.2	0.1	-83.5	0.3	14.0	32.2	4.3	0.0	0.5	0.0	1.2	0.0	13.1	0.0	2.8	0.0	1.9	7.8
Lower Arun 22	22-Jul	-12.7	0.0	-87.6	0.1	14.0	29.0	6.1	0.0	0.5	0.0	1.2	0.0	10.6	0.1	3.1	0.0	0.9	6.1
Lower Arun 23	26-Jul	-12.1	0.0	-83.4	0.2	13.3	33.8	4.2	0.0	0.4	0.0	1.3	0.0	13.0	0.1	2.8	0.0	2.0	9.5
Lower Arun 24	30-Jul	-13.6	0.0	-95.8	0.0	12.9	45.4	4.0	0.0	0.7	0.0	2.0	0.0	15.3	0.0	2.7	0.0	3.2	16.9
Lower Arun 25	3-Aug	-14.8	0.0	-105.7	0.1	12.7	75.2	12.0	0.1	0.4	0.0	3.1	0.0	20.5	0.0	2.9	0.0	6.2	29.5
Lower Arun 26	7-Aug	-13.9	0.0	-98.1	0.1	12.9	58.8	5.7	0.1	0.5	0.0	2.7	0.0	19.5	0.1	2.9	0.0	3.3	24.2
Lower Arun 27	11-Aug	-14.3	0.0	-101.5	0.1	13.1	62.4	5.8	0.0	0.3	0.0	3.0	0.0	20.1	0.1	2.9	0.0	3.8	26.5
Lower Arun 28	15-Aug	-14.4	0.0	-102.5	0.1	12.6	65.6	5.9	0.0	0.6	0.0	3.1	0.0	21.2	0.1	2.8	0.0	3.7	28.2
Lower Arun 29	19-Aug	-14.4	0.0	-102.3	0.1	13.0	63.5	5.7	0.0	0.5	0.0	3.1	0.0	21.5	0.1	3.0	0.0	2.6	27.0
Lower Arun 30	23-Aug	-14.1	0.0	-99.5	0.1	13.0	55.5	2.9	0.0	1.0	0.0	2.8	0.0	19.5	0.1	2.9	0.0	2.2	24.2
Lower Arun 31	27-Aug	-14.0	0.0	-99.1	0.1	12.5	58.6	3.2	0.0	0.9	0.0	3.1	0.0	20.7	0.1	3.1	0.0	1.7	26.0
Lower Arun 32	31-Aug	-12.6	0.0	-87.3	0.1	13.5	40.0	4.5	0.0	0.5	0.1	2.0	0.0	15.2	0.1	2.8	0.0	0.7	14.4
Lower Arun 33	4-Sep	-13.1	0.0	-90.9	0.1	13.9	27.9	4.0	0.0	0.5	0.0	1.3	0.0	10.8	0.0	2.9	0.0	0.8	7.7
Lower Arun 34	8-Sep	-12.8	0.0	-88.3	0.1	13.7	35.3	4.5	0.0	0.4	0.0	1.7	0.0	12.7	0.0	3.3	0.0	0.6	11.9
Lower Arun 35	12-Sep	-12.6	0.0	-87.6	0.1	13.6	25.3	1.9	0.0	0.8	0.0	1.3	0.0	9.5	0.0	3.0	0.0	0.6	8.2
Lower Arun 36	16-Sep	-12.7	0.0	-87.8	0.0	13.5	28.0	2.3	0.0	0.4	0.0	1.3	0.0	9.6	0.0	2.9	0.0	2.1	9.4
Lower Arun 37	20-Sep	-12.0	0.0	-82.5	0.1	13.3	27.8	2.3	0.0	0.9	0.0	1.4	0.0	9.8	0.1	3.5	0.0	0.7	9.1
Lower Arun 38	24-Sep	-12.0	0.0	-82.4	0.1	13.4	27.6	2.3	0.0	0.9	0.0	1.4	0.0	9.9	0.1	3.4	0.0	0.6	9.1
Lower Arun 39	28-Sep	-12.8	0.0	-88.5	0.1	13.7	30.1	2.3	0.0	1.0	0.0	1.5	0.0	11.5	0.0	3.3	0.0	0.6	10.0
Lower Arun 40	1-Oct	-12.5	0.0	-86.4	0.1	13.5	17.9	2.4	0.0	0.9	0.0	1.4	0.0	9.8	0.0	3.4	0.0		
Lower Arun 41	1-Oct	-12.5	0.0	-86.2	0.1	13.8	19.4	4.4	0.0	0.4	0.0	1.4	0.0	9.8	0.0	3.3	0.0		

Name	Date	δ18O (‰)	Std. Dev. δ18O (‰)	δD (‰)	Std. Dev. δD (‰)	d18-excess (‰)	Sum of dissolved ions (mg L^{-1})	Na^+ (mg L^{-1})	Std. Dev. Na^+ (mg L^{-1})	K^+ (mg L^{-1})	Std. Dev. K^+ (mg L^{-1})	Mg^{2+} (mg L^{-1})	Std. Dev. Mg^{2+} (mg L^{-1})	Ca^{2+} (mg L^{-1})	Std. Dev. Ca^{2+} (mg L^{-1})	Si (mg L^{-1})	Std. Dev. Si (mg L^{-1})	Cl^- (mg L^{-1})	SO_4^{2-} (mg L^{-1})
Sabha Khola 1	5-May	-5.8	0.0	-32.6	0.3	14.0	29.3	2.4	0.0	1.7	0.0	2.3	0.0	12.5	0.1	3.6	0.0	1.2	5.5
Sabha Khola 2	6-May	-6.0	0.0	-34.3	0.4	13.3	31.7	2.1	0.0	1.7	0.0	2.8	0.0	14.4	0.0	3.7	0.0	0.9	6.1
Sabha Khola 3	7-May	-5.5	0.0	-29.6	0.1	14.6	27.5	1.9	0.0	1.4	0.0	2.4	0.0	12.3	0.0	3.3	0.0	0.8	5.4
Sabha Khola 4	11-May	-5.8	0.0	-33.0	0.1	13.5	32.0	2.6	0.0	1.8	0.0	2.7	0.0	13.8	0.0	4.0	0.0	1.0	6.0
Sabha Khola 5	15-May	-5.5	0.0	-28.9	0.1	14.8	27.8	2.0	0.0	1.6	0.0	2.4	0.0	12.1	0.0	3.6	0.0	0.8	5.3
Sabha Khola 6	19-May	-4.9	0.0	-22.9	0.1	16.3	24.0	1.4	0.0	1.2	0.0	2.1	0.0	11.2	0.1	2.9	0.0	0.6	4.6
Sabha Khola 7	23-May	-5.4	0.0	-27.9	0.1	15.5	26.1	1.5	0.0	1.3	0.0	2.5	0.0	12.2	0.0	3.2	0.0	0.6	4.7
Sabha Khola 8	27-May	-6.1	0.0	-32.7	0.1	15.7	24.2	1.7	0.0	1.2	0.0	2.1	0.0	11.0	0.1	3.4	0.0	0.6	4.3
Sabha Khola 9	31-May	-5.5	0.0	-27.5	0.1	16.3	21.4	1.5	0.0	1.1	0.0	1.8	0.0	9.8	0.0	2.9	0.0	0.5	3.2
Sabha Khola 10	4-Jun	-6.1	0.0	-33.2	0.1	15.3	26.1	1.8	0.0	1.3	0.0	2.3	0.0	11.9	0.0	3.4	0.0	0.6	4.7
Sabha Khola 11	8-Jun	-4.5	0.0	-18.5	0.1	17.7	17.0	1.3	0.0	0.8	0.0	1.3	0.0	7.0	0.0	2.4	0.0	0.5	3.1
Sabha Khola 12	12-Jun	-4.0	0.0	-16.3	0.1	15.5	22.9	3.0	0.0	1.2	0.0	1.7	0.0	6.6	0.0	3.9	0.0	1.9	4.6
Sabha Khola 13	16-Jun	-4.1	0.0	-16.1	0.2	16.9	15.9	1.3	0.0	0.8	0.0	1.2	0.0	7.0	0.0	2.4	0.0	0.6	2.6
Sabha Khola 14	20-Jun	-5.4	0.0	-26.8	0.1	16.1	19.2	1.4	0.0	0.9	0.0	1.7	0.0	8.7	0.0	3.1	0.0	0.5	2.9
Sabha Khola 15	24-Jun	-5.3	0.0	-26.3	0.1	15.9	16.7	1.3	0.0	1.0	0.0	1.3	0.0	6.5	0.0	3.0	0.0	0.7	3.0
Sabha Khola 16	28-Jun	-6.1	0.0	-33.2	0.1	15.8	26.6	4.5	0.0	0.2	0.0	1.9	0.0	9.8	0.0	2.9	0.0	1.8	5.4
Sabha Khola 17	2-Jul	-6.4	0.0	-35.7	0.1	15.4	20.8	1.4	0.0	1.2	0.0	1.8	0.0	8.5	0.0	3.6	0.0	0.6	3.1
Sabha Khola 18	6-Jul	-7.3	0.0	-43.1	0.1	15.1	19.8	1.4	0.0	1.1	0.0	1.7	0.0	8.1	0.0	3.5	0.0	0.6	3.5
Sabha Khola 19	10-Jul	-7.3	0.0	-44.3	0.1	13.8	19.1	1.6	0.0	1.0	0.0	1.6	0.0	7.6	0.0	3.5	0.0	0.5	2.7
Sabha Khola 20	14-Jul	-7.0	0.0	-42.1	0.1	13.9	18.3	1.5	0.0	1.2	0.0	1.7	0.0	7.8	0.0	3.7	0.0	0.4	1.4
Sabha Khola 21	18-Jul	-8.5	0.0	-54.3	0.1	13.9	18.6	1.5	0.0	0.9	0.0	1.5	0.0	7.4	0.0	3.4	0.0	0.6	2.6
Sabha Khola 22	22-Jul	-10.4	0.0	-69.5	0.1	13.4	17.3	1.3	0.0	0.8	0.0	1.2	0.0	7.7	0.0	2.7	0.0	0.7	2.9
Sabha Khola 23	26-Jul	-8.3	0.0	-53.4	0.1	13.2	17.2	1.6	0.0	0.9	0.0	1.4	0.0	6.3	0.0	3.3	0.0	0.7	2.3
Sabha Khola 24	30-Jul	-8.3	0.0	-52.8	0.1	13.4	18.7	1.8	0.0	1.0	0.0	1.4	0.0	6.3	0.0	3.8	0.0	1.3	3.2
Sabha Khola 25	3-Aug	-8.2	0.0	-51.8	0.0	13.5	19.6	1.8	0.0	0.9	0.0	1.7	0.0	7.3	0.0	4.1	0.0	0.5	2.7
Sabha Khola 26	7-Aug	-8.0	0.0	-50.8	0.1	13.1	21.0	1.9	0.0	1.2	0.0	1.8	0.0	7.9	0.0	4.2	0.0	0.6	2.8
Sabha Khola 27	11-Aug	-8.4	0.0	-54.5	0.1	12.7	19.3	2.0	0.0	1.1	0.0	1.7	0.0	7.1	0.0	4.1	0.0	0.7	2.0
Sabha Khola 28	15-Aug	-8.0	0.0	-51.3	0.1	13.0	21.5	2.0	0.0	1.0	0.0	1.8	0.0	7.8	0.0	4.2	0.0	0.7	3.2
Sabha Khola 29	19-Aug	-7.8	0.0	-48.8	0.1	13.7	22.3	2.1	0.0	1.2	0.0	2.0	0.0	8.8	0.0	4.4	0.0	0.7	3.2
Sabha Khola 30	23-Aug	-8.1	0.0	-51.9	0.0	13.1	21.5	2.0	0.0	1.1	0.0	1.9	0.0	8.6	0.0	4.3	0.0	0.5	3.1
Sabha Khola 31	27-Aug	-7.5	0.0	-47.3	0.1	13.0	24.8	2.2	0.0	1.2	0.0	2.0	0.0	8.9	0.0	4.7	0.0	1.7	3.4
Sabha Khola 32	31-Aug	-8.5	0.0	-54.1	0.1	13.7	15.4	1.7	0.0	0.9	0.0	1.2	0.0	5.2	0.0	3.3	0.0	0.6	2.4
Sabha Khola 33	4-Sep	-9.5	0.0	-63.5	0.3	12.6	16.1	1.6	0.0	0.8	0.0	1.4	0.0	6.1	0.0	3.5	0.0	0.5	2.2
Sabha Khola 34	8-Sep	-8.5	0.0	-55.2	0.1	13.0	20.0	1.9	0.0	1.0	0.0	1.8	0.0	7.7	0.0	4.4	0.0	0.5	2.8
Sabha Khola 35	12-Sep	-9.5	0.0	-63.3	0.1	12.9	15.4	1.7	0.0	0.8	0.0	1.2	0.0	5.9	0.0	3.3	0.0	0.5	2.0
Sabha Khola 36	16-Sep	-9.4	0.0	-61.6	0.1	13.7	17.1	1.6	0.0	0.8	0.0	1.4	0.0	6.5	0.0	3.4	0.0	0.5	2.3
Sabha Khola 37	20-Sep	-9.0	0.0	-58.9	0.1	13.5	18.3	1.7	0.0	1.0	0.0	1.4	0.0	6.2	0.0	3.9	0.0	0.7	2.5
Sabha Khola 38	24-Sep	-9.3	0.0	-60.4	0.1	13.6	18.3	1.8	0.0	1.0	0.0	1.6	0.0	6.9	0.0	4.0	0.0	0.6	2.4
Sabha Khola 39	28-Sep	-8.7	0.0	-56.8	0.1	12.8	21.1	2.2	0.0	1.1	0.0	1.8	0.0	7.2	0.0	4.7	0.0	0.7	2.8
Sabha Khola 40	1-Oct	-8.8	0.0	-57.4	0.1	13.0	21.3	1.9	0.0	1.3	0.0	1.9	0.0	8.0	0.0	4.7	0.0	0.6	2.2
Sabha Khola 41	1-Oct	-8.8	0.0	-57.4	0.1	13.1	23.0	2.0	0.0	1.2	0.0	1.9	0.0	8.0	0.0	4.7	0.0	1.3	2.9
Barun Khola 1	29-Apr	-10.1	0.0	-63.7	0.1	16.7	20.9	1.1	0.0	0.8	0.0	0.8	0.0	7.7	0.0	2.2	0.0	0.4	6.9
Barun Khola 2	30-Apr	-10.0	0.0	-63.2	0.1	17.0	19.9	1.2	0.0	0.6	0.0	0.8	0.0	7.6	0.0	2.3	0.0	0.3	6.4
Barun Khola 3	1-May	-9.9	0.0	-63.2	0.1	16.4	20.4	1.2	0.0	0.6	0.0	0.8	0.0	7.6	0.0	2.3	0.0	0.4	6.9
Barun Khola 4	5-May	-9.5	0.0	-58.5	0.1	17.2	19.5	0.9	0.0	0.8	0.0	0.7	0.0	7.2	0.0	2.1	0.0	0.3	6.7
Barun Khola 5	9-May	-9.7	0.0	-60.2	0.2	17.2	18.6	1.1	0.0	0.6	0.0	0.7	0.0	7.3	0.0	2.2	0.0	0.3	6.4
Barun Khola 6	13-May	-8.5	0.0	-50.5	0.1	17.8	16.6	1.1	0.0	0.5	0.0	0.7	0.0	6.1	0.0	2.0	0.0	0.4	5.2
Barun Khola 7	17-May	-8.6	0.0	-51.0	0.1	17.9	16.4	1.1	0.0	0.5	0.0	0.7	0.0	6.4	0.0	2.0	0.0	0.4	5.4
Barun Khola 8	21-May	-7.3	0.0	-39.7	0.2	18.7	13.0	1.0	0.0	0.4	0.0	0.6	0.0	4.9	0.0	1.7	0.0	0.3	4.1
Barun Khola 9	26-May	-8.6	0.0	-50.6	0.1	18.0	12.7	0.9	0.0	0.4	0.0	0.6	0.0	4.8	0.0	1.7	0.0	0.3	4.0
Barun Khola 10	29-May	-9.5	0.0	-58.4	0.1	17.2	16.3	0.9	0.0	0.9	0.0	0.7	0.0	6.2	0.0	2.1	0.0	0.4	5.2
Barun Khola 11	1-Jun	-8.1	0.0	-46.5	0.1	18.2	13.8	1.0	0.0	0.4	0.0	0.6	0.0	5.1	0.0	2.0	0.0	0.4	3.7
Barun Khola 12	5-Jun	-9.5	0.0	-58.7	0.1	17.4	18.0	1.2	0.0	0.9	0.0	0.7	0.0	6.3	0.0	2.0	0.0	0.7	5.4
Barun Khola 13	9-Jun	-6.3	0.0	-30.9	0.2	19.1	9.1	0.7	0.0	0.7	0.0	0.4	0.0	3.2	0.0	1.3	0.0	0.4	2.4
Barun Khola 14	12-Jun	-9.6	0.0	-59.8	0.1	17.1	15.4	0.9	0.0	0.8	0.0	0.6	0.0	5.4	0.0	2.0	0.0	0.5	5.1
Barun Khola 15	16-Jun	-6.9	0.0	-37.2	0.1	18.0	10.7	2.4	0.0	0.2	0.0	0.4	0.0	3.6	0.0	1.3	0.0	0.3	2.5
Barun Khola 16	19-Jun	-9.8	0.0	-61.5	0.1	16.8	16.5	1.2	0.0	0.5	0.0	0.6	0.0	4.7	0.0	1.7	0.0	1.6	5.5
Barun Khola 17	22-Jun	-8.6	0.0	-51.9	0.1	16.8	12.7	1.0	0.0	0.4	0.0	0.6	0.0	4.3	0.0	2.2	0.0	0.3	3.4
Barun Khola 18	6-Jul	-13.3	0.0	-91.7	0.1	14.9	20.3	1.4	0.0	0.6	0.0	0.8	0.0	5.8	0.0	3.1	0.0	1.7	6.3
Barun Khola 19	10-Jul	-13.5	0.0	-92.7	0.1	15.1	22.3	3.3	0.0	0.6	0.0	0.9	0.0	5.7	0.0	3.0	0.0	1.9	6.1
Barun Khola 20	13-Jul	-14.0	0.0	-97.8	0.1	14.5	15.4	1.1	0.0	0.3	0.0	0.6	0.0	4.5	0.0	2.1	0.0	1.8	5.0
Barun Khola 21	17-Jul	-13.7	0.0	-94.4	0.1	14.8	14.4	1.2	0.0	0.4	0.0	0.7	0.0	5.2	0.0	2.3	0.0	0.3	4.3
Barun Khola 22	21-Jul	-13.7	0.0	-94.4	0.1	14.9	16.6	1.3	0.0	0.5	0.0	0.7	0.0	5.7	0.0	2.6	0.1	0.3	4.9
Barun Khola 23	25-Jul	-13.9	0.0	-96.4	0.3	14.5	25.1	1.3	0.0	2.9	0.0	1.7	0.0	6.0	0.0	5.9	0.0	1.2	4.8
Barun Khola 24	29-Jul	-14.0	0.0	-97.8	0.1	14.6	17.3	1.4	0.0	0.5	0.0	0.8	0.0	5.6	0.0	3.2	0.0	0.4	4.7
Barun Khola 25	2-Aug	-14.0	0.0	-97.4	0.1	14.7	16.6	1.3	0.0	0.5	0.0	0.8	0.0	5.6	0.0	2.7	0.0	0.4	4.8
Barun Khola 26	6-Aug	-14.1	0.0	-97.8	0.1	15.2	23.7	3.0	0.0	0.7	0.0	0.8	0.0	5.6	0.0	2.6	0.0	3.5	7.4
Barun Khola 27	10-Aug	-13.8	0.0	-95.5	0.1	15.3	17.7	2.2	0.0	0.9	0.0	0.8	0.0	5.6	0.0	2.7	0.0	0.5	5.1
Barun Khola 28	14-Aug	-13.7	0.0	-94.0	0.1	15.2	15.3	1.5	0.0	0.6	0.0	0.8	0.0	6.1	0.0	2.7	0.0	0.4	3.3
Barun Khola 29	18-Aug	-13.6	0.0	-93.9	0.1	14.7	19.2	3.5	0.0	1.1	0.0	0.7	0.0	4.9	0.0	2.3	0.0	1.7	3.9
Barun Khola 30	22-Aug	-13.2	0.0	-90.5	0.1	14.7	22.3	0.8	0.0	3.1	0.0	2.3	0.0	5.6	0.0	6.9	0.0	0.3	3.3
Barun Khola 31	26-Aug	-13.2	0.1	-90.6	0.1	14.9	20.6	0.7	0.0	2.8	0.0	2.1	0.0	5.3	0.0	6.4	0.0	0.3	3.1
Barun Khola 32	31-Aug	-14.6	0.0	-101.6	0.1	15.2	10.7	1.0	0.0	0.1	0.0	0.5	0.0	4.3	0.0	1.9	0.0	0.3	2.6
Barun Khola 33	4-Sep	-14.6	0.0	-103.5	0.1	13.2	31.1	6.3	0.0	1.1	0.0	2.1	0.0	13.8	0.1	2.4	0.0	0.4	4.4
Barun Khola 34	8-Sep	-14.5	0.0	-103.4	0.1	12.6	26.7	3.3	0.0	1.2	0.0	2.1	0.0	13.7	0.1	2.4	0.0	0.3	3.0
Barun Khola 35	12-Sep	-12.9	0.0	-88.4	0.1	14.9	17.0	1.2	0.0	0.6	0.0	0.7	0.0	6.4	0.0	2.5	0.0	0.5	5.0
Barun Khola 36	16-Sep	-12.7	0.0	-86.9	0.1	14.8	17.6	0.9	0.0	0.8	0.0	0.7	0.0	6.6	0.0	2.4	0.0	0.4	5.3
Barun Khola 37	20-Sep	-12.7	0.0	-86.9	0.1	14.9	18.4	1.9	0.0	0.3	0.0	0.8	0.0	6.7	0.0	2.5	0.0	0.3	4.9
Barun Khola 38	24-Sep	-12.9	0.0	-88.0	0.1	15.1	17.4	1.0	0.0	0.6	0.0	0.7	0.0	6.4	0.0	2.6	0.0	0.3	5.1
Barun Khola 39	28-Sep	-14.0	0.0	-97.6	0.1	14.8	12.1	1.4	0.0	0.1	0.0	0.5	0.0	4.4	0.0	1.7	0.0	0.3	3.1
Barun Khola 40	2-Oct	-13.6	0.0	-94.2	0.1	14.5	11.2	0.7	0.0	0.7	0.0	0.5	0.0	3.8	0.0	1.6	0.0	0.5	2.8
Barun Khola 41	6-Oct	-14.6	0.1	-100.9	0.3	15.5	10.3	1.0	0.0	0.6	0.0	0.5	0.0	3.4	0.0	1.6	0.0	0.4	2.2
Barun Khola 42	10-Oct	-14.0	0.1	-97.2	0.1	14.8	14.4	1.5	0.0	0.8	0.0	0.6	0.0	4.4	0.0	2.3	0.0	0.5	3.7
Barun Khola 43	14-Oct	-12.5	0.0	-84.5	0.2	15.3	18.2	1.4	0.0	0.3	0.0	0.8	0.0	6.8	0.0	2.5	0.0	0.3	5.4
Barun Khola 44	18-Oct	-12.4	0.1	-83.8	0.1	15.6	18.4	1.3	0.0	0.3	0.0	0.8	0.0	6.9	0.0	2.5	0.0	0.3	5.6
Barun Khola 45	28-Oct	-12.2	0.0	-82.3	0.1	15.4	19.6	1.6	0.0	0.4	0.0	0.8	0.0	7.3	0.0	2.6	0.0	0.4	5.9

Appendix B.

Sample Name	Cross-season Equivalent Sample Name	Dominant Source Water for Drainage Area	Latitude	Longitude	Date Collected	Time Collected	Mean Catchment Elevation (m)	Season	$\delta^{18}O$ (‰)	$\delta^{18}O$ std dev (‰)	δD (‰)	δD std dev. (‰)	d-excess (‰)	% Change in Snow Covered Area
K1	K1	Groundwater-sourced Spring	27.3712559	87.2136194	2-Apr-16	8:14:56AM	1113	Spring	-5.33	0.05	-35.02	0.28	7.61	
K2	K2	Groundwater-sourced Spring	27.3647195	87.2385796	2-Apr-16	9:41:12AM	565	Spring	-5.66	0.01	-39.44	0.13	5.83	
K3	K3	Groundwater-sourced Tributary	27.3607983	87.2440909	2-Apr-16	10:20:32AM	565	Spring	-5.77	0.03	-35.95	0.12	10.25	
K4	K4	Stream	27.3691333	87.2461174	2-Apr-16	12:03:41PM	1746	Spring	-6.45	0.02	-37.55	0.07	14.09	
K5	K5	Groundwater-sourced Tributary	27.3797119	87.2703115	2-Apr-16	1:42:00PM	782	Spring	-5.78	0.03	-37.21	0.12	9.04	
K6	K6	Stream	27.3807225	87.2705378	2-Apr-16	1:56:00PM	1808	Spring	-6.50	0.05	-37.65	0.09	14.35	
K7	K7	Groundwater-sourced Spring	27.3833399	87.2867028	2-Apr-16	3:39:25PM	817	Spring	-6.31	0.03	-40.44	0.11	10.04	
K8	K8	Groundwater-sourced Tributary	27.3688844	87.3253117	3-Apr-16	9:28:53AM	1463	Spring	-6.92	0.01	-43.42	0.10	11.97	
K9	K9	Groundwater-sourced Tributary	27.3842948	87.3375476	3-Apr-16	12:35:37PM	1859	Spring	-7.13	0.02	-44.34	0.06	12.73	
K10	K10	Groundwater-sourced Spring	27.3989711	87.3365462	3-Apr-16	3:34:46PM	1800	Spring	-7.85	0.03	-49.18	0.07	13.61	
K12	K12	Groundwater-sourced Spring	27.4154468	87.3312658	4-Apr-16	8:57:05AM	1222	Spring	-7.07	0.02	-44.28	0.09	12.31	
K13	K13	Stream	27.4292749	87.3426376	4-Apr-16	10:17:32AM	2429	Spring	-7.14	0.03	-41.52	0.10	15.64	
K14	K14	Groundwater-sourced Spring	27.4250792	87.3711486	4-Apr-16	1:51:07PM	1414	Spring	-6.66	0.03	-42.50	0.13	10.75	
K15	K15	Groundwater-sourced Spring	27.4238499	87.376017	4-Apr-16	3:46:21PM	1549	Spring	-7.25	0.05	-45.07	0.09	12.91	
K16	K16	Groundwater-sourced Tributary	27.4288748	87.3871325	5-Apr-16	8:10:00AM	2268	Spring	-7.45	0.03	-45.04	0.12	14.53	
K17	K17	Groundwater-sourced Tributary	27.4355067	87.4054843	5-Apr-16	10:18:42AM	2543	Spring	-8.16	0.03	-50.19	0.12	15.11	
K19	K19	Snowmelt (Headwater Tributary)	27.444108	87.3943643	6-Apr-16	8:49:26AM	2962	Spring	-6.45	0.04	-34.27	0.16	17.36	-100%
K20	K20	Groundwater-sourced Tributary	27.4280501	87.3631217	7-Apr-16	9:30:03AM	1853	Spring	-7.35	0.02	-44.84	0.11	13.98	
K21	K21	Groundwater-sourced Tributary	27.4281817	87.3431465	7-Apr-16	10:35:01AM	1521	Spring	-6.90	0.03	-42.61	0.13	12.61	
K22	K22	Groundwater-sourced Tributary	27.436996	87.3246803	7-Apr-16	1:15:02PM	1794	Spring	-5.91	0.01	-32.95	0.08	14.33	
K23	K23	Stream	27.426718	87.3089109	7-Apr-16	2:26:11PM	2204	Spring	-6.62	0.04	-37.77	0.05	15.17	
K24	K24	Groundwater-sourced Tributary	27.4330811	87.2864718	8-Apr-16	8:28:48AM	1330	Spring	-6.08	0.04	-35.28	0.08	13.40	
K25	K25	Groundwater-sourced Spring	27.4607989	87.2752232	8-Apr-16	11:35:50AM	1261	Spring	-6.12	0.03	-35.36	0.07	13.63	
K26	K26	Groundwater-sourced Tributary	27.4907261	87.2692137	9-Apr-16	8:57:54AM	1874	Spring	-7.01	0.02	-41.19	0.04	14.86	
K27	K27	Groundwater-sourced Tributary	27.4886553	87.2620984	9-Apr-16	9:42:25AM	1822	Spring	-7.26	0.03	-43.30	0.11	14.75	
K28	K28	Groundwater-sourced Tributary	27.4853242	87.2596723	9-Apr-16	10:03:52AM	1598	Spring	-7.12	0.02	-42.96	0.08	14.01	
K29	K29	Groundwater-sourced Tributary	27.4712843	87.2473186	9-Apr-16	11:21:24AM	1721	Spring	-6.77	0.02	-40.92	0.07	13.20	
K30	K30	Groundwater-sourced Tributary	27.4577887	87.2372871	10-Apr-16	7:32:42AM	1755	Spring	-7.14	0.03	-42.34	0.07	14.80	
K31	K31	Groundwater-sourced Spring	27.4229195	87.2356394	10-Apr-16	9:30:46AM	1546	Spring	-7.17	0.03	-44.72	0.16	12.62	
K32	K32	Groundwater-sourced Spring	27.3995614	87.2360543	10-Apr-16	1:41:39PM	755	Spring	-5.71	0.02	-36.63	0.10	9.06	
K33	K33	Groundwater-sourced Tributary	27.3955	87.2242834	11-Apr-16	7:23:34AM	847	Spring	-5.60	0.02	-36.55	0.09	8.25	
K34	K34	Snowmelt	27.7096847	87.2103379	16-Apr-16	2:04:27PM	4071	Spring	-6.00	-29.41	18.62	0.02	0.09	-100%
K35	K35	Snowmelt	27.725227	87.2120242	17-Apr-16	8:17:43AM	4223	Spring	-9.82	-62.41	16.13	0.03	0.19	-92%
K36	K36	Stream	27.7272875	87.2052354	17-Apr-16	8:53:32AM	5476	Spring	-12.88	-87.90	15.17	0.02	0.10	-27%
K37	K37	Snowmelt	27.7325981	87.1939349	17-Apr-16	9:47:47AM	4236	Spring	-10.89	-71.05	16.05	0.02	0.13	-91%
K38	K38	Stream	27.7347216	87.1908484	17-Apr-16	10:10:32AM	5476	Spring	-13.41	-92.46	14.80	0.04	0.14	-27%
K39	K39	Snowmelt	27.7372858	87.1881486	17-Apr-16	10:32:10AM	4367	Spring	-8.19	-48.35	17.14	0.02	0.15	-95%
K40	K40	Stream	27.7441807	87.1800239	17-Apr-16	11:52:03AM	5530	Spring	-13.44	-92.65	14.90	0.02	0.12	-25%
K41	K41	Snowmelt	27.7456888	87.1765563	17-Apr-16	12:20:04PM	4363	Spring	-8.53	-50.96	17.24	0.03	0.16	-85%
K42	K42	Snowmelt	27.7546776	87.1683302	17-Apr-16	1:03:39PM	4508	Spring	-5.66	-25.22	20.10	0.02	0.10	-44%
K43	K43	Stream	27.7595064	87.1655178	17-Apr-16	1:35:19PM	5614	Spring	-13.73	-94.63	15.18	0.05	0.18	-22%
K46	K46	Stream	27.758372	87.1654406	18-Apr-16	7:41:50AM	5614	Spring	-13.62	-94.20	14.79	0.03	0.25	-22%
K47	K47	Snowmelt	27.7723069	87.1552108	18-Apr-16	8:40:43AM	4956	Spring	-8.55	-51.73	16.65	0.02	0.16	-51%
K48	K48	Stream	27.7869082	87.1509773	18-Apr-16	10:06:26AM	5747	Spring	-16.42	-117.68	13.66	0.02	0.32	-16%
K49	K49	Glacier melt (debris covered)	27.7915324	87.1511358	18-Apr-16	10:48:22AM	5248	Spring	-10.95	-72.89	14.71	0.03	0.17	-49%
K50	K50	Glacier melt (debris covered)	27.794317	87.1349951	18-Apr-16	11:41:49AM	5170	Spring	-12.26	-83.37	14.70	0.03	0.09	-41%
K51	K51	Glacier melt (pro-glacial lake)	27.7953624	87.1180636	19-Apr-16	7:37:57AM	5728	Spring	-17.94	-130.66	12.82	0.03	0.16	-17%
K52	K52	Stream	27.8046632	87.0874269	19-Apr-16	9:27:07AM	5858	Spring	-18.23	-133.49	12.38	0.02	0.08	-11%
K53	K53	Glacier melt (pro-glacial lake)	27.8367173	87.0773813	19-Apr-16	3:50:01PM	5941	Spring	-18.52	-135.81	12.33	0.03	0.08	-10%
K55	K55	Glacier melt (debris covered)	27.8084146	87.0817284	21-Apr-16	8:05:36AM	5414	Spring	-16.43	-119.66	11.81	0.02	0.08	-19%
K56	K56	Snowmelt	27.7758252	87.1553974	21-Apr-16	12:24:38PM	4660	Spring	-6.84	-36.02	18.68	0.03	0.38	-82%
K57	K57	Snowmelt	27.7594436	87.1651687	21-Apr-16	1:15:56PM	4629	Spring	-8.37	-50.06	16.90	0.01	0.03	-75%
K58	K58	Snowmelt	27.7095473	87.2104096	22-Apr-16	10:26:11AM	4071	Spring	-5.73	-27.34	18.49	0.03	0.24	-100%
K60	K60	Stream	27.6931286	87.3635624	30-Apr-16	12:00:50PM	4757	Spring	-9.99	-64.19	15.70	0.03	0.11	-47%
K62	K62	Stream	27.3262402	87.2022251	6-May-16	7:06:00AM	1536	Spring	-5.75	0.02	-32.04	0.16	13.92	
K63	K63	Groundwater-sourced Spring	27.3257658	87.2014114	6-May-16	7:22:34AM	422	Spring	-6.12	0.04	-40.63	0.07	8.30	
K65	K65	Groundwater-sourced Spring	27.3220083	87.1913837	6-May-16	8:54:17AM	390	Spring	-5.94	0.04	-38.32	0.09	9.24	

K66	K34	Snowmelt	27.70845	87.20991	20-Oct-16	1:04:19PM	4071	Fall	-13.94	-97.25	14.30	0.04	0.28
K67	K35	Snowmelt	27.72496	87.21199	21-Oct-16	8:41:32AM	4223	Fall	-12.62	-86.35	14.64	0.05	0.15
K68	K36	Stream	27.72726	87.20515	21-Oct-16	9:17:44AM	5476	Fall	-15.77	-112.61	13.57	0.03	0.09
K69	K37	Snowmelt	27.73261	87.19395	21-Oct-16	10:06:31AM	4236	Fall	-11.58	-77.70	14.91	0.03	0.16
K70	K38	Stream	27.73475	87.19104	21-Oct-16	10:29:17AM	5476	Fall	-15.97	-114.75	13.01	0.03	0.09
K71	K39	Snowmelt	27.73744	87.18823	21-Oct-16	10:58:01AM	4367	Fall	-13.20	-91.59	14.05	0.02	0.10
K72	K40	Stream	27.74424	87.17977	21-Oct-16	11:33:20AM	5530	Fall	-16.21	-116.28	13.38	0.01	0.19
K73	K41	Snowmelt	27.74566	87.17651	21-Oct-16	12:00:03PM	4363	Fall	-13.78	-96.92	13.30	0.03	0.17
K74	K42	Snowmelt	27.75363	87.16845	21-Oct-16	12:39:03PM	4508	Fall	-11.90	-80.67	14.56	0.03	0.09
K76	K43	Stream	27.75853	87.16549	21-Oct-16	2:28:43PM	5614	Fall	-16.60	-119.59	13.24	0.03	0.24
K77	K46	Stream	27.75853	87.16541	22-Oct-16	7:11:14AM	5614	Fall	-16.78	-120.96	13.26	0.03	0.11
K78	K57	Snowmelt	27.76135	87.16451	22-Oct-16	7:32:45AM	4629	Fall	-14.04	-98.45	13.90	0.03	0.09
K79	K47	Snowmelt	27.77151	87.15578	22-Oct-16	8:21:04AM	4956	Fall	-13.63	-94.90	14.14	0.02	0.07
K80	K56	Snowmelt	27.77579	87.15535	22-Oct-16	8:45:50AM	4660	Fall	-13.22	-91.13	14.63	0.04	0.11
K81	K48	Stream	27.78697	87.15114	22-Oct-16	9:48:03AM	5747	Fall	-17.79	-129.30	13.03	0.03	0.13
K82	K49	Glacier melt (debris covered)	27.79162	87.1511	22-Oct-16	10:36:10AM	5248	Fall	-13.94	-97.69	13.84	0.02	0.12
K83	K50	Glacier melt (debris covered)	27.79428	87.13501	22-Oct-16	11:36:25AM	5170	Fall	-14.66	-103.35	13.92	0.04	0.07
K84	K51	Glacier melt (pro-glacial lake)	27.79498	87.11643	22-Oct-16	2:12:51PM	5728	Fall	-17.70	-128.83	12.81	0.05	0.11
K85	K52	Stream	27.80464	87.08735	23-Oct-16	9:00:26AM	5858	Fall	-18.98	-139.43	12.38	0.03	0.07
K86	K55	Glacier melt (debris covered)	27.80841	87.08177	23-Oct-16	9:31:54AM	5414	Fall	-17.22	-125.77	12.02	0.02	0.11
K87	K53	Glacier melt (pro-glacial lake)	27.83663	87.07732	23-Oct-16	11:42:12AM	5941	Fall	-19.36	-142.11	12.80	0.03	0.11
K88		Glacier melt (debris covered)	27.78308	87.15728	24-Oct-16	12:51:27PM	4768	Fall	-14.24	-100.37	13.57	0.04	0.18
K89	K58	Snowmelt	27.70855	87.21001	25-Oct-16	1:45:50PM	4071	Fall	-13.52	-93.52	14.61	0.05	0.08
K91	K60	Stream	27.69314	87.36361	31-Oct-16	2:22:11PM	4757	Fall	-12.04	-81.55	14.76	0.03	0.32
K92	K1	Groundwater-sourced Spring	27.37127	87.21371	5-Nov-16	7:25:17AM	1113	Fall	-6.37	0.03	-41.38	0.19	9.57
K93	K2	Groundwater-sourced Spring	27.36473	87.23861	5-Nov-16	8:37:59AM	565	Fall	-6.38	0.04	-42.92	0.06	8.14
K94	K4	Stream	27.36043	87.24001	5-Nov-16	9:10:15AM	1746	Fall	-7.66	0.03	-48.54	0.12	12.77
K95	K3	Groundwater-sourced Tributary	27.36052	87.24425	5-Nov-16	9:38:49AM	565	Fall	-5.86	0.04	-37.81	0.34	9.06
K96	K5	Groundwater-sourced Tributary	27.38018	87.26996	5-Nov-16	12:14:07PM	782	Fall	-6.58	0.03	-44.17	0.09	8.46
K97	K6	Stream	27.3807	87.27059	5-Nov-16	12:26:40PM	1808	Fall	-7.82	0.04	-50.11	0.11	12.48
K98	K7	Groundwater-sourced Spring	27.38333	87.28675	5-Nov-16	1:43:09PM	817	Fall	-6.29	0.02	-40.73	0.12	9.58
K99	K8	Groundwater-sourced Tributary	27.36902	87.32531	6-Nov-16	8:29:30AM	1463	Fall	-7.48	0.02	-47.73	0.10	12.08
K100	K9	Groundwater-sourced Tributary	27.38414	87.33758	6-Nov-16	9:49:27AM	1859	Fall	-7.94	0.01	-50.27	0.07	13.23
K101	K10	Groundwater-sourced Spring	27.39908	87.33663	6-Nov-16	1:42:42PM	1800	Fall	-7.69	0.02	-48.13	0.09	13.43
K102	K12	Groundwater-sourced Spring	27.41559	87.33143	7-Nov-16	8:28:17AM	1222	Fall	-7.13	0.03	-45.61	0.08	11.47
K103	K13	Stream	27.4293	87.34255	7-Nov-16	9:40:59AM	2429	Fall	-8.69	0.04	-56.05	0.07	13.46
K104	K21	Groundwater-sourced Tributary	27.42811	87.34345	7-Nov-16	10:01:07AM	1521	Fall	-7.68	0.02	-49.27	0.11	12.20
K105	K20	Groundwater-sourced Tributary	27.42754	87.36287	7-Nov-16	11:47:05AM	1853	Fall	-8.09	0.03	-51.17	0.09	13.52
K106	K14	Groundwater-sourced Spring	27.42498	87.37121	7-Nov-16	12:54:00PM	1414	Fall	-6.81	0.04	-43.53	0.10	10.98
K107	K15	Groundwater-sourced Spring	27.42388	87.37633	7-Nov-16	1:41:28PM	1549	Fall	-7.54	0.02	-46.66	0.16	13.66
K108	K16	Groundwater-sourced Tributary	27.42886	87.38715	8-Nov-16	8:00:37AM	2310	Fall	-8.64	0.02	-54.67	0.09	14.44
K109	K17	Groundwater-sourced Tributary	27.43556	87.40554	8-Nov-16	9:27:31AM	2543	Fall	-9.38	0.02	-60.38	0.11	14.65
K110	K19	Groundwater-sourced Tributary (Headwaters)	27.44547	87.39364	9-Nov-16	7:12:28AM	2962	Fall	-9.51	0.03	-61.30	0.06	14.77
K111		Groundwater-sourced Tributary	27.43899	87.40648	9-Nov-16	8:13:39AM	1700	Fall	-7.55	0.02	-46.36	0.10	14.01
K112	K22	Groundwater-sourced Tributary	27.4373	87.32476	10-Nov-16	12:10:35PM	1794	Fall	-7.70	0.02	-47.23	0.10	14.34
K113	K23	Stream	27.42684	87.30898	10-Nov-16	1:12:19PM	2204	Fall	-8.34	0.02	-52.67	0.08	14.06
K114	K24	Groundwater-sourced Tributary	27.43267	87.28683	11-Nov-16	7:58:17AM	1330	Fall	-7.38	0.02	-45.37	0.11	13.68
K115	K25	Groundwater-sourced Spring	27.46071	87.27546	11-Nov-16	10:12:17AM	1261	Fall	-6.72	0.03	-41.08	0.33	12.65
K116	K26	Groundwater-sourced Tributary	27.49075	87.26914	12-Nov-16	7:58:04AM	1874	Fall	-8.00	0.02	-49.24	0.08	14.80
K117	K27	Groundwater-sourced Tributary	27.48864	87.26203	12-Nov-16	8:26:30AM	1822	Fall	-7.46	0.03	-44.86	0.08	14.82
K118	K28	Groundwater-sourced Tributary	27.48518	87.25987	12-Nov-16	8:50:33AM	1598	Fall	-8.01	0.03	-49.42	0.08	14.66
K119	K29	Groundwater-sourced Tributary	27.47125	87.2474	12-Nov-16	9:48:56AM	1721	Fall	-7.37	0.04	-44.85	0.11	14.13
K120	K30	Groundwater-sourced Tributary	27.45785	87.23749	13-Nov-16	7:33:25AM	1755	Fall	-7.48	0.02	-45.32	0.08	14.55
K121	K31	Groundwater-sourced Spring	27.42285	87.23575	13-Nov-16	9:10:33AM	1546	Fall	-6.76	0.02	-41.71	0.05	12.40
K122	K32	Groundwater-sourced Spring	27.39954	87.23614	13-Nov-16	10:44:13AM	755	Fall	-5.55	0.02	-35.52	0.06	8.85
K123	K33	Groundwater-sourced Tributary	27.39579	87.22418	14-Nov-16	7:34:18AM	847	Fall	-6.86	0.01	-43.44	0.06	11.46
K124	K62	Stream	27.32616	87.20225	14-Nov-16	4:09:52PM	1536	Fall	-7.48	0.03	-47.28	0.09	12.59
K125	K63	Groundwater-sourced Spring	27.32567	87.20122	14-Nov-16	4:38:26PM	422	Fall	-6.27	0.03	-41.24	0.05	8.92
K127	K65	Groundwater-sourced Spring	27.32208	87.19137	14-Nov-16	5:52:17PM	390	Fall	-5.96	0.03	-37.69	0.18	10.02

Appendix C.

Name	Type	Season	δ18O (‰)	δ18O STD (‰)	δD (‰)	δD STD (‰)	d18-excess (‰)	Na^+ (mgL^{-1})	Na^+ STD (mgL^{-1})	K^+ (mgL^{-1})	K^+ STD (mgL^{-1})	Mg^{2+} (mgL^{-1})	Mg^{2+} STD (mgL^{-1})	Ca^{2+} (mgL^{-1})	Ca^{2+} STD (mgL^{-1})	Si (mgL^{-1})	Si STD (mgL^{-1})	Cl^- (mgL^{-1})	SO_4^{2-} (mgL^{-1})
K1	Groundwater	Spring	-5.33	0.05	-35.02	0.28	7.61	11.40	0.02	4.87	0.00	2.01	0.00	4.45	0.01	13.27	0.01	12.07	0.60
K2	Groundwater	Spring	-5.66	0.01	-39.44	0.13	5.83	5.82	0.01	1.40	0.01	0.84	0.00	5.68	0.01	5.37	0.01	3.35	2.35
K3	Groundwater	Spring	-5.77	0.03	-35.95	0.12	10.25	6.05	0.02	1.51	0.02	3.09	0.01	2.46	0.01	11.95	0.03	1.70	1.05
K4	Stream	Spring	-6.45	0.02	-37.55	0.07	14.09	3.00	0.01	1.04	0.01	3.14	0.01	14.90	0.03	4.38	0.02	1.83	5.40
K5	Groundwater	Spring	-5.78	0.03	-37.21	0.12	9.04	8.17	0.02	2.25	0.02	4.47	0.01	12.01	0.03	9.38	0.01	2.65	5.70
K6	Stream	Spring	-6.50	0.05	-37.65	0.09	14.35	2.44	0.01	1.54	0.02	3.06	0.02	14.79	0.09	4.66	0.03	0.92	5.60
K7	Groundwater	Spring	-6.31	0.03	-40.44	0.11	10.04	6.99	0.04	7.08	0.05	11.47	0.12	39.06	0.09	15.63	0.04	6.99	9.80
K8	Groundwater	Spring	-6.92	0.01	-43.42	0.10	11.97	1.86	0.01	2.36	0.02	5.74	0.03	28.66	0.11	4.84	0.04	1.51	6.10
K9	Groundwater	Spring	-7.13	0.02	-44.34	0.06	12.73	2.62	0.01	0.99	0.01	2.85	0.00	11.89	0.02	6.08	0.02	0.76	3.20
K10	Groundwater	Spring	-7.85	0.03	-49.18	0.07	13.61	3.00	0.03	0.82	0.02	0.63	0.01	2.07	0.02	7.17	0.06	1.35	1.05
K12	Groundwater	Spring	-7.07	0.02	-44.28	0.09	12.31	1.35	0.01	1.65	0.01	1.79	0.01	2.53	0.02	4.01	0.03	1.93	1.60
K13	Stream	Spring	-7.14	0.03	-41.52	0.10	15.64	1.50	0.01	0.89	0.01	2.00	0.01	12.39	0.04	3.17	0.02	1.50	4.90
K14	Groundwater	Spring	-6.66	0.03	-42.50	0.13	10.75	1.88	0.01	0.82	0.01	0.31	0.00	0.88	0.00	5.06	0.02	0.70	2.05
K15	Groundwater	Spring	-7.25	0.05	-45.07	0.09	12.91	2.94	0.01	0.41	0.01	0.29	0.00	1.30	0.00	7.31	0.02	0.40	1.05
K16	Groundwater	Spring	-7.45	0.03	-45.04	0.12	14.53	1.94	0.01	0.53	0.02	0.35	0.00	1.29	0.01	4.63	0.02	0.46	2.10
K17	Snowmelt	Spring	-8.16	0.03	-50.19	0.12	15.11	1.77	0.00	1.03	0.01	3.07	0.01	17.85	0.08	3.28	0.02	1.33	5.60
K19	Stream	Spring	-6.45	0.04	-34.27	0.16	17.36	1.32	0.01	0.80	0.01	1.09	0.01	7.30	0.03	2.03	0.01	1.16	4.50
K20	Groundwater	Spring	-7.35	0.02	-44.84	0.11	13.98	2.17	0.03	0.85	0.05	0.57	0.00	1.48	0.01	5.51	0.02	0.90	2.50
K21	Groundwater	Spring	-6.90	0.03	-42.61	0.13	12.61	2.31	0.01	1.24	0.02	1.80	0.00	7.11	0.01	5.67	0.01	1.36	5.30
K22	Groundwater	Spring	-5.91	0.01	-32.95	0.08	14.33	1.34	0.00	2.67	0.02	5.69	0.02	23.00	0.09	4.04	0.02	1.44	7.40
K23	Stream	Spring	-6.62	0.04	-37.77	0.05	15.17	1.68	0.01	1.38	0.01	2.68	0.01	14.53	0.07	3.57	0.03	1.01	5.50
K24	Groundwater	Spring	-6.08	0.04	-35.28	0.08	13.40	3.09	0.01	1.69	0.01	2.99	0.01	9.62	0.04	5.95	0.03	0.69	5.80
K25	Groundwater	Spring	-6.12	0.03	-35.36	0.07	13.63	5.74	0.02	2.47	0.02	1.46	0.00	2.97	0.01	13.66	0.06	1.08	0.60
K26	Groundwater	Spring	-7.01	0.02	-41.19	0.04	14.86	4.00	0.02	1.26	0.02	0.96	0.00	2.67	0.01	4.46	0.00	2.10	2.30
K27	Groundwater	Spring	-7.26	0.03	-43.30	0.11	14.75	2.42	0.01	1.35	0.01	0.89	0.00	2.85	0.01	5.80	0.03	0.50	1.80
K28	Groundwater	Spring	-7.12	0.02	-42.96	0.08	14.01	1.66	0.01	0.78	0.02	0.47	0.00	1.90	0.01	4.31	0.03	1.51	1.40
K29	Groundwater	Spring	-6.77	0.02	-40.92	0.07	13.20	2.66	0.02	0.89	0.00	0.38	0.00	1.45	0.01	6.35	0.03	0.84	0.25
K30	Groundwater	Spring	-7.14	0.03	-42.34	0.07	14.80	1.80	0.02	1.08	0.01	0.44	0.00	1.47	0.00	4.65	0.01	1.29	0.60
K31	Groundwater	Spring	-7.17	0.03	-44.72	0.16	12.62	2.59	0.01	0.81	0.01	1.23	0.00	1.90	0.00	6.37	0.01	1.69	1.90
K32	Groundwater	Spring	-5.71	0.02	-36.63	0.10	9.06	9.12	0.06	1.51	0.01	0.79	0.01	2.78	0.02	17.14	0.08	1.44	0.25
K33	Groundwater	Spring	-5.60	0.02	-36.55	0.09	8.25	5.80	0.02	1.10	0.01	0.84	0.00	2.60	0.00	8.71	0.02	2.88	1.30
K62	Stream	Spring	-5.75	0.02	-32.04	0.16	13.92	2.29	0.01	1.65	0.01	2.96	0.01	14.10	0.06	3.67	0.02	1.01	5.70
K63	Groundwater	Spring	-6.12	0.04	-40.63	0.07	8.30	15.25	0.08	1.68	0.01	2.53	0.02	8.91	0.06	31.44	0.15	0.67	0.00
K65	Groundwater	Spring	-5.94	0.04	-38.32	0.09	9.24	9.73	0.02	1.19	0.02	1.82	0.00	7.07	0.02	20.28	0.05	5.60	0.50
K92	Groundwater	Fall	-6.37	0.03	-41.38	0.19	9.57	10.10	0.04	1.35	0.03	1.31	0.01	3.54	0.01	11.81	0.04	11.48	0.66
K93	Groundwater	Fall	-6.38	0.04	-42.92	0.06	8.14	5.34	0.02	0.90	0.01	0.20	0.00	0.29	0.00	4.22	0.01	1.77	0.32
K94	Stream	Fall	-7.66	0.03	-48.54	0.12	12.77	2.30	0.01	1.22	0.01	2.28	0.01	9.89	0.05	5.30	0.02	1.88	4.10
K95	Groundwater	Fall	-5.86	0.04	-37.81	0.34	9.06	4.16	0.01	2.69	0.01	2.84	0.01	2.91	0.01	11.93	0.04	0.61	0.98
K96	Groundwater	Fall	-6.58	0.03	-44.17	0.09	8.46	3.61	0.02	1.70	0.02	1.91	0.01	4.65	0.03	7.50	0.01	0.93	2.76
K97	Stream	Fall	-7.82	0.04	-50.11	0.11	12.48	2.24	0.01	1.37	0.01	2.35	0.00	10.60	0.04	5.35	0.02	0.44	3.23
K98	Groundwater	Fall	-6.29	0.02	-40.73	0.12	9.58	5.68	0.03	6.52	0.03	9.73	0.05	33.54	0.09	15.52	0.02	5.22	9.17
K99	Groundwater	Fall	-7.48	0.02	-47.73	0.10	12.08	1.88	0.01	1.42	0.01	5.75	0.04	27.03	0.06	5.60	0.03	1.11	4.77
K100	Groundwater	Fall	-7.94	0.01	-50.27	0.07	13.23	2.01	0.01	0.52	0.01	1.87	0.02	7.95	0.02	5.40	0.02	0.36	2.04
K101	Groundwater	Fall	-7.69	0.02	-48.13	0.09	13.43	3.32	0.02	1.13	0.00	0.54	0.00	1.97	0.01	7.32	0.03	0.62	0.72
K102	Groundwater	Fall	-7.13	0.03	-45.61	0.08	11.47	1.38	0.01	1.79	0.00	2.52	0.01	5.22	0.01	5.91	0.03	0.48	0.46
K103	Stream	Fall	-8.69	0.04	-56.05	0.07	13.46	1.47	0.01	0.90	0.01	1.85	0.01	10.94	0.01	4.07	0.00	0.36	3.47
K104	Groundwater	Fall	-7.68	0.02	-49.27	0.11	12.20	1.51	0.01	0.98	0.01	1.14	0.01	5.20	0.01	5.27	0.01	0.36	2.69
K105	Groundwater	Fall	-8.09	0.03	-51.17	0.09	13.52	1.77	0.01	0.35	0.02	0.41	0.00	1.17	0.01	4.76	0.03	0.98	1.57
K106	Groundwater	Fall	-6.81	0.04	-43.53	0.10	10.98	1.64	0.01	1.14	0.01	0.28	0.00	0.86	0.00	4.75	0.02	0.74	0.53
K107	Groundwater	Fall	-7.54	0.02	-46.66	0.16	13.66	2.94	0.02	0.41	0.03	0.27	0.00	1.55	0.01	7.98	0.03	0.34	0.66
K108	Groundwater	Fall	-8.64	0.02	-54.67	0.09	14.44	1.43	0.00	0.29	0.01	0.27	0.00	1.11	0.00	4.11	0.01	0.33	0.76
K109	Snowmelt	Fall	-9.38	0.02	-60.38	0.11	14.65	1.47	0.01	0.55	0.02	2.16	0.01	12.94	0.01	3.25	0.01	0.49	3.78
K110	Stream	Fall	-9.51	0.03	-61.30	0.06	14.77	1.06	0.01	0.84	0.01	1.68	0.00	10.33	0.02	3.11	0.00	0.61	4.54
K111	Groundwater	Fall	-7.55	0.02	-46.36	0.10	14.01	0.99	0.00	1.39	0.01	2.51	0.00	9.83	0.02	6.06	0.02	0.42	5.33
K112	Groundwater	Fall	-7.70	0.02	-47.23	0.10	14.34	2.01	0.01	2.38	0.03	4.17	0.01	17.53	0.01	3.94	0.01	0.46	4.29
K113	Stream	Fall	-8.34	0.02	-52.67	0.08	14.06	1.51	0.01	1.17	0.01	2.49	0.01	12.93	0.02	4.40	0.01	0.39	3.75
K114	Groundwater	Fall	-7.38	0.02	-45.37	0.11	13.68	2.22	0.01	1.20	0.01	1.92	0.01	6.45	0.01	5.47	0.01	0.40	2.50
K115	Groundwater	Fall	-6.72	0.03	-41.08	0.33	12.65	4.67	0.03	2.11	0.02	1.19	0.01	2.68	0.01	12.27	0.07	0.78	1.04
K116	Groundwater	Fall	-8.00	0.02	-49.24	0.08	14.80	1.61	0.00	0.73	0.01	0.62	0.00	1.86	0.00	4.00	0.01	0.58	2.44
K117	Groundwater	Fall	-7.46	0.03	-44.86	0.08	14.82	2.02	0.00	1.16	0.01	0.67	0.00	2.32	0.01	5.12	0.01	0.37	1.69
K118	Groundwater	Fall	-8.01	0.03	-49.42	0.08	14.66	1.73	0.01	0.79	0.01	0.40	0.00	1.94	0.00	3.89	0.01	0.40	1.27
K119	Groundwater	Fall	-7.37	0.04	-44.85	0.11	14.13	1.98	0.01	0.74	0.01	0.30	0.00	1.30	0.00	4.84	0.01	0.87	0.71
K120	Groundwater	Fall	-7.48	0.02	-45.32	0.08	14.55	2.17	0.01	1.09	0.02	0.45	0.00	1.62	0.00	4.78	0.01	0.68	0.94
K121	Groundwater	Fall	-6.76	0.02	-41.71	0.05	12.40	2.67	0.02	1.01	0.01	1.23	0.01	2.08	0.02	6.34	0.02	1.76	1.98
K122	Groundwater	Fall	-5.55	0.02	-35.52	0.06	8.85	9.27	0.03	1.74	0.03	0.80	0.00	3.48	0.01	16.89	0.08	3.07	0.57
K123	Groundwater	Fall	-6.86	0.01	-43.44	0.06	11.46	4.27	0.01	0.73	0.01	0.44	0.00	1.59	0.00	7.17	0.01	1.45	1.35
K124	Stream	Fall	-7.48	0.03	-47.28	0.09	12.59	2.77	0.01	1.35	0.02	2.38	0.01	10.13	0.03	5.79	0.02	0.77	3.81
K125	Groundwater	Fall	-6.27	0.03	-41.24	0.05	8.92	14.65	0.09	1.54	0.02	2.17	0.01	8.36	0.02	30.74	0.02	0.89	0.44
K127	Groundwater	Fall	-5.96	0.03	-37.69	0.18	10.02	11.87	0.08	1.84	0.02	1.85	0.01	5.15	0.02	20.59	0.07	7.06	0.26

Table S1. Sample isotope and ion values for Sabha Khola in Spring (pre-monsoon) and Fall (post-monsoon) seasons. Type is described as the dominant water source for drainage area.

Name	Type	Season	δ18O (‰)	δ18O STD (‰)	δD (‰)	δD STD (‰)	d18-excess (‰)	Na^+ (mgL^{-1})	Na^+ STD (mgL^{-1})	K^+ (mgL^{-1})	K^+ STD (mgL^{-1})	Mg^{2+} (mgL^{-1})	Mg^{2+} STD (mgL^{-1})	Ca^{2+} (mgL^{-1})	Ca^{2+} STD (mgL^{-1})	Si (mgL^{-1})	Si STD (mgL^{-1})	Cl^- (mgL^{-1})	SO_4^{2-} (mgL^{-1})
K34	Snowmelt	Spring	-6.00	0.02	-29.41	0.09	18.62	0.75	0.00	0.26	0.02	0.28	0.00	0.65	0.00	1.51	0.02	0.46	0.80
K35	Snowmelt	Spring	-9.82	0.03	-62.41	0.19	16.13	0.72	0.00	0.21	0.00	0.26	0.00	0.90	0.00	2.32	0.01	0.59	1.60
K36	Stream	Spring	-12.88	0.02	-87.90	0.10	15.17	1.26	0.00	0.65	0.01	0.90	0.00	8.25	0.02	2.15	0.01	0.28	7.30
K37	Snowmelt	Spring	-10.89	0.02	-71.05	0.13	16.05	0.99	0.01	0.47	0.01	0.45	0.00	5.77	0.03	3.27	0.01	0.33	1.80
K38	Stream	Spring	-13.41	0.04	-92.46	0.14	14.80	1.76	0.01	1.29	0.01	0.96	0.01	8.87	0.08	2.19	0.01	0.33	8.10
K39	Snowmelt	Spring	-8.19	0.02	-48.35	0.15	17.14	0.43	0.00	0.20	0.02	0.27	0.00	1.46	0.01	1.42	0.01	0.31	1.10
K40	Stream	Spring	-13.44	0.02	-92.65	0.12	14.90	1.02	0.01	0.92	0.02	0.95	0.00	8.82	0.03	2.05	0.00	0.29	8.30
K41	Snowmelt	Spring	-8.53	0.03	-50.96	0.16	17.24	0.66	0.01	0.07	0.02	0.30	0.00	2.61	0.01	1.74	0.01	0.41	1.00
K42	Snowmelt	Spring	-5.66	0.02	-25.22	0.10	20.10	0.62	0.00	0.07	0.02	0.21	0.00	2.07	0.01	0.64	0.01	0.40	1.10
K43	Stream	Spring	-13.73	0.05	-94.63	0.18	15.18	1.24	0.01	0.84	0.01	1.04	0.01	9.35	0.10	2.01	0.02	0.59	9.20
K46	Stream	Spring	-13.62	0.03	-94.20	0.25	14.79	1.34	0.01	0.62	0.01	1.03	0.01	9.20	0.04	2.04	0.01	0.40	9.10
K47	Snowmelt	Spring	-8.55	0.02	-51.73	0.16	16.65	0.51	0.00	0.51	0.02	0.58	0.00	4.67	0.01	2.26	0.01	0.56	1.00
K48	Stream	Spring	-16.42	0.02	-117.68	0.32	13.66	1.59	0.01	0.64	0.00	1.16	0.01	6.43	0.03	2.25	0.03	0.29	10.20
K49	Glacier melt (debris covered)	Spring	-10.95	0.03	-72.89	0.17	14.71	1.33	0.01	0.52	0.01	0.68	0.00	22.18	0.02	1.51	0.00	0.25	8.90
K50	Glacier melt (debris covered)	Spring	-12.26	0.03	-83.37	0.09	14.70	0.64	0.01	0.86	0.01	0.93	0.00	7.05	0.01	1.44	0.01	0.29	11.90
K51	Glacier melt (pro-glacial lake)	Spring	-17.94	0.03	-130.66	0.16	12.82	1.60	0.01	0.95	0.00	1.15	0.01	4.39	0.02	2.12	0.01	0.39	10.40
K52	Stream	Spring	-18.23	0.02	-133.49	0.08	12.38	2.13	0.00	1.04	0.02	1.09	0.00	5.47	0.01	2.46	0.01	0.28	12.80
K53	Glacier melt (pro-glacial lake)	Spring	-18.52	0.03	-135.81	0.08	12.33	2.17	0.01	0.98	0.01	1.03	0.00	5.36	0.02	2.32	0.03	0.50	11.80
K55	Glacier melt (debris covered)	Spring	-16.43	0.02	-119.66	0.08	11.81	1.12	0.01	0.98	0.01	1.35	0.01	9.15	0.04	1.61	0.00	0.28	19.20
K56	Snowmelt	Spring	-6.84	0.03	-36.02	0.38	18.68	0.72	0.00	0.24	0.01	0.37	0.00	3.58	0.01	1.57	0.01	0.59	1.80
K57	Snowmelt	Spring	-8.37	0.01	-50.06	0.03	16.90	0.57	0.00	0.49	0.03	0.48	0.00	7.95	0.07	1.78	0.01	0.44	2.50
K58	Snowmelt	Spring	-5.73	0.03	-27.34	0.24	18.49	0.39	0.00	0.33	0.01	0.25	0.00	0.57	0.00	1.52	0.02	0.36	0.80
K60	Stream	Spring	-9.99	0.03	-64.19	0.11	15.70	0.95	0.00	0.84	0.01	0.84	0.00	7.51	0.03	2.21	0.01	0.32	6.90
K66	Snowmelt	Fall	-13.94	0.04	-97.25	0.28	14.30	0.72	0.00	0.03	0.01	0.17	0.00	0.56	0.00	1.97	0.01	0.26	1.00
K67	Snowmelt	Fall	-12.62	0.05	-86.35	0.15	14.64	0.74	0.01	0.18	0.02	0.21	0.00	0.79	0.00	2.37	0.00	0.26	1.24
K68	Stream	Fall	-15.77	0.03	-112.61	0.09	13.57	1.14	0.00	0.74	0.01	0.88	0.00	7.48	0.03	2.51	0.02	0.28	7.14
K69	Snowmelt	Fall	-11.58	0.03	-77.70	0.16	14.91	1.02	0.00	0.48	0.00	0.40	0.00	5.26	0.01	3.44	0.01	0.26	2.06
K70	Stream	Fall	-15.97	0.03	-114.75	0.09	13.01	1.12	0.00	0.78	0.02	0.92	0.00	7.82	0.03	2.40	0.00	0.29	3.35
K71	Snowmelt	Fall	-13.20	0.02	-91.59	0.10	14.05	0.70	0.01	0.03	0.00	0.24	0.00	1.46	0.00	1.96	0.01	0.51	2.16
K72	Stream	Fall	-16.21	0.01	-116.28	0.19	13.38	1.13	0.01	0.79	0.02	0.94	0.01	7.93	0.01	2.40	0.01	0.25	0.56
K73	Snowmelt	Fall	-13.78	0.03	-96.92	0.17	13.30	0.76	0.01	0.24	0.02	0.33	0.00	3.67	0.01	2.09	0.00	0.31	2.66
K74	Snowmelt	Fall	-11.90	0.03	-80.67	0.09	14.56	0.87	0.00	0.17	0.00	0.26	0.00	4.87	0.02	2.25	0.01	0.28	1.53
K76	Stream	Fall	-16.60	0.03	-119.59	0.24	13.24	1.12	0.01	0.89	0.01	0.98	0.00	8.02	0.03	2.17	0.01	0.98	2.60
K77	Stream	Fall	-16.78	0.03	-120.96	0.11	13.26	2.82	0.03	0.46	0.02	1.03	0.01	8.03	0.02	2.34	0.01	0.25	8.69
K78	Snowmelt	Fall	-14.04	0.03	-98.45	0.09	13.90	0.74	0.00	0.05	0.02	0.31	0.00	1.10	0.00	1.99	0.01	0.24	1.80
K79	Snowmelt	Fall	-13.63	0.02	-94.90	0.07	14.14	0.93	0.01	0.18	0.01	0.34	0.00	5.01	0.01	1.66	0.00	0.24	1.56
K80	Snowmelt	Fall	-13.22	0.04	-91.13	0.11	14.63	0.91	0.00	0.31	0.02	0.46	0.00	5.52	0.04	2.34	0.02	0.25	2.91
K81	Stream	Fall	-17.79	0.03	-129.30	0.13	13.03	1.28	0.01	0.74	0.01	1.01	0.00	5.11	0.01	2.28	0.01	0.25	8.48
K82	Glacier melt (debris covered)	Fall	-13.94	0.02	-97.69	0.12	13.84	0.92	0.00	0.53	0.00	0.73	0.01	22.50	0.08	1.56	0.01	0.27	10.54
K83	Glacier melt (debris covered)	Fall	-14.66	0.04	-103.35	0.07	13.92	0.89	0.00	0.73	0.02	1.11	0.00	7.42	0.01	1.48	0.00	0.22	11.60
K84	Glacier melt (pro-glacial lake)	Fall	-17.70	0.05	-128.83	0.11	12.81	1.07	0.01	0.88	0.01	1.18	0.00	2.68	0.01	2.05	0.01	0.25	7.68
K85	Stream	Fall	-18.98	0.03	-139.43	0.07	12.38	2.15	0.02	0.32	0.00	0.69	0.00	3.81	0.01	1.89	0.01	0.25	7.58
K86	Glacier melt (debris covered)	Fall	-17.22	0.02	-125.77	0.11	12.02	1.30	0.01	1.35	0.01	1.34	0.00	10.24	0.02	1.90	0.00	0.22	18.89
K87	Glacier melt (pro-glacial lake)	Fall	-19.36	0.03	-142.11	0.11	12.80	1.35	0.01	0.98	0.02	0.73	0.01	3.69	0.01	2.26	0.01	0.28	6.90
K88	Glacier melt (debris covered)	Fall	-14.24	0.04	-100.37	0.18	13.57	0.71	0.00	0.67	0.01	0.62	0.00	18.14	0.07	1.16	0.00	0.24	10.52
K89	Snowmelt	Fall	-13.52	0.05	-93.52	0.08	14.61	0.77	0.00	0.02	0.01	0.17	0.00	0.58	0.01	2.04	0.01	0.23	1.11
K91	Stream	Fall	-12.04	0.03	-81.55	0.32	14.76	1.67	0.02	0.43	0.01	0.80	0.01	7.44	0.02	2.61	0.01	0.84	6.28

Table S2. Sample isotope and ion values for Barun Khola in Spring (pre-monsoon) and Fall (post-monsoon) seasons. Type is described as the dominant water source for drainage area.

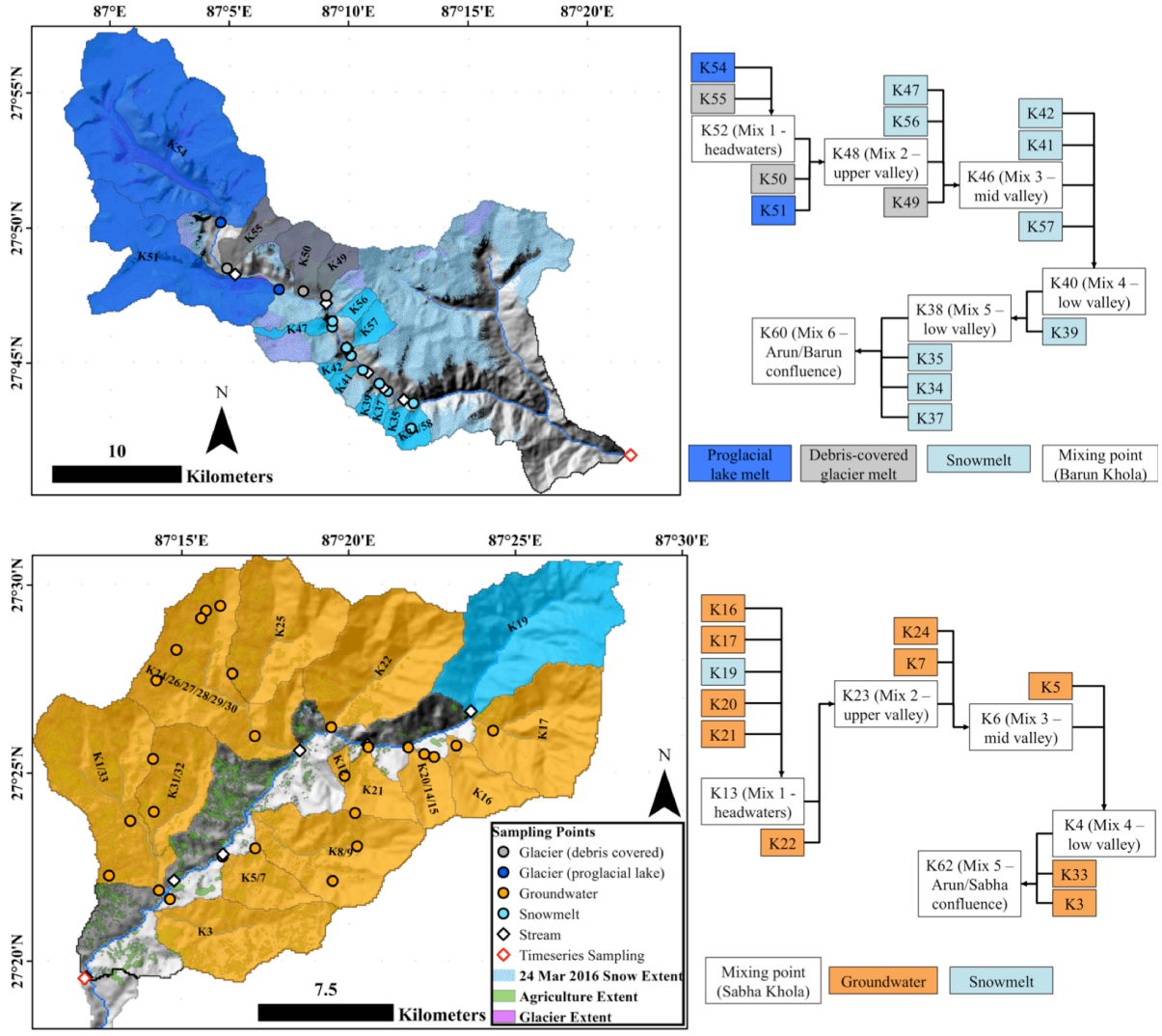

Figure S1. Schematic of Barun Khola (top) and Sabha Khola (bottom) inputs and mixing points with corresponding sample name and dominant source water type for the drainage area of the specific sample.

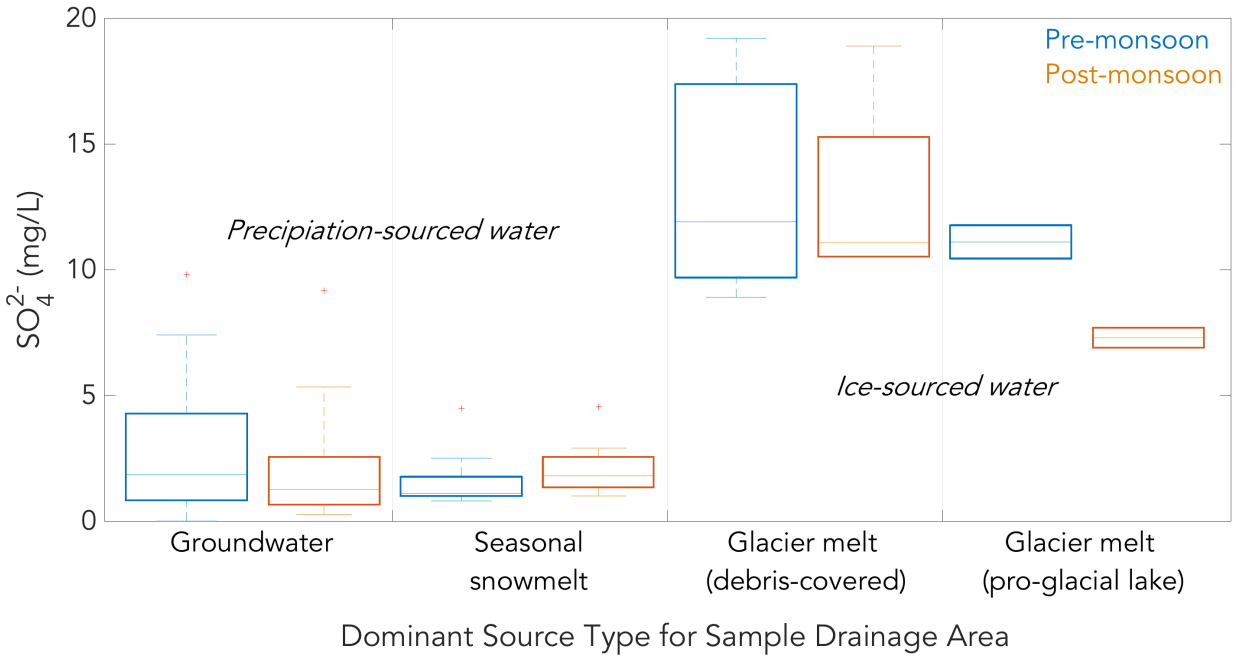

Figure S2. Sulfate concentrations are noticeably higher in glacier melt-dominated drainages relative to groundwater and drainages with seasonal snowmelt. This pattern holds across seasons and renders sulfate a useful tracer to separate glacier melt from other source water types.

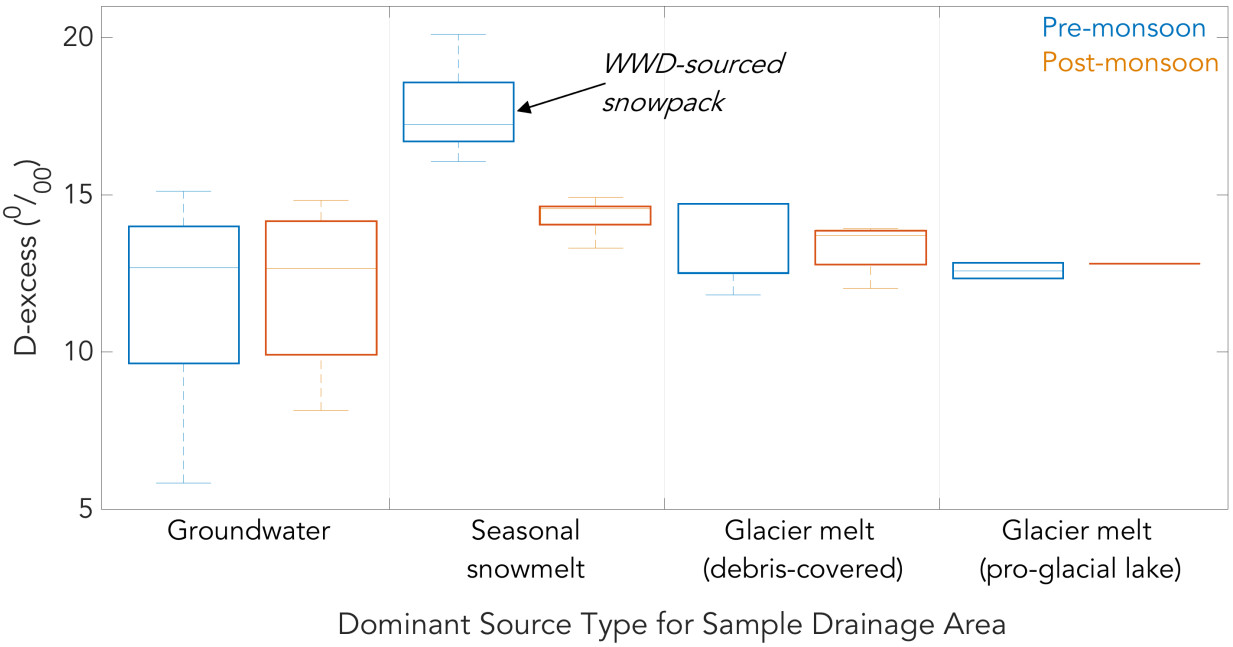

Figure S3. Deuterium-excess values are noticeably higher in the pre-monsoon in drainages with extensive WWD-sourced snowpack. The decline in d-excess in the post-monsoon is indicative of a transition to ISM-sourced precipitation inputs(R. G. Wirsing, 2013; R. Wirsing et al., 2012).

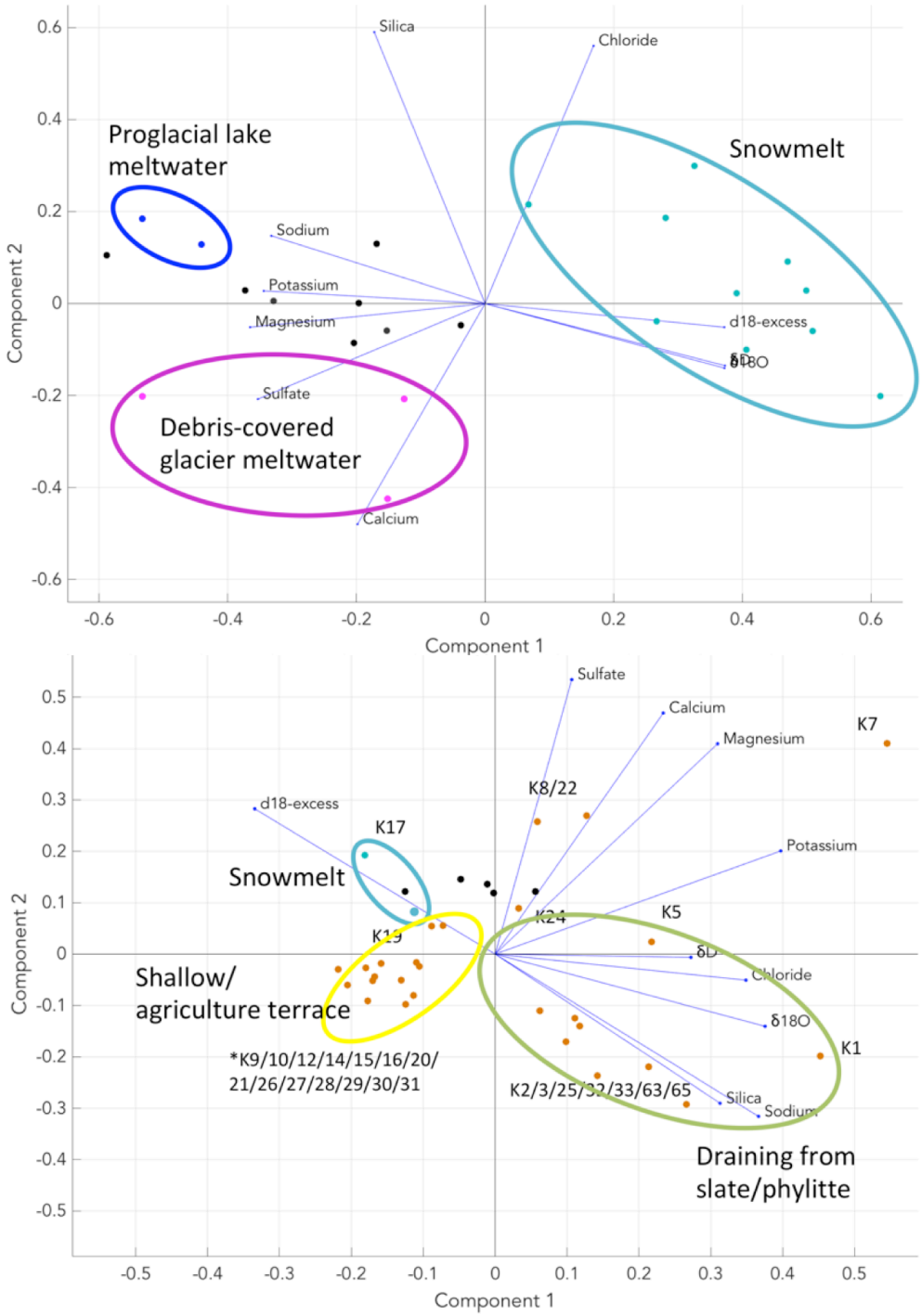

Figure S4. Results of principal component analysis in the Barun Khola (top) and Sabha Khola (bottom) in the pre-monsoon season. The analysis indicates that snowmelt-dominated samples broadly have high isotope-related values and low dissolved ion concentrations. Glacial melt-dominated samples have high dissolved ion concentrations, with sulfate particularly high in samples draining from debris-covered glacier melt. Groundwater samples has higher dissolved ion concentrations compared to snowmelt-sourced samples.

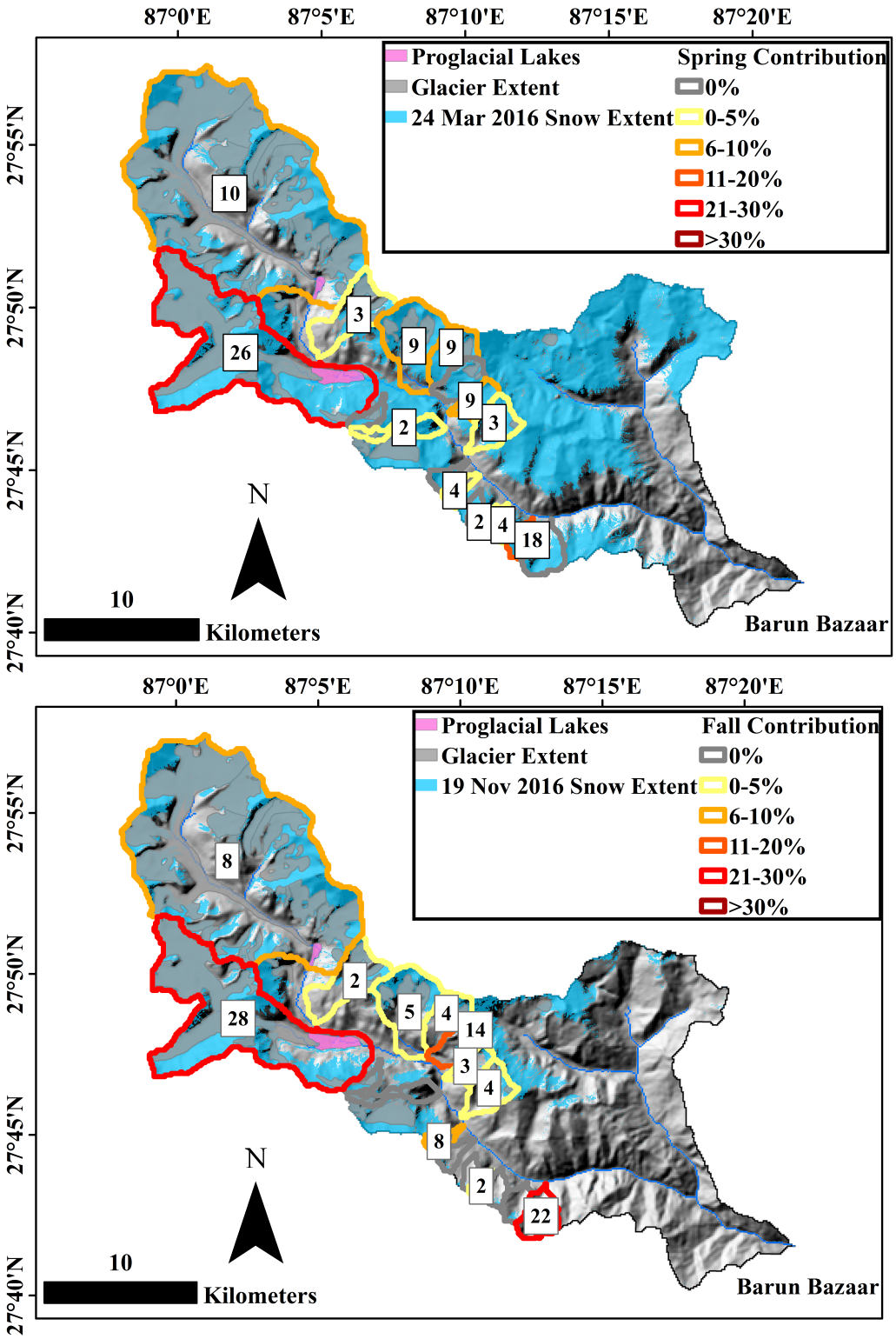

Figure S5. Estimated contributions from individual sample drainage areas in the pre-monsoon (top) and post-monsoon (bottom) seasons in the Barun Khola.

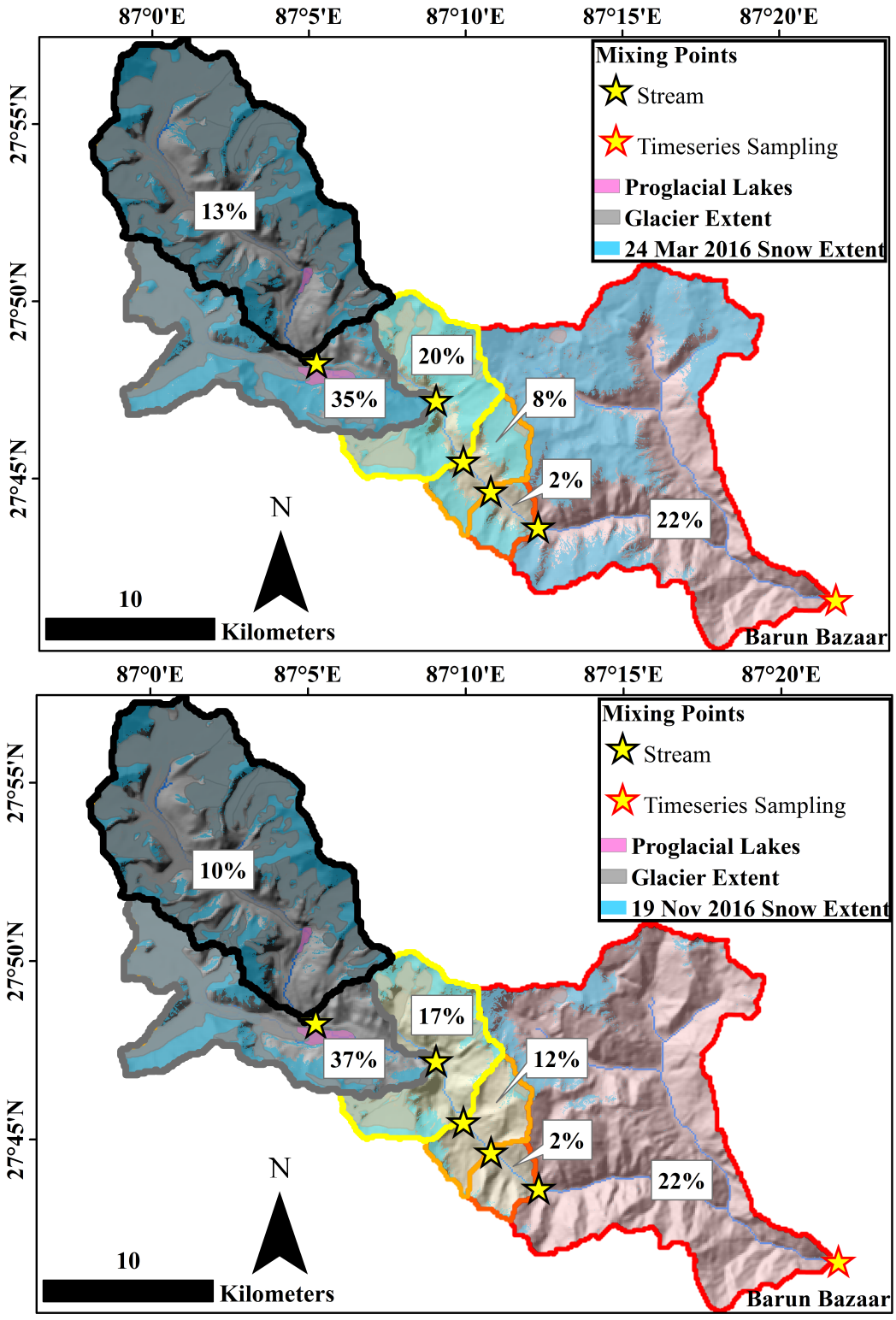

Figure S6. Contributions for each contributing area between mixing points in the pre-monsoon (top) and post-monsoon (bottom) seasons in the Barun Khola.